Role of N-terminal domains of p400 ATPase in the ATM interaction and DNA damage response

A thesis presented in partial fulfillment of the requirements for a the degree of

Master of Science (Msc)

in

Genetics

At Massey University, Manawatū,
New Zealand

Lauren Elizabeth Weber

2016

Abstract

Efficient repair of damaged DNA and preservation of genomic integrity is integral in the maintenance of proper cellular function and prevention of unrestricted cell proliferation. One critical threat to the stability of the genome is the double strand break (DSB), arguably one of the most cytotoxic lesions to DNA. Interference with the DSB repair mechanism can lead to dysregulation of cellular systems and the prospective development of malignancies. Two critical proteins in DBS repair are the Ataxia Telangiectasia Mutated (ATM) kinase, a serine/threonine kinase from the Phosphatidylinositol 3-Kinase-related Kinase (PIKK) family, and p400, an ATPase chromatin remodeler. ATM is one of the first responders to DSBs and is responsible for the phosphorylation of a multitude of protein substrates including the histone variant H2AX. Beyond its phosphorylation ability, ATM has been proposed as a potential shuttle for other repair machinery, aiding in the early and efficient recruitment of proteins to the DNA damage foci. One such proposed protein is p400. The exact role of p400 in DSB repair is unknown but previous studies show that there is a decrease in repair efficiency in its absence. A prospective interaction is supported by previous studies in which p400 and p400 N-terminal derivatives co-immunoprecipitate with ATM *in vivo* in HEK293T cells.

This study aimed to confirm the interaction of ATM and p400 N-terminal derivatives *in vitro* and explore the functional implications of the association *in vivo* in U2OS cells. It was not possible to isolate full-length p400 derivatives *in vitro* and thus no conclusive results were obtained. Functional assays revealed the ability of one p400 fragment, F1, to inhibit DNA repair and cell proliferation after DNA double-strand break induction with bleomycin. Ectopic expression of the other two p400 N-terminal fragments, F2 and F3, induced an inhibition of cell proliferation under standard growth conditions. Although no conclusive results were acquired, a trend emerged suggesting that N-terminal fragment F1 is able to interfere with ATM protein-protein interactions resulting in a decrease in the efficiency of the DNA damage response and repair. These results implicate F1 as a potential target for further research in both DNA repair and cancer therapy.

Acknowledgements

No words can described how appreciative I am to everyone who has made the writing of this thesis possible. Firstly, I would like to thank my supervisor Jeong Park for all of the knowledge he shared and for helping to guide me through this degree. JP treated all of his students as an extension of his family and I will always remember the wonderful get-togethers he and his family prepared for us. I would also like to show my gratitude for Rebecca Smith. I learned more from Bex than just research skills. She always had time to help me in my times of need or confusion, which were more than I care to admit.

I would also like to thank Kathryn Stowell for her wisdom, sound advice, and quirky sense of humor. Her door was always open and I definitely popped my head to ask for assistance more than a few times. The random appearance of confectionary in the walk-in-center and chocolate Easter eggs from the “Easter bunny” added something special to the far end of Science Tower D.

I am also very appreciative for the help I received from Tracey Hale and Helen Fitzsimons for helping with my tissue culture needs as well as all of the good conversations.

A special thank you goes out to the members of ParkLand and the Twilight Zone (as well as the downstairs lab associates). Some of the study-break chats in the computer room left me in stitches. Even on the most stressful of days, I could always count on the ridiculous banter to lighten the mood.

Abbreviations

°C	degrees Celsius
-ve	negative
A	ampere
Ac	acetylation
Amp	ampicillin
APS	ammonium persulphate
AT	Ataxia Telangiectasia
ATM	ataxia telangiectasia mutated
ATP	adenosine triphosphate
ATR	ataxia telangiectasia mutated and Rad3-related protein
BCA	bicinchoninic acid
BME	β-mercaptoethanol
bp	base pair
BSA	bovine serum albumin
c-Abl	Abelson murine leukemia viral oncogene homolog 1
cDNA	complementary DNA
CIP	calf intestinal phosphatase
CMV	cytomegalovirus
Co-IP	co-immunoprecipitation
DAPI	4’, 6-diamidino-2-phenylindole
ddH_2O	double distilled water
DMEM	Dulbecco’s Modified Eagle Medium
DMSO	dimethylsulfoxide
DNA	Deoxyribose nucleic acid
DNA-PKcs	DNA-dependent protein kinase catalytic subunit
dNTPs	Deoxyribonucleic triphosphate
DSB	Double strand break
DTT	Dithiothreitol
E. coli	*Escherichia coli*
EDTA	ethylene diamine tetra-acetic acid
EtBr	ethidium bromide
EtOH	ethanol
FAT	FRAP-ATM-TRRAP
FAT-C	FAT domain located at the protein’s C-terminus
FBS	fetal bovine serum
g	gram
g	relative centrifugal force (force x gravity)
GSH	glutathione
GST	glutathione S-transferase
h	hours

H2Av	Drosophila H2A.Z and H2A.X homologue
H2AX	histone variant of H2A
γH2AX	histone variant H2A.X phosphorylated at serine 139
HA	hemagglutinin
HAT	histone acetyl transferase
HCl	hydrochloric acid
HEK293T	human embryonic kidney cell line
HD	high definition
HF	high fidelity
HP1	heterochromatin binding protein 1
HR	homologous recombination
HRP	horseradish peroxidase
HSA	helicase and SANT associated
IF	immunofluorescence
IP	immunoprecipitation
ITPG	isopropyl β-D-1-thiogalactopyranoside
K	lysine
kb	kilobase
kDa	kilodalton
L	liter
LB	Luria-Bertani bacteriological media
M2 agarose	α-FLAG antibody immobilized on agarose beads
mA	milliampere
Mb	megabase
MCS	multiple cloning site
mg	milligram
min	minute
mL	milliliter
mM	millimol
mRNA	messenger ribonucleic acid
MRN	Mre11-Rad3-Nsb1
Mre11	meiotic recombination 11
MW	molecular weight
NBS	Nijmegen breakage syndrome
ng	nanogram
NHEJ	non-homologous end joining
NLS	nucelar localization sequence
nm	nanometer
NP-40	tergitol-type nonyl phnoxypolyethocyethanol 40 (Igapal CA-630)
OD	optical density
PAGE	polyacrylamide gel electrophoresis
P3	generation 3 of baculovirus
PBS	phosphate buffered saline

PCR	polymerase chain reaction
PEG	polyethylene glycol
pen/strep	penicillin-streptomycin solution
PFA	paraformaldehyde
PHYRE2	protein homology/analogy recognition engine V 2.0
PI3K	phosphatidylinositol 3-kinase
PIKK	phosphatidylinositol 3-kinase-like protein kinase
pmol	picomol
PMSF	phenylmethanesulfonyl fluoride solution
PVDF	polyvinylidene fluoride transfer membrane
qPCR	quantitative real-time PCR
RE	restriction endonuclease
RNA	ribose nucleic acid
RNase	ribonuclease
RT	reverse transcription/reverse transcriptase
RT-qPCR	reverse transcription quantitative real-time PCR
S	serine
s	second
SANT	SWI3-ADA2-N-CoR-TFIIIB
SDS	sodium dodecyl sulphate
SDS-PAGE	sodium dodecyl sulphate polyacrylamide gel electrophoresis
Sf9	clonal isolate of *Spodoptera frugiperda* Sf21 cells
siRNA	small interfering RNA
SWI2/SNF2	switch 2/sucrose non-fermentable 2
TAT	transactivator of transcription
TBE	tris boric acid EDTA
TBS/T	tris-buffered saline with tween-20
TE	tris EDTA buffer
TEMED	N, N, N’, N’-tetramethylethylenediamine
TIP48	transactivation-domain interacting protein of 48 kDa
TIP49	transactivation-domain interacting protein of 49 kDa
TIP60	HIV-I TAT interacting protein of 60 kDa
Tris	2-amino-2-hydromethyl-1,3-propanidol
TRRAP	transformation/transcription domain-associated protein
μg	microgram
μL	microliter
UV	ultraviolet light
V	volts
v/v	volume per volume
w/v	weight per volume
WT	wild type

List of Figures

List of Tables

Table of Contents

1 Introduction

1.1 Cancer and Current Cancer Therapies

DNA is under constant attack by genotoxic events, which can result in spontaneous DNA lesions [1]. These range from single strand (SS) damage to more deleterious aberrations such as DNA Double-strand Breaks (DSBs). DSBs can be generated through replication-associated errors, endogenous cellular metabolic processes and exogenous sources such as Ionizing Radiation (IR) and chemotherapeutic agents. There are also instances in which DSBs are generated in a programmed manner, as in the case of meiosis in order to produce gametes with increased variation or during V(D)J recombination and class switch recombination for the development of lymphocytes. Whatever their origin, it is critical that DSBs be efficiently and accurately repaired in order to ensure the veracity of the cell. Insufficient or inaccurate restorations can cause genomic mutations and chromosomal translocations or fragment loss leading to an increased risk of malignancy or cell death [1]. Because of this, cells have developed a well-coordinated network of signaling cascades, called the DNA Damage Response (DDR), to ensure the integrity of DNA. The DDR senses the damage, transmits damage signals to effector proteins, and induces cellular responses such as cell cycle arrest, activation of DNA repair pathways, and programmed cell death [2].

Unfortunately the DDR isn't always successful which can leave damaged cells to continue to replicate with potentially harmful genomic alterations. Current cancer therapies enlist the use of many different types of chemotherapeutic agents and radiotherapy mechanisms in order to combat these abnormal cells. The chemicals can inflict a variety of lesions on the DNA or disrupt the DDR. Chemotherapeutic drugs such as methyl-methane sulfonate and temozolomide are alkylating agent that attach alkyl groups to DNA bases while etoposide inhibits topoisomerase I and II, which induces the formation of Single Strand Breaks (SSBs) or DSBs by trapping topoisomerase-DNA covalent complexes. Radiotherapy employs the use of particles or waves moving at high frequency to target and damage the DNA of replicating cells in a specific physical region [3]. Many therapies are used in conjunction to amplify the effects of one another such as the combination of radiotherapy with inhibitors of the DDR proteins ATM (Ataxia Telangiectasia kinase Mutated) and the MRN (MRE11-RAD50-NBS1) complex, which produces a profound radiosensitizing effect [4].

Regrettably, these therapies work not only on cancerous cells but on healthy cells as well. Radiotherapy can cause severe local adverse effects such as radiodermatitis and chemotherapy treatment can kill healthy, rapidly dividing cells and cause new mutations in previously healthy cells due to the aggressive ability to generate DNA damage. Furthermore, these treatments aren't always successful and the high levels of chemotherapeutic agents required to successfully eradicate malignant cells can cause the patients an immense amount of physical and psychological stress. Because of this, there has been a strong push to develop novel cancer therapies that make use of the machinery of the human body itself. One way to achieve this is through the manipulation or inhibition of the DDR. This study proposes a potential inhibition of ATM by the expression of N-terminal derivatives of the ATPase chromatin remodeler E1A-binding protein p400 (p400), another DDR protein naturally occurring in the human body. To comprehend how the DDR may be manipulated it is necessary to understand the structure and function of chromatin, DNA damage and repair, and the roles of ATM and p400 in the cell and in regards to each other.

1.2 Chromatin and Gene Regulation

The blueprint to every cellular characteristic and metabolic function is contained within the DNA molecules of the cell. DNA is packaged in the nucleus as chromatin, a highly ordered and complex mechanism by which to maintain genomic integrity while enabling efficient access and regulation of genes. The basic unit of chromatin is the nucleosome, which consists of 147 base pairs (bp) of DNA wrapped 1.67 turns around an octamer of histones and one linker DNA up to 80 bp in length. The octamer is comprised of two of each of the four canonical histones structured as one H3-H4 heterotetramer and two H2A-H2B heterodimers [5, 6]. The primary chromatin structure, known as the 10 nm fiber, is the most basic form of the chromatin folding hierarchy and consists of multiple nucleosomes in a sequence. The secondary structure is the 30 nm fiber, which is constructed from the folding of the 10 nm and is stabilized by H1 histones in order to maintain this higher level of folding [7]. The 30 nm fiber folds upon itself to create the tertiary chromatin structure. This requires both the H1 histone as well as HP1 (Heterochromatin Protein 1) as seen in Figure 1.1 [8].

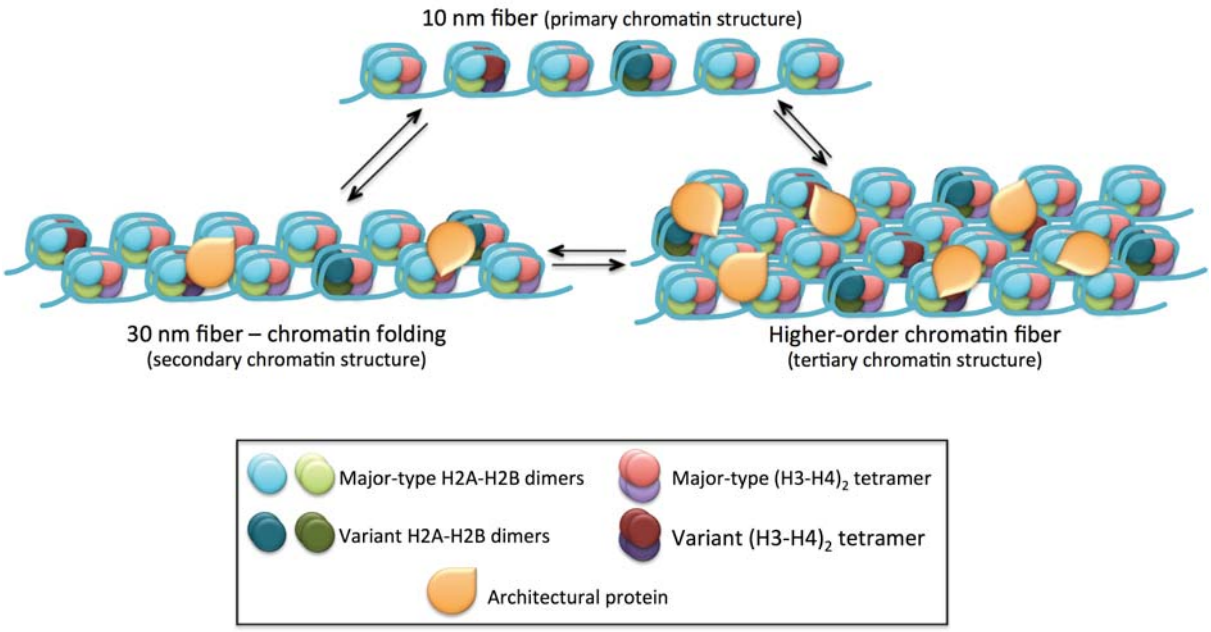

Figure 1.1 Chromatin Folding Mechanisms. Chromatin can assume different forms of folding. One of these determining elements is post-translational modification as well as presence or absence of architectural proteins. The 10 nm fiber is the most basic chromatin structure, which consists of nucleosomes connected by linker DNA. Next is the 30 nm fiber, which is maintained by the assistance of architectural proteins such as H1. Higher-order chromatin fibers are derived from 30 nm fibers organized with higher levels of complexity and maintained by architectural proteins such as H1 and HP1 as well as posttranslational modifications of the core histones. (Adapted from Luger et. al, 2012) [9]

1.2.1 Role of histones in chromatin accessibility

The majority of nucleosomes are comprised of four canonical core histones, H2A, H2B, H3, and H4. Supplementary to these core histones are the histone variants, which have distinct amino acid sequences and functions that help to determine the structure, stability, and dynamics of both the nucleosome and chromatin. All histones have two major domains, the globular domain and the histone tail, which extends out from the nucleosome core. At the core of the nucleosome, a strong four-helix bundle interaction between the two H3 histones forms the $(H3/H4)_2$ tetramer. This tetramer interacts with the two heterodimers of H2A/H2B located at the DNA entry and exit sites of the nucleosome [10]. H2B and H4 share an interaction through a weak four-helix bundle while the two H2A histones interact with the nucleosome through the L-loop. These interactions keep the nucleosome intact but also allow for modifications. Post-

Translational modifications (PTMs) of histone tails such as methylation, phosphorylation, acetylation, ubiquitination, ribosylation, and sumoylation can alter nucleosome stability and/or serve as docking sites for a wide range of proteins [11, 12]. These modifications are highly dynamic and reversibly added or removed by a variety of enzymes depending on the needs of the cell. Together, variations in histone composition and PTMs help to regulate the configuration of chromatin as either euchromatin or heterochromatin.

Euchromatin is characterized by an open chromatin structure associated with actively transcribed regions of DNA. Specific histone modifications such as high levels of acetylation of histone H4 on lysine 16 or the dimethylation of histone H3 on lysine 4 and 36 promote this accessible configuration [13, 14]. Acetylation of the positively charged lysine residue neutralizes the overall charge, eliminating the interaction between the lysine and the negatively charged DNA phosphate group. This promotes a more relaxed and open structure and prevents folding of the 30 nm structure [15, 16].

Heterochromatin, in contrast to euchromatin, is retained in a highly folded state characterized by inactive regions of DNA folded into 30 nm fibers and higher order chromatin structures. Heterochromatin typically occupies regions of DNA with a low density of genes and many stretches of repetitive sequences [14, 17]. Levels of histone acetylation in heterochromatin are typically low as opposed to the high levels of acetylation in euchromatin. Modifications to maintain a heterochromatin state include trimethylation of histone H3 at lysine 9, which serves as a docking site for HP1, and trimethylation of H3 lysine 27 [18-20]. In addition, H2AZ is monoubiquinated, which provides a binding site for heterochromatin promoting factors [21, 22].

1.2.2 Alteration of chromatin structure by chromatin remodeling complexes

Chromatin Remodeling Complexes (CRCs) are multisubunit protein complexes containing an ATPase subunit that disrupt histone interactions or mobilize histones in an ATP-dependent manner and play a principal role in chromatin remodeling activities [23, 24]. CRCs are able to evict nucleosomes to create sections of open or relaxed DNA or slide nucleosomes by shifting their position relative to the DNA in order to expose or bury specific DNA sequences [25-27]. They can also exchange canonical histones for histone variants and vice versa to alter chromatin structure [28]. Replacing canonical histones with histone variants can regulate gene activation or repression [12, 29].

1.3 H2A Histone Variants

The H2A histone variants H2AX and H2AZ both play a role in DNA repair. They are of particular interest to this study because of their direct interactions with ATM and p400 respectfully.

H2AZ diverged from H2A early in eukaryotic evolution and has remained distinct from H2A. This variant is relatively conserved between species and universal to nearly all eukaryotes [30]. H2AZ accounts for roughly 15% of total H2A in a cell and preferentially localized at promoter and enhancer regions of genes [31, 32]. It is introduced into the nucleosome as a H2AZ/H2B dimer by the SRCAP (SNF2-Related CBP Activator Protein) or the Tip60 (TAT Interacting Protein 60)/p400 complexes [13, 33, 34]. Canonical H2A and H2AZ share a 64% sequence identity, resulting in some key structural differences between the two (Figure 1.2). One notable difference is the extended acidic patch in the C-terminal region. This extension has been argued to act as both a stabilizer of higher order chromatin structures as well as a stimulation point for chromatin remodeling activity [33, 35, 36]. Conversely, the structurally distinct H2AZ L1 loop, located within the docking domain of the $(H3/H4)_2$ tetramer, was found to compromise three hydrogen bonds due to a glutamine-to-glycine substitution in H2AZ [35]. This structural variance weakens the histone-histones interactions, resulting in a subtle difference in chromosome stability.

H2AZ can both stabilize and destabilize chromatin depending on PTMs, differences in DNA sequence, and whether H2AZ is heterotypic or homotypic in a hybrid nucleosome [37, 38]. The type of PTMs on H2AZ in promoter regions determines positive or negative regulation of transcription. Acetylation of H2AZ on lysine (K) 4, K7, K11, and K13 typically promotes an open chromatin structure [39, 40]. When H2AZ is methylated on K4 or K7 transcription will be discouraged. These methylation marks prevent the acetylation of H2AZ at K4 and K7, indicating that these marks are mutually exclusive [41]. This supports involvement of H2AZ in both positive and negative regulation of gene expression and chromosome stability.

Figure 1.2 Protein alignment of histone H2A variants. MUSCLE from EMBL-EBI was used to align the protein sequences for H2A (NP_003507.1), H2A.Z (NP_002097.1), and H2A.X (NP_002096.1). Asterisks (*) represent single, fully conserved residues between all three histone variants, colons (:) denote conservations between residues with strongly similar properties (0.5 in the Gonnet PAM 250 matrix) and periods (.) symbolize conservation between residues of weakly similar properties (=< 0.5 in the Gonnet PAM 250 matrix). Red indicates residues that are small and hydrophobic, blue represents acidic residues, magenta denotes basic residues, and green specifies hydroxyl, sulfhydryl, amine, and G residues. The red arrow designates serine (S) 139 of H2A.X, which is phosphorylated by members of the PIKK family of kinases during the DNA damage response. (http://www.ebi.ac.uk/Tools/msa/muscle/)

H2AX is located throughout the genome and is deposited throughout chromatin in a random manner. Canonical H2A and H2AX share a 95% homology to one another. The most distinct difference between H2AX and H2A is the H2AX C-terminal extension containing an SQ motif that is recognized by PIKK (Phosphoinositide-3-Kinase-related protein Kinase) family members, which generates the phosphorylated H2AX (γH2AX) mark during DNA repair [42]. The phosphorylation of serine (S) 139 in the SQ motif (indicated by the red arrow in Figure 1.2) by PIKK family members such as ATM, promotes the assembly of signaling complexes onto the chromatin. This is a critical step for initiation and amplification of DNA damage signals including the timely engagement of MDC1 (Mediator of DNA damage Checkpoint protein 1), 53 BP1 (p53 Binding Protein 1), and BRCA1 (Breast Cancer 1) [43]. It is also vital for the delineation of the chromatin region involved in the DDR [44]. The phosphorylation of H2AX spreads several kilobases either side of the break site with little to none

phosphorylated at the break site itself, which may be due to nucleosome eviction at that location [45-47].

H2AX knockout mice display an increase in chromosomal abnormalities and deficiencies in DSB repair with an overall increase in sensitivity to DNA damage [48-50]. Similarly, the mutation of H2AX's S139 to a non-phosphorylatable amino acid results in a decrease in the accumulation of DNA repair proteins as well as an overall reduction in repair efficiency [48, 51-53]. In addition, the inability to acetylate H2AX during DNA repair inhibits the exchange of modified H2AX to unmodified H2AX, reducing the efficiency of DNA repair [54]. These PTMs and others are critical for H2AX to effectively perform its function as a signal and protein-docking site in DNA repair.

1.4 DNA repair

Maintaining the integrity of the DNA is of the upmost importance in a cell as unrepaired DNA aberrations may lead to mutations within the cell [55]. To prevent this cells have evolved a number of repair systems. Two different kinds of damage that can occur are SSBs and DSBs. The cell has developed mechanisms for the repair of each of them. SSB repair is comprised of base excision repair, nucleotide excision repair, and mismatch repair while DSB repair involves Non-Homologous End Joining (NHEJ) and Homologous Recombination (HR). This study is concerned with only DSBs as these are the breaks that involved both ATM and p400.

1.4.1 Double Strand Break Repair

Double strand breaks are more critical for the cell as they can lead to massive alterations in DNA such as chromosomal translocations and loss of chromosomal fragments [56]. These breaks can arise from endogenous or exogenous sources and replication-associated errors as well as in a programmed generated manner. Although the DSB repair mechanism has not been fully characterized there are three well-defined events that occur rapidly after a break transpires; accumulation of the MRN complex at the break site, ATM kinase activation, and phosphorylation of H2AX.

There are a multitude of proteins involved in DNA repair. They exist in a hierarchical order and are described as sensors, transducers, mediators, and effectors, dependent in part on their subcellular localization [57]. Sensors, such as the large

multisubunit MRN complex, are the one of first to respond to assaults on DNA and bind directly to chromatin. MRE11 (Meiotic Recombination 11 homologue), RAD50, and NBS1 (nibrin) congregate at nuclear foci to form the MRN complex, which acts as a bridge between the two strands [58]. MRE11 contains two DNA binding domains that have been shown to avidly bind SS DNA regions that occur at break sites [59]. It also acts as a binding site for both NBS1 and RAD50 [60, 61]. NBS1 promotes the accumulation of repair machinery through its ability to bind to a variety of proteins including γH2AX and MDC1 (Mediator of DNA-damage Checkpoint 1) and is crucial for ATM recruitment and retention at DSBs [62-66]. RAD50 aids in bridging the break site and encourages DNA end processing through MRE11 [67]. When one or more of the MRN complex subunits is mutated, the cell experiences chromosomal instabilities and deficiencies in DNA repair [68]. Although the MRN complex can bind to DSBs independently of ATM, when the two interact MRN accumulation is more strongly promoted [69]. The association also aids in the activation of ATM, suggesting that the MRN complex may amplify ATM [70].

Transducers, mediators, and effectors guide the DNA damage actions [2]. When activated, transducers relay a strong and widespread signal to numerous downstream effectors and sensors, which can create feedback loops. ATM is the main transducer of DSB repair loops [71-73]. Once activated, ATM is capable of phosphorylating a large array of proteins, with one of the most critical phosphorylation targets being the histone H2AX, whose role in DNA repair was previously discussed. This phosphorylation is significant enough to support the need for redundancy between ATM, ATR (ATM and RAD3-related) and DNA-PKcs (DNA-dependent Protein Kinase catalytic subunit), which are all able to phosphorylate H2AX during DNA damage [64, 74]. In both mouse embryo fibroblasts and human fibroblasts lacking either DNA-PKcs or ATM, phosphorylation of H2AX occurred at similar levels after exposure to IR but was significantly reduced in ATM deficient cells treated with a drug that inhibits DNA-PK (DNA-dependent Protein Kinase) [74]. ATR can phosphorylate H2AX but does not display an ability to phosphorylate any other ATM phosphorylation substrates [53]. Once the DNA lesion is repaired, the chromatin structure is restored to a pre-damaged state, which is accomplished in part by the exchange of modified histones for unmodified histones through the chromatin remodeling actions of p400 [75, 76]

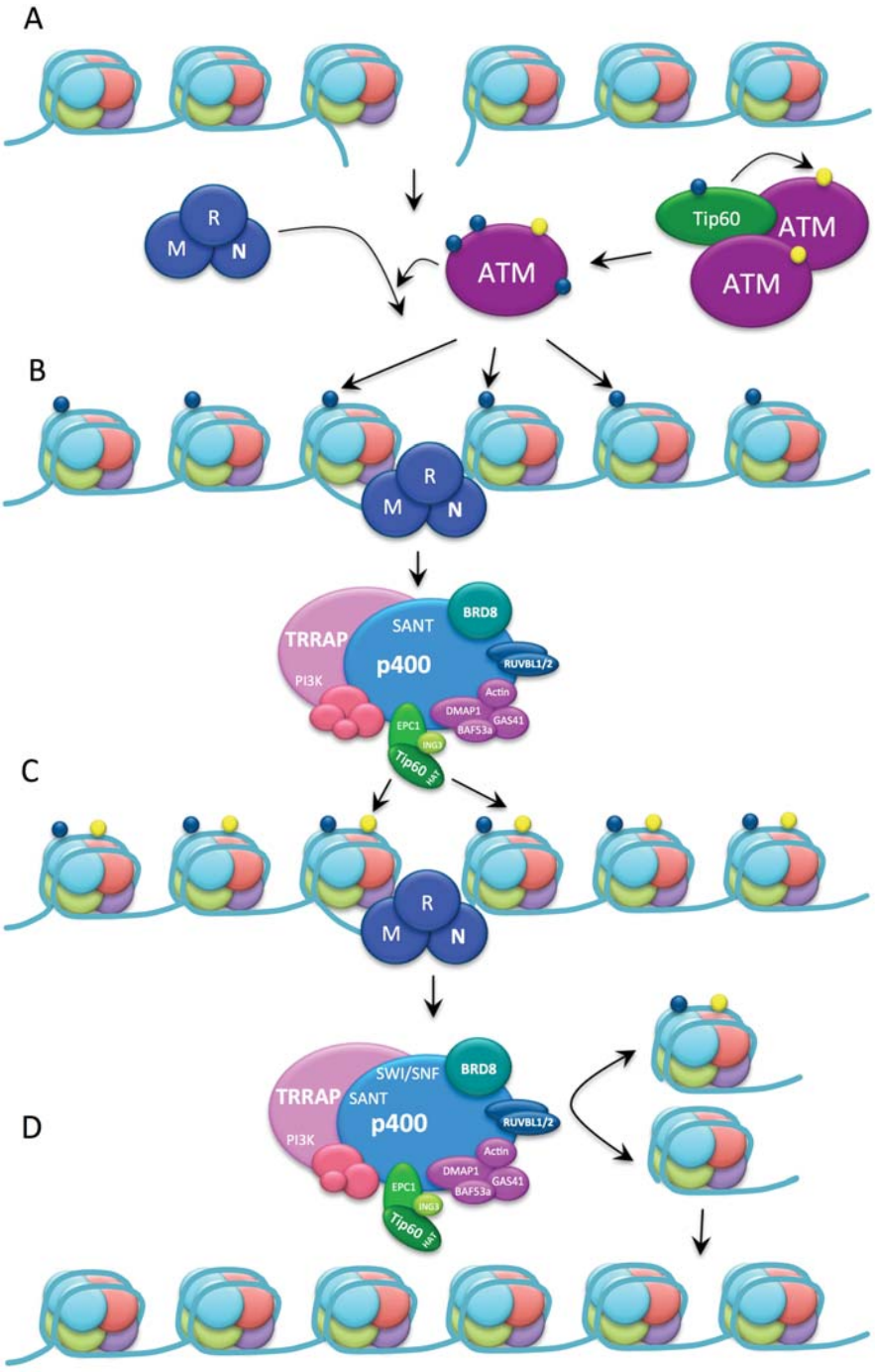

Figure 1.3 The DNA double strand break repair response. A-B) Upon DNA damage, the MRN complex binds to the DSB and acts as a scaffold as well as a signal to repair proteins such as ATM. ATM is activated through its acetylation by Tip60, which induces autophosphorylation. The MRN complex helps to optimize ATM activity and aids in ATM's localization to the DSB site. Activated ATM phosphorylates H2AX around the break site. C) The MRN complex and γH2AX act as docking sites for additional repair proteins including the Tip60 complex. Acetylation of H4 by Tip60 loosens the chromatin structure allowing for remodeling complexes to bind. D) Once the DNA is repaired, chromatin-remodeling complexes such as the Tip60/p400 complex are recruited to the break site and aid in the exchange of modified histones for unmodified histones. (Adapted from Smith, 2014) [77]

1.4.1.1 DSB repair by non-homologous end joining and homologous recombination

There are several distinctions between NHEJ and HR. One main difference between the two pathways is the stage at which the breaks occur. NHEJ can repair damage at any phase of the cell cycle although many studies have indicated that it occurs mainly during G1 and early S phase. On the contrary, HR occurs only during DNA replication and the G2 stage of the cell cycle [78, 79]. Another key difference between NHEJ and HR is the way in which the two ends of the DNA strands are processed. NHEJ works by simply locating the broken ends of the DNA strands and religating them back together with limited processing. When minimal trimming is required, NHEJ predominantly uses the MRN complex to tether the two ends, proceeded by their ligation by DNA ligase [80]. This method is error prone and can result in loss of genetic information [80]. HR repair takes advantage of the sister chromatid as a template for the damaged DNA. During HR the break site is processed into SS DNA and used to search for the homologous region of the sister chromatid via strand invasion with the assistance of RAD51 [81]. Once the appropriate section has been located, the sister chromatid is used as a template to repair the damage, resulting in a much less error-prone repair mechanism [82]. Due to the added complexity of HR, it requires a larger number of proteins to process and repair the DNA [83].

1.5 ATM kinase

ATM is a critical 350 kDa serine/threonine protein kinase in the DNA damage repair system. Mutations and loss of function of ATM has critical effects as seen in patients diagnosed with the genetic disease Ataxia Telangiectasia (AT), an autosomal recessive, multisystem disease [84]. Symptoms of homozygous patients include progressive neurodegeneration; telangiectasia (dilation of the capillaries); immunodeficiency that spans the B and T cell system; thymic and gonadal atrophy; marked predisposition to malignancies; acute sensitivity to IR; osteoporosis; and premature aging [85, 86]. Heterozygotes have an increased risk of breast cancer, developing diabetes and cardiovascular disease [87-89]. The cellular phenotype of AT includes increased chromosomal breakages; premature senescence of primary fibroblast cultures; sensitivity to DNA damaging agents (especially DSB inducing agents); defects in activation of cellular responses to DSBs; and hypersensitivity to IR and radio mimetic drugs. Cells that are homozygous typically demonstrate an attenuation of the

DSB response rather than a complete abolition, indicating that some roles of ATM may be accomplished by the redundant functions of PIKK family members [85]. Complete loss of ATM is less detrimental to the cell than possession of a mutated form [90-92].

Spontaneous mutations in ATM also have serious implications in the development of cancers. Mutated ATM alleles have been found in breast and colorectal cancers [93-95], while ATM heterozygous deficient mice show an increase in the development of mammary carcinomas and display ATM as a haploinsufficient tumor suppressor [96]. Complete loss of ATM causes an increase in cancer development in mice models, which further supports ATM as a target for cancer therapy. [90].

1.5.1 Structure and Function of ATM

ATM is a member of the PIKK family, which is part of the larger phosphatidylinositol 3-kinase (PI3K) superfamily. Members of the PI3K superfamily phosphorylate lipid moieties but members of the PIKK subfamily, with the exception of TRRAP (transformation/transcription domain-associated protein), phosphorylate protein substrates on serine or threonine residues followed by glutamine [(S/T)Q] motif. ATM along with ATR, TRRAP, DNA-PKcs, SMG1 (Suppressor with Morphological effect on Genitalia family member 1), and mTOR/FRAP (Mammalian Target Of Rapamycin/FKBP Adarapamycin associated Protein) constitute the PIKK family. All of the PIKK members possess a similar domain structure, which includes the FAT (FRAP-ATM-TRRAP) domain, FATC (FAT domain located at the C-terminus) domain, PIKK regulatory domain, and a PI3K kinase domain [86, 97]. FATC is a modular domain that can be replaced by the homologous domain of another PIKK protein, while retaining the original function of the chimeric protein [98]. All members display active kinase activity with the exception of TRRAP, which lacks a functional kinase domain. The six members of the PIKK family are involved in various cellular stress responses. Some display redundant functions to other PIKK members as mentioned previously [98].

Although very few distinct features have been identified, the landmark domain of ATM has been determined to be its carboxy-terminal active site, which occupies approximately 10% of the protein and contains a PI3K signature [97]. A nuclear localization sequence (NLS), ^{385}KRKK^{388}, in the N-terminal is recognized by the conventional nuclear import receptor importin α1/β1 heterodimer, which localizes ATM to the nucleus [99]. It is suspected that the rest of ATM contains regulatory and

interaction domains that determine its modes of activation and broad substrate specificity (Figure 1.4). Proteomic screens indicate the presence of hundreds of putative ATM substrates while, currently, ATM has been shown to interact with upwards of 30 different proteins including MDC1, CHK2 (Checkpoint Kinase 2), DNA-PK, RAD51, and BRCA1 [71-73, 100].

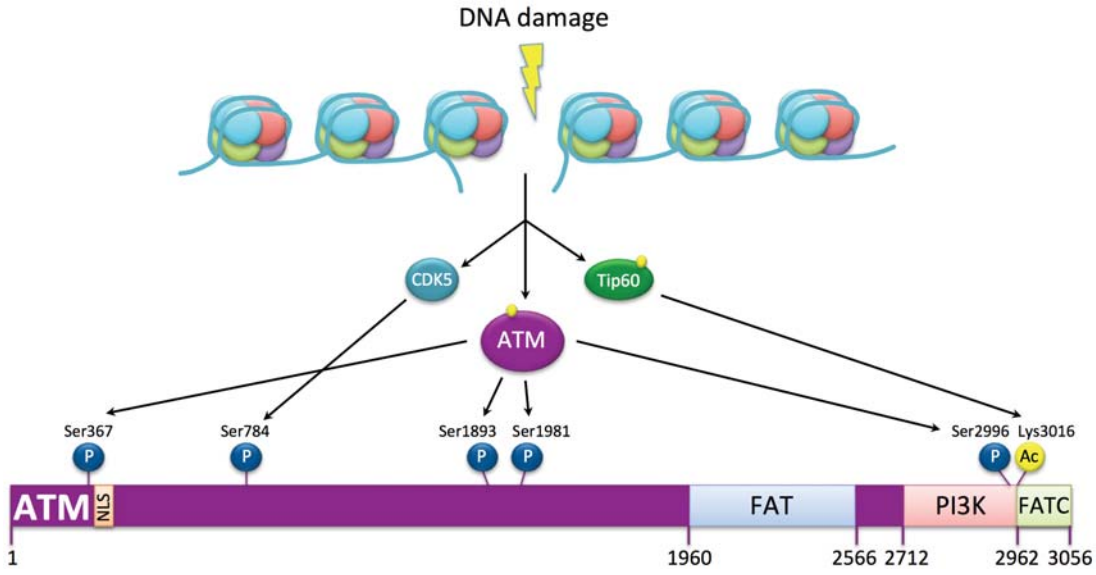

Figure 1.4 Schematic Representation of ATM and its Phosphorylation Sites. ATM is 3056 amino acids in length and contains a nuclear localization sequence (amino acid 355-388), the FAT domain (amino acid 1960-2566), the PI3K domain (amino acid 2712-2962), and the FATC domain (amino acid 2962-3056). In the presence of DNA damage ATM is acetylated by Tip60 (KAT5) on lysine 3016, which enables monomerization of ATM and autophosphorylation of S367, S1893, S1981, and S2996. (Adapted from Shiloh, 2003) [86]

In the absence of DNA damage ATM exists as a homodimer. This dimerization is facilitated by the kinase domain and FAT domain along with essential binding sequences flanking S1981 [101]. This has been supported using *in vitro* purified proteins as well as *Xenopus laevis* extracts [65, 102]. ATM in its dimerized state is inactive but a mere few DSBs are sufficient to induce massive quantitative activation of

the ATM pool [101]. Research suggests that the ATM homodimer may also be in complex with Tip60 (KAT5) [103]. This association of ATM and Tip60 may assist in the swift activation of ATM as acetylation of ATM K3016 by Tip60 followed by autophosphorylation at S1981 is one of route of ATM activation [104]. The autophosphorylation of S1981 is the first PTM associated with activated ATM, however, it is not required for monomerization [65].

1.5.2 ATM Activation

In the presence of DNA damage, ATM undergoes spatial relocalization within the nucleus and catalytic activation [105]. A portion of ATM is rapidly recruited to the break site where it remains for hours while the rest presumably stays nucleoplasmic [106]. The total amount of ATM appears to stay constant in the presence or absence of DNA damage [107-109]. The exact mechanism for ATM recognition of DNA damage and its subsequent activation is currently under debate. There are currently five evidence-supported initiation schemes thought to result in ATM activation (Figure 1.5).

Three of the five mechanisms implicate the physical form of the DNA as an activation initiator. The first suggests that ATM must bind to broken DNA; specifically to SS DNA stretches at DSBs [110, 111]. This is supported by the presence of hSSB1, a novel ssDNA-binding protein that may be required for ATM activation [112]. Another proposed mechanism reasons that SS oligonucleotides emanating from DSBs following end resection are the triggers for ATM activation [113]. Cells deficient in Trex1, an exonuclease that degrades ssDNA to mononucleotides, display a chronic ATM dependent damage response, implying that the build up of oligonucleotides maintains the cells in a constant state of activated ATM [114, 115]. In light of these speculations, a contradicting theory argues that chromatin conformation change following a DSB event prompts activation rather than the direct contact of ATM with broken DNA. [101, 116].

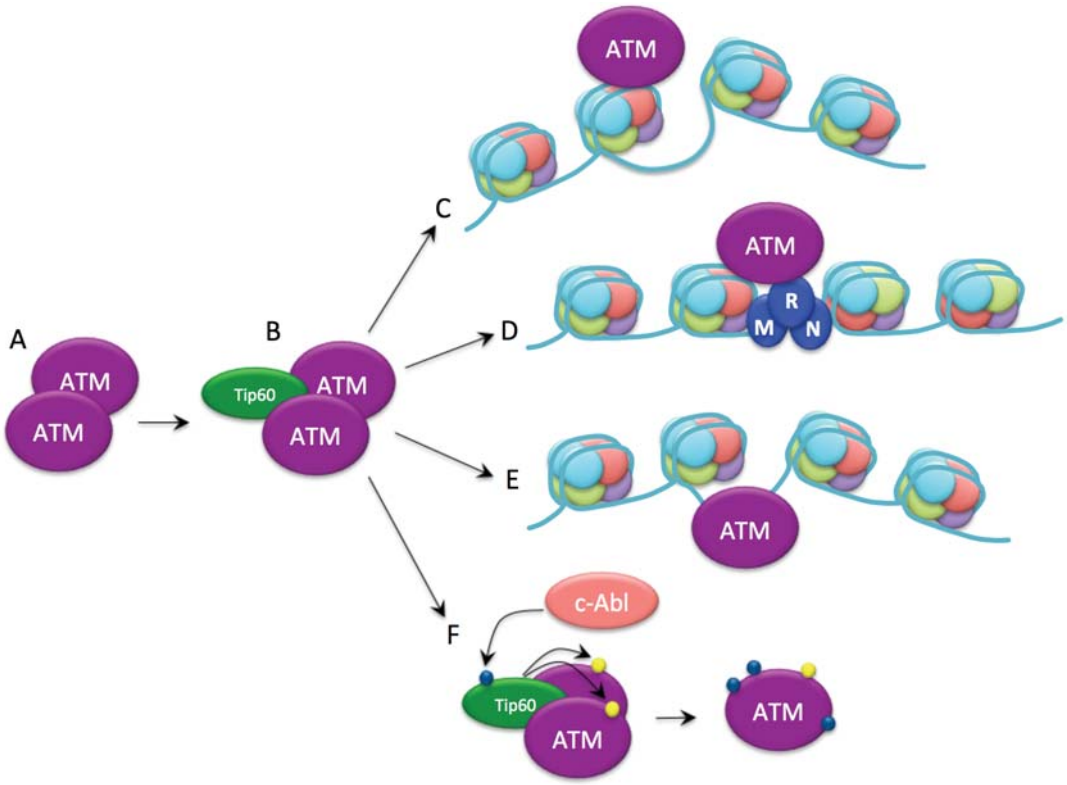

Figure 1.5 ATM activation mechanism. A) ATM exists as a homodimer in its inactive state and/or B) in a complex with Tip60. Activation of ATM is necessary in order for it to perform its function in DNA repair. This is done by C) binding to distorted chromatin, D) binding to DNA repair proteins such as NSB1 of the MRN complex, E) binding directly to free DNA ends or detection of oligonucleotides or F) when c-Abl phosphorylates Tip60, which then acetylates ATM, promoting autophosphorylation by ATM. Dark blue circles represent phosphorylation while yellow circles represent acetylation.

The other two mechanisms by which ATM activation is triggered involve the binding of ATM to repair proteins of the DDR. One way in which this has been shown is with the tethering of ATM to undamaged chromatin through the interaction of ATM with proteins such as MDC1 and the MRN complex [117]. Lastly, activation of ATM can be accomplished by a chain reaction of PTMs whose initial trigger has not been elucidated. Experimental evidence has shown that the tyrosine kinase c-Abl phosphorylates Tip60 in the presence of DNA DSBs or changes in chromatin structure. Once phosphorylated, Tip60 is activated and acetylates lysine 3016 of ATM. This acetylation is followed by ATM's monomerization and autophosphorylation of S1981, the most crucial PTM for ATM activation, as well as S367 and S1893 [101, 118]. Although there is evidence to support all of these proposed mechanisms, the biophysical

nature of the activation process and the mechanism of activation of ATM's physical trigger are still unknown.

1.5.3 Role of ATM in DNA Damage Response

The active form of ATM is essential for efficient induction of cellular responses to DSBs. This is accomplished through ATM phosphorylation of a multitude of DNA repair proteins and other phosphorylation targets such as H2AX, which is of particular importance [119]. γH2AX is a marker of DNA damage and spreads several kilobases either side of the break site while simultaneously acting as a critical docking site for repair protein assembly [51]. One of these repair proteins is MDC1. The phosphorylation of MDC1 by ATM enhances oligomerization at sites of DSBs [120-122]. In addition, MDC1 is anchored to the DSB site via γH2AX, whereby the MDC1 is able to bind to more ATM. This allows ATM to phosphorylate additional H2AX moieties further down the break site, followed by the association of more MDC1 molecules. These MDC1 proteins bind further ATM resulting in an enhanced process that accelerates the expansion of the DSB-associated focus [123]. The phosphorylation of both H2AX and MDC1 by ATM encourages a positive feedback loop between ATM and a protein that is required for proper positioning of repair proteins at DSB sites.

ATM is also responsible for the phosphorylation of MRE11 and RAD50, two of the three proteins that constitute the MRN complex [124-126]. The MRN complex is one of the first complexes to be recruited to the DSB site where it acts as a damage sensor as well as a physical bridge linking the two ends of the DNA [58]. Although the MRN complex is not required for ATM activation, it is vital for optimal stimulation of ATM, which contributes greatly to the timely commencement of various DDR branches [125, 127]. This creates a positive feedback loop that maintains ATM activity.

Another role for ATM during DNA damage is the regulation of cell cycle arrest. Changes in gene expression and degradation of checkpoint proteins is incited by phosphorylation events derived from the kinase activity of ATM. This facilitates cell cycle arrest at various checkpoints, preventing the replication of cells that may contain damaged DNA [128-130]. A further mechanism is the phosphorylation of p53. ATM-dependent activation and stabilization of p53 is essential to the regulation of cellular transcription following induction of DSBs [131, 132]. Activated p53 is able act in a cell survival manner by driving the expression of genes involved in the activation of cell

cycle checkpoints but it is also able to stimulate genes that promote programmed cell death or senescence [133, 134]. ATM is able to activate p53 directly by phosphorylating p53 at S15 or indirectly through a complex signaling sub-network within the larger DDR system where extensive PTM-mediated modulation of a range of proteins affects p53 activity and stability [135]. It is suspected that the type and extent of DNA damage influences the interplay between the opposing mechanisms and determines cell fate.

1.6 The ATPase chromatin remodeler p400

The ATPase chromatin remodeler p400 was originally discovered as part of a protein complex essential for transformation with the adenovirus E1A (Early region 1A) oncoprotein [136]. p400 belongs to the INO80 family, part of the larger SWI/SNF (Switch/Sucrose Non-Fermentable) super family, and plays an essential role in the regulation of gene transcription as well as DNA damage repair [136, 137]. It is considered a member of the SWR1-class of remodelers and is responsible for the exchange of the canonical histone H2A and histone variant H2AZ in nucleosomes [75, 76, 138, 139]. Not much is known about many of p400's domains but due to the presence of the SWI2/SNF2 (Switch2/Sucrose Non-Fermentable 2) homology domain, which exhibits ATP dependent histone exchange, p400 was revealed to be involved in histone exchange [136]. This multidomain protein also contains a SANT (SWI3-ADA2-N-CoRTFIIIB) domain, a HSA (Helicase and SANT Associated) domain, and a poly Q (poly-glutamine) domain [140].

p400 exists in two complexes, the Tip60 complex and the p400 complex (Figure 1.6). The two are nearly identical with the key difference being the inclusion or exclusion of the acetyltransferase Tip60 subunit [136, 141]. This is indicative of a possible dynamic exchange between the p400 and Tip60 complexes and explains the absence of histone acetylase activity of the p400 complex [136, 141, 142]. The Tip60/p400 complex is comprised of more than fifteen proteins, which include TRRAP, a member of the PIKK family; inhibitor of growth family member 3 (ING3); MRG15 (histone acetyltransferase subunit MORF4-related gene on chromosome 15); Brd8 (Bromo-containing protein 8); BAF53 (53 kDa BRG1/human BRG1-Associated Factor); TAP53α and TAP53β (Tip60 Associated Proteins 53α and 53β), and Tip49 (TBP-Interacting Protein) amongst others [136, 143]. The Tip60 subunit it exhibits a direct interaction with both p400 and TRRAP in the Tip60 complex [77].

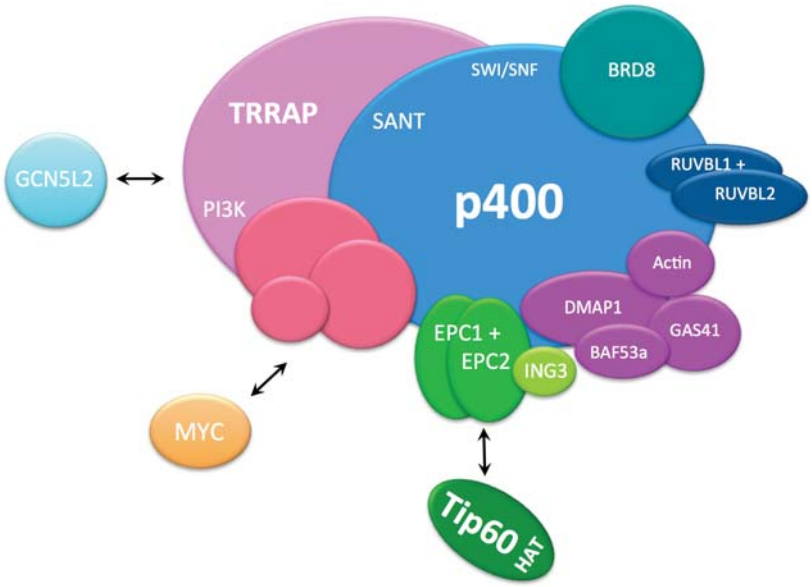

Figure 1.6 Hypothesized structure of p400 complex. p400 is a known member of two different complexes, the Tip60 complex and the p400 complex. The difference between the two complexes is the inclusion or exclusion of Tip60. The Tip60 complex contains Tip60 and displays acetyltransferase activity while p400 does not. In addition, Myc (c-Myc) and GCN5L2 (KAT2A) are able to associate with the p400 complex as well.

1.6.1 Role of p400 in H2AZ exchange

The importance of the p400 and theTip60/p400 complex as a chromatin remodeler is evident through the presence of homologues in all eukaryotic cells. Previous studies indicate that the yeast *Saccharomyces cerevisiae* p400 homologue, Swi2/Snf2 related (Swr1p), is responsible for the deposition of the histone variant H2AZ in euchromatin regions flanking heterochromatic regions [75]. When Swr1p is silenced there is a reduction in H2AZ deposition, resulting in the subsequent spread of heterochromatin. Swr1p is found in both the yeast SWR1 and NuA4 complexes, which are functionally conserved complexes of proteins homologous to the human Tip60 and p400 complexes and carry out many of the same functions [143-145]. The SWR1 complex has also been shown to be involved in chromosome segregation and stability [146]. The *Drosophila melanogaster* homologue for human p400, Domino, is part of the Drosophila Tip60 (dTip60) complex and catalyzes the exchange of H2A for H2Av, a homologue of human H2AX/H2AZ, at DNA damage sites [137]. This demonstrates both a physical and functional conservation between species [76].

1.6.2 Role of p400 in Gene Regulation

p400 plays a major role in the epigenetic regulation of gene expression through the incorporation of H2AZ in promoter regions [29, 147] and is implicated in proliferation control through physical and/or functional interactions with growth transcription factors such as c-Myc, p53, E2F, and E1A [136, 147-150]. p400-dependet deposition of H2AZ at the promoter regions of estrogen receptor α (ERα) nuclear receptor target genes is essential for their expression [151]. The incorporation of H2AZ at the proximal promoter of TFF1, an ERα-dependent model gene, induces stabilization of the nucleosomes and is fundamental for the recruitment of the transcriptional machinery.

p400 is involved in cell proliferation control through the regulation of p21. When p400 is depleted in untransformed human fibroblasts and human osteosarcoma U2OS cells there is cell-cycle arrest at G1, an increase in p21 mRNA, and premature induction of senescence [31, 152]. Expression of p21 by p400 is also accomplished in a p53-dependent and c-Myc-modulated manner through its co-localization with p53 at the p53-binding site of the p21 promoter and c-Myc at a TATA region [147, 153]. This interaction is able to block cell proliferation and lead to cellular senescence.

1.6.3 Role of p400 in DNA repair

Although the main role of p400is in gene regulation, it also plays an important part in DNA repair through chromatin remodeling. During DNA repair p400 in the Tip60/p400 complex relaxes the chromatin adjacent to DSB sites by destabilizing the nucleosomes through the exchange of histone H2A for the histone variant H2AZ. This creates a more open chromatin structure, which is necessary for the accumulation of DNA repair proteins, and facilitates efficient DNA repair [154, 155]. This exchange of histones, as well as other chromatin modifications by the Tip60/p400 complex, is essential for the recruitment and accumulation of repair proteins at locations of DSBs and ultimately, the maintenance of chromosomal integrity [156]. When p400 activity is altered with the use of ATPase mutants or through shRNA knockdown, its absence is marked by an increase in nucleosome stability around break sites [47]. One example of how p400-mediated alteration in the chromatin structure can aid in DNA repair is the RNF8-dependent ubiquitination of chromatin and the subsequent recruitment of BRCA1 to DSBs is [47]. In addition, previous studies show that while in the Tip60

complex, p400 is necessary for the acetylation of the N-termini of histones H4 and H2AX by the Tip60 subunit at sites of DNA damage, promoting a more relaxed chromatin structure [156, 157]. Besides its histone exchange functions in DNA repair, p400 is also important in the recruitment of Rad51 to the DSB site in HR where p400 and Rad51 show a direct interaction and co-localization at DSB damage foci [158].

1.6.4 Disruption of p400

Disrupting p400 has critical effects on the cell. The Tip60/p400 ratio is crucial in colon carcinomas [159]. One study observed that both *p400* and *Tip60* mRNA were under-expressed in colon carcinomas. A restoration of the normal Tip60/p400 ratio was sufficient to promote growth arrest and apoptosis of these cancerous cells. It was also observed that when the levels of Tip60 were higher than that of p400, there was an increase in p21 expression and cell senescence, while an inhibition of Tip60 resulted in decreased p21 expression [159]. In another study, the knockdown of p400 incited an increase in ATM phosphorylation and the induction of the DNA double strand break response [160]. Conversely, an overexpression of the p400 SANT domain reduces ATM phosphorylation [142]. Additionally, mice with an N-terminally deleted p400 mutation died *in utero* with a primitive erythropoiesis [161]. Within two weeks of induction of conditional knockout mice, the deletion resulted in the death of the mice with a rapid loss of bone marrow cells including hematopoietic progenitor and stem cells. It was determined to be a result of the reduced expression of cell-cycle regulatory genes involved in cell-cycle progression [161]. Lastly, it was shown that a loss of p400 activity results in an overall increase in cell radiosensitivity and chromosomal aberrations, indicating a role for p400 in the stability of nucleosomes [47, 54].

1.7 Thesis outline and hypothesis

Because of their critical roles in DNA repair, inhibiting or altering in function of ATM or p400 can have detrimental effects on healthy cells. This suggests that a mechanism by which to manipulate this dysregulation and prevent DNA repair could be used in the treatment of cancer cells in order to induce cell death. A prospective interaction between ATM and p400 was initially proposed due to the commonality of binding partners and overlap in DSB repair. p400 exhibits a direct association with the PIKK family member TRRAP, as part of the Tip60/p400 complex. TRRAP and ATM

are both part of the PIKK family of kinases and share many structural similarities as well as homologous domains such as FATC, which is known to be essential in protein-protein interactions. This resemblance implicates a potential direct association between ATM and p400. In addition, both ATM and p400 have direct interactions with Tip60. In a previous study, ATM was shown to co-immunoprecipitate with p400 *in vivo* [77]. Further examination into this interaction revealed that the N-terminal derivatives of p400 were responsible for this association. It was suggested that this interaction may have a functional effect on the activity of ATM.

This study aims to demonstrate a direct interaction between the N-terminal fragments of p400 and ATM in an *in vitro* environment. Additionally, the potential functional effect of p400 N-terminal derivatives on ATM will be examined in order to elucidate one or more N-terminal fragments as novel targets for cancer treatments in conjunction with traditional chemotherapeutic therapies.

1.7.1 Hypothesis

This project examined two hypotheses:

1) One or more p400 derivatives are capable of a direct interaction with ATM in vitro.
2) An interaction between p400 and ATM can influence a cell's sensitivity to DNA damage.

1.7.2 Objectives

1) Clone and express six GST-p400 derivatives in *Escherichia coli (E. coli)* BL21 cells and isolate the fusion-recombinant proteins using GST purification.
2) Express ATM in Sf9 cells and extract a cell lysate to use in a GST pull-down assay.
3) Examine the interaction between GST-p400 derivatives and ATM in an in vitro system through GST pull-down.
4) Clone and express six FLAG-tagged p400 derivatives in mammalian U2OS cells.
5) Functionally analyze the interaction of p400 and ATM by examining ATM's activity via autophosphorylation of ATM and ATM's phosphorylation of the histone variant H2AX.
6) Examine functional implications of the interaction between p400 and ATM through a growth assay and bleomycin sensitivity assay.

2 Materials and Methods

2.1 Materials

Supplier and Materials
Abcam, England
P-ATM serine 1981 antibody (ab36810)
Applied Biological Materials Inc., Canada
qPRC lentivirus titration kit
Axygen, USA
1.5 mL microfuge tubes, 0.6 mL microfuge tubes, PCR tubes, pipette tips
Bioline, England
Agarose
BioRad, USA
40% acrylamide-bis (29:1), BCA protein assay dye reagent concentrate, Poly-prep® Chromatography column (Catalog 732-1550)
Calbiochem, Germany
ATM polyclonal antibody (819844)
Eastman Kodak, USA
Biomax general blue film, Biomax MS intensifying screen cassette 8”x10”
Greiner Bio-One, Germany
96 well tissue culture plate, 6 well tissue culture plate, 60 mm tissue culture plate, 100mm tissue culture plate, 15 mL centrifuge tubes, 50 mL centrifuge tubes, 5 mL pipette, 10 mL pipette, 25 mL pipette
Leica Microsystems, Germany
TRITC (tetramethylrhodamine-5-(and 6)-isothiocyanate)
Merck, Germany
40% acrylamide-bis solution, absolute ethanol, boric acid, chloroform, methanol
Millipore, USA
H2AX polyclonal antibody (07-627), H2AX-P polyclonal antibody (07-164)
New England Biolabs, USA
*BamH*I, *CIP*, *Cla*I, *Eco*RI, *Eco*RV, *Hind*III, *Not*I, T4 DNA polymerase, T4 ligase
Oxoid, UK
Agar Bacteriological
Promega Corporation, USA
FuGENE® 6, FuGENE® HD
Roche, NZ
cOmplete™ Mini EDTA-free protease inhibitor cocktail tablets
Santa Cruz Biotechnology, USA
Goat anti-rabbit HRP conjugate antibody (SC2054), goat anti-mouse HRP conjugated antibody (SC2055)

Sigma Chemical Company, USA
1Kb+ DNA marker, ANTI-FLAG® M2 affinity agarose gel, ampicillin trihydrate (amp), β-mercaptoethanol (BME), Bromophenol Blue sodium salt, Coomassie brilliant blue R concentrate, deoxyribonuclease (DNase) I (D4263), ethidium bromide, formaldehyde solution, glutathione-agarose (Sep4B – s-nitrosoglutathione in alginate) (G510-10ML), glycerol, glycine, Igapal CA-630 (NP40), imidazide, isopropyl β-D-1-thiogalactopyranoside (IPTG), LB broth, oligonucleotides, paraformaldehyde (PFA), phenol, phenylmethanesulfonylfluoride solution (PMSF), potassium acetate, potassium chloride, potassium phosphate monobasic, puromycin dihydrochloride, sodium acetate anhydrous, sodium carbonate, sodium chloride, sodium deoxycholate, sodium dodecyl sulphate, sodium hydroxide, sodium phosphate monobasic, sodium phosphate dibasic, tertamethylethylene diamie (TEMED), triton X-100, tween-20 Antibodies: β-actin (A5316), FLAG M2 monoclonal (F3165), HA (SAB4300603)
Thermo Fisher Scientific, USA
0.5% trypsin-EDTA (10x), Charge SwitchPro PCR clean up kit, CyQUANT® Cell proliferation assay kit, Dulbecco's modified Eagle medium (DMEM) + GlutaMAX, foetal bovine serum, Halt™ protease inhibitor cocktail, OPTI-MEM, penicillin/streptomycin/amphotericin B mix, Phusion polymerase and HF buffer, Pierce™ ECL western blotting substrate, Prolong Gold with DAPI, Purelink Quick gel extraction kit, PureLink Quick plasmid midiprep Kit, SuperSignal™ West Femto maximum sensitivity substrate

2.2 DNA Methods

2.2.1 Restriction Enzyme Digestion

On average, 1 μL of enzyme (5000U/μl) was used to digest 2 μg of DNA in buffer conditions specified by the manufacturer. Digestions were allowed to proceed for two hours at 37°C to ensure complete digestion. Where applicable, the restriction enzymes were heat deactivated according to manufacturer's instructions. The products of these digestions were analyzed by gel electrophoresis (section 2.2.5). When appropriate, DNA fragments were purified by gel purification (section 2.2.6).

2.2.2 DNA Fill in of Cohesive Ends

T4 DNA polymerase was to make blunt ends after a restriction enzyme digestion that makes cohesive ends. To fill in the 5' overhangs after the first restriction digest, 20 μL

of digestion product (section 2.2.1) was incubated with 10 μL dNTP, 3 μL NEB2 buffer, 5 μL 10x BSA, 12 μL double distilled water (ddH_2O), and 1 μL of T4 DNA polymerase (1 U/μL) at 18°C for 15 min.

2.2.3 PCR Purification

Plasmid DNA from section 2.2.2 was purified using High Pure PCR product purification kit according to the manufacturer's instructions. In this method, DNA is bound to glass fleece by means of a chaotropic salt while contaminants such as proteins, salts, and nucleotides are washed away prior to DNA elution. DNA is eluted using a low salt buffer.

2.2.4 Calf Intestinal Phosphatase Digestion

Calf intestinal phosphatase (CIP) treatment was used to remove 5' phosphate groups on digested plasmid DNA in order to reduce religation of empty vector DNA. One μL of CIP was added to plasmid digestion reactions and allowed to incubate for 2 hours at 37°C to ensure maximal removal of phosphate groups. No additional buffer is needed when using the NEB system, as CIP is active in all NEB buffers. CIP treatment was accomplished before purification of plasmid DNA by gel electrophoresis (section 2.2.5).

2.2.5 Agarose Gel Electrophoresis

Agarose gel electrophoresis was typically carried out on 1% agarose (w/v) in 0.5x TBE (44.5 mM Tris-HCl, 44.5 mM boric acid, and 10 mM EDTA) in order to separate DNA molecules. Ten percent (v/v) DNA loading dye (30% glycerol, 0.25% bromophenol blue) was added to DNA samples before being loaded into wells. In general, electrophoresis was executed at 150 V for 1 hour. Visualization of DNA was accomplished by staining the gel with 0.5 μg/mL ethidium bromide in 0.5x TBE for 15 minutes. The gel was destained in 0.5x TBE for 5 minutes before being visualized under UV light on a gel documentation system. A 1+kb DNA standard marker was run on the gel during separation of the DNA bands and was used to estimate DNA sizes.

2.2.6 DNA Purification from Agarose Gel

Once DNA fragments are separated through gel electrophoresis (section 2.2.5), DNA bands were identified under long wavelength UV light and extracted from the gel with minimal excess of agarose. DNA was purified using E.Z.N.A® gel extraction kit from Omega, which binds DNA to the HiBind® matrix while allowing for other contaminants to be washed away. DNA is released from the matrix by either deionized water or a low salt buffer.

2.2.7 DNA Ligation

Digested and purified DNA was used in ligation reactions where typically 50-100 ng DNA was employed in a molar ratio of 3:1 insert to vector DNA. According to the manufacturer's instructions, reactions were made up to 10 μL with buffer and 1 μL ligase (1 U/μL). Ligations were incubated at 16°C overnight before being used for transformation of *E. coli* (section 2.2.9).

2.2.8 Preparation of Competent *Escherichia coli (E. coli)* cells

In this study the *E. coli* strain DH5α was used for all transformations. Competent cell preparations were made by streaking *E. coli* onto LB plates (20 g/L LB, 1.5% (w/v) bacto-agar) and incubating them overnight at 37°C. A single colony inoculation in 5 mL LB (20 g/L LB) was grown at 37°C overnight on a shaker. A 100 mL broth was inoculated with 1 mL of overnight culture and incubated on a shaker at 37°C for two and a half hours then split into two 50 mL tubes and centrifuged at 1500 g for 10 min at 4°C. After removal of the supernatant, the pellets were resuspended in 5 mL of ice cold 0.1 M $CaCl_2$ then pooled and centrifuged again at 1500 g for 10 min at 4°C. The supernatant was removed once again and the pellet was resuspended in 3.2 mL of 0.1 M $CaCl_2$ then incubated on ice overnight. After incubation, 0.8 mL of 50% glycerol (10% final concentration (v/v)) was added to the cell suspension and mixed gently. Cells were dispensed as 100 μL aliquots into microfuge tubes that were pre-chilled at -20°C for 1 hour. The aliquots were then placed at -80°C for storage.

2.2.9 Transformation of DH5α *E. coli*

After thawing *E. coli* aliquots on ice, 0.5 μL of purified plasmid or 4 μL of ligation product were added to the cells, mixed gently and incubated on ice for 30 min. The cells were heat shocked for 90 sec at 42°C then placed back on ice for 30 sec. Typically, 800 μL of LB was added to the cell mixture and mixed gently before being incubated at 37°C for two hours with shaking. The cells were then spun down at 3000 g for 10 min and approximately 700 μL of supernatant was removed. The cell pellet was resuspended in the remaining 200 μL of supernatant. Approximately 150 μL of the reaction was spread onto an LB plate containing ampicillin. The cell suspension was allowed to fully absorb into the LB plate at room temperature before being inverted and incubated at 37°C overnight.

2.2.10 Plasmid Purification from *E. coli*

Depending on the application of the DNA, several purification methods were employed to purify plasmid DNA from *E. coli*.

2.2.10.1 Rapid Boil

This method was derived from the rapid boiling method described in the journal article "A rapid Boiling Method for the Preparation of Bacterial Plasmids with several modifications [162]. After a sample of the overnight culture has been centrifuged, the pellet is resuspended in 350 μL of STET buffer (10 mM Tris-HCl, pH8.0, 1 mM EDTA, 0.1 M NaCl, 5% Triton x-100) supplemented with 25 μL freshly prepared lysozyme solution (10 mg/mL) and no addition of 8% sucrose. Another modification to this method was the separation of the gelatinous pellet and the supernatant. A sterile toothpick was utilized to remove the gelatinous cell debris rather than the supernatant being drawn off with a pipet. Lastly, the precipitation of the DNA was accomplished through a phenol/chloroform step. After the pellet was discarded, an addition of 200 μL phenol: chloroform: isoamyl alcohol (30:29:1) was added to the supernatant. Samples were vortexed on high for approximately 1 min then spun down at 16000 g for 5 min. The aqueous phase, located above the organic phase, was transferred to a new microfuge tube and subsequently mixed well with 200 μL of room temperature isopropanol. The solution was allowed to stand at -20°C for 20-30 min then centrifuged

at 12000 g for 5 min. The supernatant was removed and the pellet was washed with 500 µL ice-cold 98% EtOH before being centrifuged at 12000 g for 1 min. The EtOH was removed as much as possible before being centrifuged again at 12000 g for 1 min. Any remaining ethanol was removed and the pellet was allowed to air-dry upside down at room temperature until all traces of ethanol had disappeared. The pellet was then resuspended in 50 µL sterile TE (10 mM Tris-HCl, pH 8.0, 1 mM EDTA, pH 8.0) supplemented with RNase (0.1 mg/mL) and stored at -20°C or used for restriction endonuclease digestion section 2.2.1) for confirmation of plasmid identity.

2.2.10.2 Small-Scale High Quality Plasmid Isolation

The High Pure plasmid isolation kit from Roche was used for small-scale plasmid isolations. This was performed according to the manufacturer's specifications using 1.5 mL of *E. coli* culture. Cells are lysed using an alkaline lysis, which releases the DNA into the supernatant. A chaotropic salt containing buffer allows for plasmid DNA to bind to glass fibers within the filter while genomic DNA, cell debris and other contaminants are washed through using centrifugation. The plasmid DNA is released from the glass by using a low salt buffer. Plasmid DNA can then be quantified (section 2.2.12) and utilized for further applications.

2.2.10.3 Large-Scale High Quality Plasmid Isolation

The QIAGEN plasmid midiprep kit was used for large-scale plasmid isolations. Plasmid isolation was performed according to the manufacturer's specifications using 100 mL of *E. coli* culture. Cells are lysed using an alkaline lysis, which releases the DNA into the supernatant. Anion-exchange properties of the column and centrifugation allow for the separation of plasmid DNA from genomic DNA and cell debris. Plasmid DNA binds to the column in low-salt conditions, while genomic DNA, cell debris and other contaminants are removed using a medium-salt rinse. A high-salt buffer is used to elute plasmid DNA from the column followed by precipitation of the DNA by isopropanol. The resulting DNA pellet was washed with 70% EtOH then resuspended in TE buffer (10 mM Tris-HCl, pH 8.0, 1 mM EDTA, pH 8.0). Plasmid DNA can then be quantified (section 2.2.12) and utilized for further applications.

2.2.11 DNA Sequencing

DNA was submitted to the Massey Genome Service for Sanger sequencing. DNA was supplied at 500 ng per 15 μL reaction buffer with 4 pmol of primer.

2.2.12 DNA Quantification

The quantity of DNA in the sample was assessed by spectrophotometry at an absorbance of 260 nm using a Nanodrop® ND-100.

2.2.13 RT-qPCR Lentivirus titration

An RT-qPCR lentivirus titration kit (ABM) was used to titrate concentrated lentivirus samples from section 2.4.6 in order to confirm lentivirus production and estimate virus titer. The kit allows for a one step titration assay for lentiviral vectors by employing a fast RNA extraction step coupled with a qRT-PCR. Titrations were carried out as per the manufacturer's protocol. As the kit does not come with qPCR mastermix or reagent mix (RT/Taq + primers), SYBR Green I Mastermix and reagent mix from Thermo Fisher Scientific were used. The qRT-PCR was performed in a Light Cycler® 480 by Roche and were carried out using the following protocol.

Table 2.1 RT-qPCR lentivirus titration protocol

Step	Temp	Duration	Cycles
Reverse Transcription	42°C	20 min	1
Enzyme Activation	95°C	10 min	1
Denaturation	95°C	15 sec	40
Annealing and Extension	60°C	1 min	40

2.3 Protein Methods

2.3.1 IPTG induced Protein Expression

The *E. coli* strain BL21 was used for ITPG induced expression of GST-fusion proteins. *E. coli* were transformed as in section 2.2.9. A single colony was picked and used to inoculate 5 mL LB broth containing ampicillin. The seed culture was grown overnight at 37°C with shaking. After incubation, DNA was extracted from 1 mL of the culture

(section 2.2.10) in order to confirm the presence of the appropriate plasmid. Once confirmed, a 1% inoculation (1 mL into 100 mL LB), ampicillin (100μg/mL) was performed and allowed to grow for 2.5 hours at 30°C with agitation to reach an optical density (OD) of 0.6. Samples were put on ice and allowed to cool during the addition of ITPG (0.6 mM) and tetracycline (5μg/mL) then incubated for 1-2 hours at 25°C with shaking. Cell suspension was then placed on ice before being processed (section 2.3.2).

2.3.2 BCA Assay

Total protein concentration was determined using Bio-Rad bicinchoninic acid (BCA) Protein Assay Dye Reagent Concentrate. A standard of BSA protein as well as 1 μL of each protein sample were added into wells of a 96-well plate containing 20 μL BCA reagent and 180 μL ddH_2O. The solutions were mixed thoroughly, incubated at room temperature for 15 minutes, and analyzed using the BMG LABTECH FLUOstar® Omega microplate reader at 562 nm. A standard curve generated from the BSA standard was used to determine sample concentrations.

2.3.3 GST-fusion Protein Purification

Cells from the 100 mL cell suspension from section 2.3.1 were harvested into one 50 mL tube through two rounds of centrifugation. The first 50 mL of the culture was poured into the 50 mL tube and centrifuged at 7000 g for 5 min. The supernatant was removed then the second half of the 100 mL culture was added to the pellet-containing 50 mL tube and centrifuged again as specified above. The supernatant was removed and the pellet resuspended in 10 mL lysis buffer (PBS (137 mM NaCl, 2.7 mM KCl, 4.3 mM $Na_2H_2PO_4$, 1.47 mM KH_2PO_4,), 10 mM BME, 0.2 mg/mL lysozyme, 1 mM PMSF, 0.1 mg/mL DNase, 0.1% NP40). The solution was sonicated at 20% for 15 seconds 6 times and placed on ice in between each sonication. Solution was centrifuged at 35,000 g for 30 min and the supernatant collected into 15 mL tubes. From the total volume of lysate, 30 μL was reserved and kept at -20°C for future analysis. A volume of 250 μL glutathione-sepharose pre-equilibrated with BC150 (0.2 mM EDTA, 20 mM Tris pH 7.5, 0.15 M KCl, 20% glycerol) + 0.1% NP-40 and 0.2 mg BSA was added to the remaining lysate and incubated at 4°C overnight with rocking. The solution was poured into Poly-prep® Chromatograhpy columns and allowed to flow through. Approximately

500 μL of flow through was reserved as an input and stored at -20°C for future analysis. The columns were washed twice with 10 mL wash buffer (PBS (137 mM NaCl, 2.7 mM KCl, 4.3 mM $Na_2H_2PO_4$, 1.47 mM KH_2PO_4,), 10 mM BME, 1 mM PMSF, 0.1% NP40). GST-fusion proteins were eluted from the glutathione-Sep4B in three extraction steps using elution buffer (10 mM reduced glutathione in 50 mM Tris, pH 8.5). For each extraction 0.5 mL elution buffer was added to the column and allowed to rest for 1 hour before collection. Samples were placed in dialysis tubing from SpectrumLabs prepared according to manufacturer's specifications and underwent dialysis for extraction of glutathione from GST-fusion proteins. Nitrocellulose tubing containing the sample was submerged in 1 L dialysis buffer (20 mM Tris pH 7.5, 0.15 M KCl, 0.2 mM EDTA, 20% glycerol, 0.1% NP40) and incubated at 4°C for 6 hours. The dialysis buffer was discarded and replenished with 1 L fresh dialysis buffer and allowed to incubate at 4°C for another 6 hours. This was repeated once more before the samples in the tubing were extracted and retained for future processing. Samples were stored at -20°C when not being immediately analyzed.

2.3.4 ATM Cell Lysate Preparation from Sf9 Cells

The frozen pellet from section 2.4.2 was resuspended in 6 mL lysis buffer F (20 mM Tris-HCl, pH 7.9, 500 mM KCl, 4 mM $MgCl_2$, 20% (v/v) glycerol, 0.4 mM EDTA, 2 mM DDT, 0.5 mM PMSF, 1x protease inhibitor mix). A solution of 10% NP-40 was added for a final concentration of 0.05% and mixed well. Cells were disrupted with a dounce homogenizer with 10 strokes every 10 min for 30 min and ultracentrifuged at 30K g for 30 min at 4°C. Supernatant was transferred to 50 mL centrifuge tubes and 14 mL of dilution buffer (BC 0, 0.05% NP40, 2 mM DTT, 0.5 mM PMSF, 1x protease inhibitor mix) was added so a final condition of BC150 + 0.05% NP40. The solution was dispensed in 5 mL aliquots in 15 mL centrifuge tubes and stored at -80°C for future processing. The residual solution was used in SDS-PAGE (section 2.3.5) to confirm the presence of ATM and appropriate volume for use in GST-pull-down (section 2.3.4)

2.3.5 GST-Pull-Down Assay

A 50% slurry of glutathione sepharose 4B in equilibration buffer (BC150, 0.05% NP40, 0.2 mg/mL BSA) was prepared by centrifuging a vial of 50% slurry of glutathione sepharose 4B suspended in 20% ethanol, removing the supernatant, and suspending the

beads in 50% equilibration buffer (BC150, 0.05% NP40, 0.2 mg/mL BSA) in a 1:1 (v/v) ration of beads to buffer. The first step of the GST-pull-down assay involved a reaction of 50 μL 10x protease inhibitor, 30-300 μL purified GST-fusion protein sample depending on quantity of fusion protein present (determined by western blot analysis), 40 μL BSA (10 mg/mL), 20 μL 50% glutathione-sepharose 4B slurry and equilibration buffer up to a total reaction volume of 410 μL, which was mixed for 1 hour at 4°C with rocking. A volume of 1 mL FLAG-ATM (section 2.3.3) was added to the reaction mix and incubated overnight at 4°C with rocking. The solution was centrifuged at 3000 g for 5 min at 4°C, the supernatant was discarded, 0.5 mL equilibration buffer without BSA was added and subsequently mixed by vortex on low for 1 min. This was repeated four additional times. The solution was centrifuged, supernatant removed, and centrifuged again in order to pipette out any residual liquid. The sample was resuspended in 20 μL of 2x SDS-PAGE sample buffer and gently vortexed. The samples were then resolved using SDS-PAGE (section 2.3.5)

2.3.6 Sodium Dodecylsulphate Polyacrylamide Gel Electrophoresis (SDS-PAGE)

The Mini-PROTEAN Tetra System by Bio-Rad was used to conduct all gel electrophoresis. A range of 4-12% polyacrylamide gels were prepared using 2.5 mL resolving gel buffer (1.5 M Tris, pH 8.8, 0.4% SDS) added to 1-3 mL 40% acrylamide-bis (29:1) with water to a final volume of 10 mL. The gel was poured immediately after the addition of 100 μL of 10% ammonium persulphate (APS) and 20 μL TEMED, covered with 70% EtOH and allowed to set for 15 min. The ethanol was removed prior to the addition of a stacking gel comprising of 1 mL Tris/SDS (0.5 M Tris, pH6.8, 0.4% SDS), 0.4 mL 40% acrylamide, 2.6 mL water, 40 μL 10% APS and 8 μL TEMED on top of the resolving gel. A comb was inserted and the stacking gel was allowed to set for 30 min before use. Gradient polyacrylamide gels (4-12%) were created using the Hoefer SG30 gradient maker with a stacking gel overlaid as described above. Two-step gradient gels were also used. This was accomplished in a two-step process by pouring a higher percentage polyacrylamide gel (10%) halfway up the glass plate and allowing it to solidify before the addition of a second layer of a lower percentage polyacrylamide gel (5%) to just below the top of the plate. The second layer is allowed to set before pouring the stacking gel, as described above. A 6X SDS sample buffer (60 mM Tris, 10% glycerol, 2% SDS, 0.01% bromophenol blue, 1.25% β-mercaptoethanol (BME))

was added to protein samples and then heated at 95°C for 5 min. Samples were then loaded into the gel and run in SDS electrophoresis buffer (25 mM Tris, 192 mM glycine, 0.1% SDS) at a constant amperage of 30 mA between 1 h and 1 h 15 min.

2.3.7 Western Blotting

After the protein samples were resolved by SDS-Page (section 2.3.1), the gel was allowed to equilibrate in chilled transfer buffer (25 mM Tris, 192 mM glycine, 20% methanol) for 10 min. A PVDF membrane was charged by submerging it in methanol for 10 s, washing with ddH_2O for 10 s, and finally immersing it in chilled transfer buffer for a minimum of 5 min. Transfer of the protein from the polyacrylamide gel to the membrane was conducted in the Mini-PROTEAN Tetra System by sandwiching the gel and the membrane between blotting paper and submerging the sandwich in chilled transfer buffer at a constant amperage of 150 mA for 2 h. The membrane was then removed from the blotting equipment and submerged in blocking buffer (10 mM Tris-HCl, pH7.6, 150 mM NaCl, 0.2% Tween-20, 5% skim milk, 0.2% sodium azide) and placed on an orbital shaker at room temperature for 30 min. The membrane was then washed with TBS/T (10 mM Tris-HCl, pH 7.6, 150 mM NaCl, 0.2% Tween-20) three times then submerged in a solution of primary antibody diluted in antibody dilution buffer (10 mM Tris-HCl, pH 7.6, 150 mM NaCl, 0.2% Tween-20, 1% skim milk, 0.05% sodium azide) and incubated on an orbital shaker at 4°C overnight. After removal of the primary antibody, the membrane was subjected to three 10 min washes in TBS/T then incubated in a solution of secondary antibody diluted in antibody dilution buffer at room temperature for 30 min with shaking. The secondary antibody was removed and the membrane was subjected to three 15 min washes in TBS/T. The proteins were detected using a chemiluminescent reagent and X-ray film.
Appendix Figure A1.1 contains a list of antibody concentrations.

2.3.8 Coomassie Blue Staining

Once proteins were resolved using SDS-PAGE (section 2.3.3) the gel was submerged in BioRad's Brilliant Blue Coomassie Stain at room temperature for 15 min with shaking. Stain was removed and replaced by destain solution (20% methanol, 10% acetic acid). Gel is destained until bands become visible.

2.3.9 Immunoprecipitation

Cells were lysed according to section 2.4.6 for each immunoprecipitation reaction. From the lysate, 20 μL was retained as an input sample while the remaining 480 μL was combined with 20 μL of 50% M2 antibody agarose bead conjugates. The solution was incubated overnight at 4°C on an orbital rotator. The beads were pelleted by centrifugation at 3000 g for 5 min at 4°C. The supernatant was removed and the beads were resuspended and washed with 1 mL F buffer (20 mM HEPES pH 7.4, 120 mM NaCl, 1.5 $MgCl_2$, 1 mM EGTA, 50 mM NaF, 0.2% Tween-20, 0.5 mM DTT, 1 mM PMSF). The solution was centrifuged again at the above specifications and the supernatant removed. This wash step was repeated five times with an extra final spin to ensure complete removal of the supernatant. The beads were resuspended in 20 μL 2x SDS-PAGE sample buffer for examination by western blotting (section 2.3.4).

2.4 Cell Culture

ESCO Class II Biohazard safety cabinets were utilized for all human cell culture work. Both human cell lines were maintained using growth medium consisting of Dulbecco's Modified Eagle Medium (DMEM), 10% v/v Fetal Bovine Serum (FBS) and 0.05% v/v penicillin/streptomycin (pen/strep) unless otherwise specified and incubated in standard conditions of 5% CO_2 at 37°C in the presence of atmospheric humidity.

2.4.1 Subculturing SF9 Cell Cultures

Sf9 cells were propagated in supplemented Grace's insect media with 10% FBS, 0.1% pluronic acid, 10 μg/mL gentamycin and penicillin (5 U/mL), streptomycin (0.5 mg/mL), amphotericin B (0.125 μg/mL). Cells were grown in suspension in a spinner flask at 25°C in normal atmospheric conditions on a magnetic stirrer until a density of $1x10^6$ cells/mL was reached. To reduce the cell density to approximately $2.5x10^5$ cells/mL, a volume of cell suspension was removed and discarded and replaced by fresh media.

2.4.2 SF9 Infection with Baculovirus

Sf9 cells propagated as in section 2.4.1 were grown to a density of 1 $x10^6$ cells/mL then 10 mL of that cell suspension was plated onto a 100 mm plate and allowed to adhere at

room temperature for 15 min. An optimized volume of virus (typically 1 mL of the P3 generation) was added drop-wise to the plate then incubated at 25°C for 48 h. Cells were centrifuged at 3000 g for 10 min at 4°C, the supernatant was removed and the pellet was frozen at -80°C before being processed.

2.4.3 Subculturing Mammalian Cell Cultures

Mammalian cells were maintained in Dulbecco's modified Eagle medium (DMEM) supplemented with 5% fetal bovine serum (FBS), penicillin (5U/mL), and streptomycin (0.5 mg/mL) in standard conditions of 5% CO_2 at 37°C in humidified atmosphere. Cells were grown to approximately 90% confluence before subculturing. The cells were passaged by first aspirating the medium from the plate then washing the cells for 2 min with PBS (137 mM NaCl, 2.7 mM KCl, 4.3 mM $Na_2H_2PO_4$, 1.47 mM KH_2PO_4,). The PBS was then aspirated and cells immersed in trypsin/EDTA (1 mL per 100 mm plate) for approximately 30 seconds. After the aspiration of the trypsin, the cells were dislodged from the plate by gentle tapping and resuspended in 10 mL fresh media. Cells were diluted in a ratio of 1 mL resuspended cells to 9 mL fresh media in a new plate. The new plate was returned to the humidified incubator.

Cells that were older than 20 subcultures were not used for transfections as cell lines in continuous culture are prone to genetic drift and finite cell lines are fated for senescence.

2.4.4 Mammalian Cell Transient Transfection

HEK293T cell line was used for all transfections. Cells were split onto 100 mm plates and transfected either 24 hours after passaging at 50-60% confluence. For transfection reaction mix, 200 μL pre-warmed OPTI-MEM was dispensed into sterile microfuge tubes followed by the addition of 12 μL Fugene6 from Promega. The solutions were mixed by gently tapping then 4 μg of DNA was added. The samples were mixed by gently tapping then briefly centrifuged at 1000 g to bring down all of the liquid. The reactions were allowed to incubate for 15-30 min before being added drop-wise onto the plates followed by gentle swirling to mix. Transfected cells were typically incubated for 48 hours in conditions of 5% CO_2 at 37% with a humidified atmosphere before any further processing.

2.4.5 Lentivirus Production

The HEK293T cell line was used for lentivirus production. Cells were split onto 100 mm plates and grown in standard conditions of 5% CO_2 at 37°C for 24 hours before transfection. Reaction mix was made in sterile microfuge tubes containing 500 μL pre-warmed OPTI-MEM. Each microfuge tube had 32 μL Fugene6 added and was mixed well by gentle tapping followed by the addition of 3 μg packaging plasmid mix and 5 μg lentivirus plasmid DNA with gentle tapping to mix. The microfuge tubes were spun down at 1000 g to consolidate the liquid then incubated at room temperature for 15-30 min. The solution was added to the cells drop-wise and swirled gently to mix. Cells were placed in an incubator with 5% CO_2 at 37°C in a humidified atmosphere for 17 hours. The medium was aspirated and replaced with 10 mL fresh growth medium (DMEM supplemented with 10% FBS, 1% penicillin/streptomycin, 1 mM caffeine) and returned to the incubator for a further 24 hours. The medium was collected and transferred to a sterile 50 mL centrifuge tube followed by the addition of 10 mL fresh medium to the cells and placed in the appropriate incubator. The 50 mL centrifuge tubes were stored at 4°C. After another 24 hours the medium from the cells was harvested and added to the 50 mL centrifuge tubes containing the media harvested from the previous day and stored at 4°C.

2.4.6 Lentivirus Concentration

The viral solution from section 2.4.5 was centrifuged at 3000 g for 5 min at 4°C and supernatant was transferred to a new sterile 50 mL centrifuge tube followed by the addition of 6 mL 50% PEG6000 (final concentration of 8.5%). After mixing the solution thoroughly, 3 mL of 4 M NaCl was added to a final concentration of 0.3 M NaCl. The tubes were stored at 4°C for either 1.5 hours with mixing every 30 min or overnight. The tubes were centrifuged at 7000 g for 10 min at 4°C and the supernatant decanted. The pellet was resuspended in 2 mL cold DMEM and tapped to mix well without the production of foam. The solution was incubated overnight at 4°C and mixed by gentle pipetting. The viral solution was dispensed into 200 μL aliquots into 4 screw cap tubes and stored at -80°C for future use. The residual liquid in the 50 mL centrifuge tube is used for viral titration (section 2.2.13).

2.4.7 Mammalian Cell Infection with Lentivirus

The human cell line U2OS were used in all lentiviral infections. The cells were subcloned onto 100 mm plates 24 hours before infection for a 50% confluent culture. Growth medium was prewarmed and 9.5 mL was dispensed into each sterile 15 mL centrifuge tube followed by the addition of 10 μL polybrene (8 mg/mL) and 0.5 mL virus solution and thorough mixing. The medium from the cells was aspirated and replaced by 10 mL virus-containing medium from the 15 mL centrifuge tubes. The cells were incubated in 5% CO_2 at 37°C for 24 hours before the medium was aspirated and replaced with 10 mL fresh medium containing 1.5 μg/mL puromycin. Cells were incubated for 48 hours followed by a replacement with fresh growth medium containing 1.5 μg/mL puromycin and another 48 hours of incubation. The remaining cells were maintained in 0.5 μg/mL for future processing.

2.4.8 Induction of DNA Damage by Bleomycin

Bleomycin (1 mg/mL in PBS) was added directly to the cell culture media for a range of final concentrations (typically 10 or 20 μg/mL). Incubation times varied depending on the assay and future processing.

2.4.9 ATM Activation Assay

For the purpose of the assay, the puromycin was terminated in order to reduce any stress symptoms the cells may display. Each of the stable cell lines produced in section 2.4.7 were passaged (section 2.4.3) onto four 100 mm tissue culture plates 24 hours before assay to allow adherence to the plate surface. A confluence of approximately 60-70% should be achieved. Bleomycin was added drop-wise to the cells to achieve a final concentration of 20 μg/mL and swirled gently to mix. Cells were exposed to bleomycin for 1 h before the removal of bleomycin and addition of fresh growth medium. Cells were allowed to recover for 0, 1, 3, or 7 h. The medium was aspirated and cells were rinsed with 10 mL PBS before being harvested and processed (section 2.4.10 and 2.4.11). Modifications to the processing (section 2.4.10) include a reduction of centrifuge speed to 1200 g instead of 3000 g, a decrease of lysis buffer from 500 μL to 100 μL, and a removal of the vortexing step. The primary antibodies used are listed below.

Table 2.2 Antibodies used during western blotting

Antibody	Catalogue Number	Stock Concentration	Immunoblot Concentration	Rabbit or Mouse	Insoluble or soluble Fraction
α-ATM	819844	0.1mg/mL	1 μg/mL	Rabbit	Soluble
α-ATM-P	ab36810	1 mg/mL	1 μg/mL	Mouse	Soluble
α-βactin	A5316	1 mg/mL	1 μg/mL	Mouse	Soluble
α-H2A.X	07-627	1 mg/mL	3 μg/mL	Rabbit	Insoluble
α-γH2A.X	07-164	1 mg/mL	3 μg/m	Rabbit	Insoluble

2.4.10 Cell Lysis

Plates containing cells at 80-90% confluence were removed from the incubator and placed on ice. The growth medium was aspirated from the samples followed by the addition of 1 mL PBS to the plate. Cells were liberated from the plate surface by scraping with a cell scraper and the cell suspension transferred to a microfuge tube. The sample was centrifuged at 3000 g for 5 min at 4°C and the supernatant removed. The cell pellet was resuspended in 500 μL of lysis buffer (25 mM Tris, pH7.05, 50 mM NaCl, 30 mM Na pyrophosphate, 50 mM Na Fluoride, 10% glycerol, 0.5% Triton X-100, 1 mM PMSF, 1% w/v protease inhibitor cocktail) and incubated on ice for 10 min before vortexing at high speed for 1 min. The sample was centrifuged at 16000 g for 10 min at 4°C and the supernatant transferred to a new microfuge tube while the pellet was retained for histone extraction (section 2.4.10). Thirty μL of the cell lysate was kept as an input sample and the remaining lysate was used for immunoprecipitation (section 2.3.8).

2.4.11 Histone Extraction

The pellet from section 2.4.9 was resuspended in 1 mL ddH_2O and centrifuged at 16000 g for 10 min. After the removal of the supernatant, the pellet was centrifuged again at 16000 g for 1 min and any residual supernatant was removed to ensure no liquid was left on the pellet. The pellet was resuspended in 60 μL 0.2 N HCl and mixed by vortexing on low overnight at 4°C. The sample was centrifuged at 16000 g for 10 min at

4°C. The supernatant was transferred to a new microfuge tube then neutralized with 20 μL of 2 M Tris/SDS (pH8.6) for analysis through SDS-PAGE (section 2.3.5).

2.4.12 Bleomycin Sensitivity Assay

Similarly to section 2.4.9, the use of puromycin was terminated in order to reduce any stress symptoms the cells may display. New stable U2OS cell lines were produced according to section 2.4.7 before for each attempt of the bleomycin sensitivity assay. Each of the stable cell lines was passaged (section 2.4.3) onto two 100 mm tissue culture plates 24 hours before assay to allow adherence to the plate surface. A confluence of approximately 60% should be achieved before addition of bleomycin (10 μg/mL). The plates were gently swirled to distribute bleomycin evenly and then returned to standard conditions of 5% CO_2 at 37°C for 12 h. The medium was removed and cells rinsed with PBS. The PBS was aspirated and 10 mL prewarmed, fresh, bleomycin-free growth medium was carefully pipetted onto the plates. The cells were dislodged from the plate, on plate at a time, through trypsinization (detailed within section 2.4.3) and resuspended in 5 mL fresh, prewarmed growth medium. Cells were counted using a hemocytometer and a cell suspension was made with a cell density of 10,000 cells/mL. Each cell suspension was dispensed in triplicate in a volume of 200 μL per well for each of the seven 96-well plates. One plate per day was emptied of its medium, rinsed with PBS (137 mM NaCl, 2.7 mM KCl, 4.3 mM $Na_2H_2PO_4$, 1.47 mM KH_2PO_4,), tapped to dry and stored at -80°C until all plates had been harvested. The final plate was frozen at -80°C for a minimum of 30 min before being processed in a BMG LABTECH POLARstar® Omega microplate reader. The plates were processed with the CyQUANT® Cell Proliferation Assay Kit as per the manufacturer's instructions. Fluorescence was measured at 480 nm excitation and 520 nm emission maxima.

2.4.13 Mammalian Cell Freezing

To optimize successful reanimation, cells that were in exponential growth were used for freezing. The basic growth medium (DMEM, 10% FBS, 5 U/mL penicillin, 0.5 mg/mL streptomycin) of one 100 mm plate containing cells at approximately 80-90% confluence was aspirated. The cells were then washed in PBS (137 mM NaCl, 2.7 mM

KCl, 4.3 mM $Na_2H_2PO_4$, 1.47 mM KH_2PO_4,) for 2 min before the PBS was aspirated. Cells were immersed in 1 mL of 0.05% Trypsin/EDTA for 30 sec before the Trypsin/EDTA was aspirated. Gentle tapping was employed to dislodge the cells from the plate then resuspension was carried out through the addition of 5 mL of fresh basic growth medium. The cell suspension was pelleted by centrifugation at 1000 g for 5 min and the supernatant removed. Cells were resuspended in 1 mL freezing medium (10% dimethylsulfoxide (DMSO), 25% FBS, 65% DMEM) and dispensed into 2 cryovials each containing 500 μL cell suspension. Before being placed at -80°C, cryovials were inserted into a CoolCell® in order to freeze the cells slowly and prevent ice crystal formation. For long-term storage, the seed stocks were relocated to liquid nitrogen.

2.4.14 Mammalian Cell Reanimation

Cells were quickly thawed in a 37°C water bath to ensure minimal damage to the cells from thawing. Cells were then transferred to a 15 mL tube containing 5 mL pre-warmed fresh growth medium and mixed gently. The cell suspension was then centrifuged at 1000 g for 5 min and the supernatant was discarded. The cells were then resuspended in 10 mL pre-warmed fresh growth medium and plated onto a 100 mm plate and placed in the incubator.

2.4.15 Confocal Microscopy

2.4.15.1 Preparation of Coverslips

All confocal microscopy was preformed using category #1 22 x 22 mm coverslips. The coverslips were washed in a mild detergent and rinsed in warm water followed by a rinse in ddH_2O. Coverslips were submerged in 98% ethanol and allowed to air dry before being sterilized by UV light for 30 min.

2.4.15.2 Preparation of Immunofluorescent Samples

Coverslips were placed in a 6 well plate with one coverslip per well and seeded with the stable U2OS cell lines (section 2.4.7) 24 h prior to treatment in order to adhere cells. Each cell line was seeded onto two separate slides. Cells were at approximately 50% confluence when either treated with bleomycin or kept as a control. Bleomycin was added drop-wise to the cells to achieve a final concentration of 20 μg/mL and swirled

gently to mix. Cells were exposed to bleomycin for 1 hour before being processed. The medium from all wells was aspirated and cells rinsed with 2 mL PBS for three 5 min washes with no shaking. Cells were fixed to the slides by submerging them in 4% paraformaldehyde in PBS for 15 min at room temperature followed by two 10 min PBS washes with no shaking. Cells were permeabilized using 0.2% Triton X-100 in PBS for 5 min at room temperature with gentle swirling every couple of minutes. Another two washes with PBS for 10 min each were employed before the cells were immersed in blocking buffer (PBS, 5% BSA, 0.5% Tween-20) and incubated for 60 min at room temperature on an orbital rocker. Coverslips were inverted onto a droplet of 200 μL primary antibody diluted in blocking buffer on Parafilm M® and incubated overnight at 4°C in an air tight container. Slides were removed from the Parafilm M®, placed in a clean 6-well plate, and underwent three 5 min washes in PBS with 0.1% Triton X-100. From this point onward, coverslips were exposed to as minimal light as possible and kept in the dark when not in use in order to prevent photobleaching. Coverslips were inverted onto secondary antibody diluted in blocking buffer in the same manner as the primary antibody treatment and incubated for 1 h at room temperature. Coverslips were removed from the secondary antibody followed by three 5 min washes in PBS with 0.1% Triton X-100 and one wash in PBS alone. Coverslips were mounted onto slides using 15 μL ProLongGold® and fixed in place using nail polish.

Table 2.3 Antibodies used during confocal microscopy

Antibody	Catalogue Number	Immunostain Concentration	Primary or Secondary	Species in which grown
γH2A.X polyclonal	ab2893	0.33 μg/mL	Primary	Rabbit
TRITC	ab6718	1.33 μg/mL	Secondary	Goat anti-rabbit

A Lieca DM6000B confocal laser-scanning microscope (CLSM) was used to examine the samples. The two dyes used and their excitation and absorption wavelengths are given in table 2.4.

Table 2.4 Excitation of dyes used during confocal microscopy

Dye	Excitation (nm)	Absorption (nm)
DAPI	405	407-496
TRITC	547	572

3 Examination of the *in vitro* interaction between p400 derivatives and ATM

3.1 Introduction

DSB repair machinery must operate in an orchestrated effort in order to efficiently process and repair DNA damage. There are many protein-protein interactions that are able to stimulate or hinder the actions of the DSB repair mechanism. The premise for this project arose from a recent study that indicated a potential direct interaction between ATM and p400, two proteins of the DSB break repair pathway [77]. This idea arose from several key observations including similarities between PIKK members such as ATM and TRRAP as well as the existence of common binding partners such as Tip60. Previous work explored this potential interaction through *in vivo* co-immunoprecipitation assays in both human HEK293T cells and insect Sf9 cells with full-length ATM and six p400 fragment constructs. This study demonstrated that the three N-terminal fragments (F1, F2, and F3) were able to co-immunoprecipitate with ATM in both mammalian and insect cell lines. Although the study excluded several of the other Tip60/p400 complex proteins as mediators of the interaction, a direct interaction between the p400 N-terminal fragments and ATM was not established. In order to confirm a direct association, an *in vitro* investigation into the association was developed. This study aimed to clone six p400 fragments (F1, F2, F3, F4, F5, and F6) into pGTK expression vectors in order to isolate GST-p400 fragment fusion proteins to be used in a GST pull-down assay with ATM. All six p400 derivatives, with the exception of F1, span part or all of a p400 domain region, which may help to isolate which domain region of p400 may be interacting with ATM (Figure 3.1).

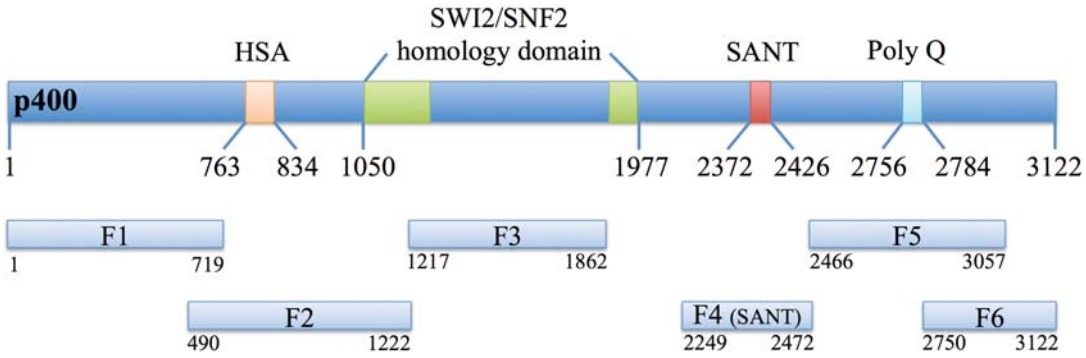

Figure 3.1 Schematic representation of full-length p400 and its derivatives. Full-length p400 consists of 3122 amino acids and several functional domains including HSA (amino acid 763-834), SWI2/SNF2 homology domain (amino acid 1050-1977), and the SANT domain (amino acid 2372-2426). p400 also contains a helicase superfamily C-terminal domain, DEXH box which contains the ATP-binding domain, and the Poly Q domain (amino acid 2756-2784). Fragment 1 (amino acid 1-719), Fragment 2 (amino acid 490-1222), Fragment 3 (amino acid 1217-1862), Fragment 4 (SANT domain) (amino acid 2249-2472), Fragment 5 (amino acid 2466-3057) and Fragment 6 (amino acid 2750-3122) were provided from previous study. All derivatives are FLAG-tagged in the CBF mammalian expression vector then inserted into the pGTK expression vector with GST located on the N-terminal.

3.2 Cloning and expression of GST-p400 fragment fusion protein

To investigate the ability of each p400 protein fragment to bind directly to ATM in vitro, six constructs were generated using the pGTK vector. Insertion of the p400 fragments into the pGTK vector enables a fusion protein product with a glutathione S-transferase (GST) tag located on the N-terminus. GST is a 211 amino acid protein (26 kDa) commonly used in expression vectors for production of recombinant fusion proteins. Expression results in a functional GST protein fused to the p400 fragment protein. GST promotes greater expression and solubility of recombinant proteins through its capacity to rapidly fold in to a stable, highly soluble protein upon translation [163]. GST also allows for the purification of the fusion protein with its ability to bind to its substrate glutathione (GSH) [164]. The six p400 fragments used in this study had previously been constructed through PCR with the addition of EcoRV restriction site at the 5’ end and a TAG stop codon followed by a HindIII enzyme digestion site at the 3’

end. The fragments were cloned into a CβF vector at the EcoRV and HindIII sites within the multiple cloning site (MCS).

The cloning strategy for insertion of the p400 fragments into a pGTK vector took advantage of these EcoRI and HindIII cut sites (Figure 3.1). In preparation for insertion into the pGTK vector, the p400 fragments were digested with EcoRV and HindIII (section 2.2.1) and gel purified according to section 2.2.6. The pGTK vector was first digested with EcoRI followed by a T4 DNA polymerase to fill in the cohesive ends of the EcoRI cut site in order to create blunt ends for future ligation reactions (section 2.2.2). The vector was then digested with HindIII and subjected to calf intestinal phosphatase (CIP) digestion to remove 5' phosphate groups on digested plasmid DNA in order to reduce religation of empty vector DNA (section 2.2.4). The digested pGTK vector DNA was gel purified before the ligation with the p400 fragments. Ligation reactions between the pGTK vector and p400 fragments were carried out according to section 2.2.7.

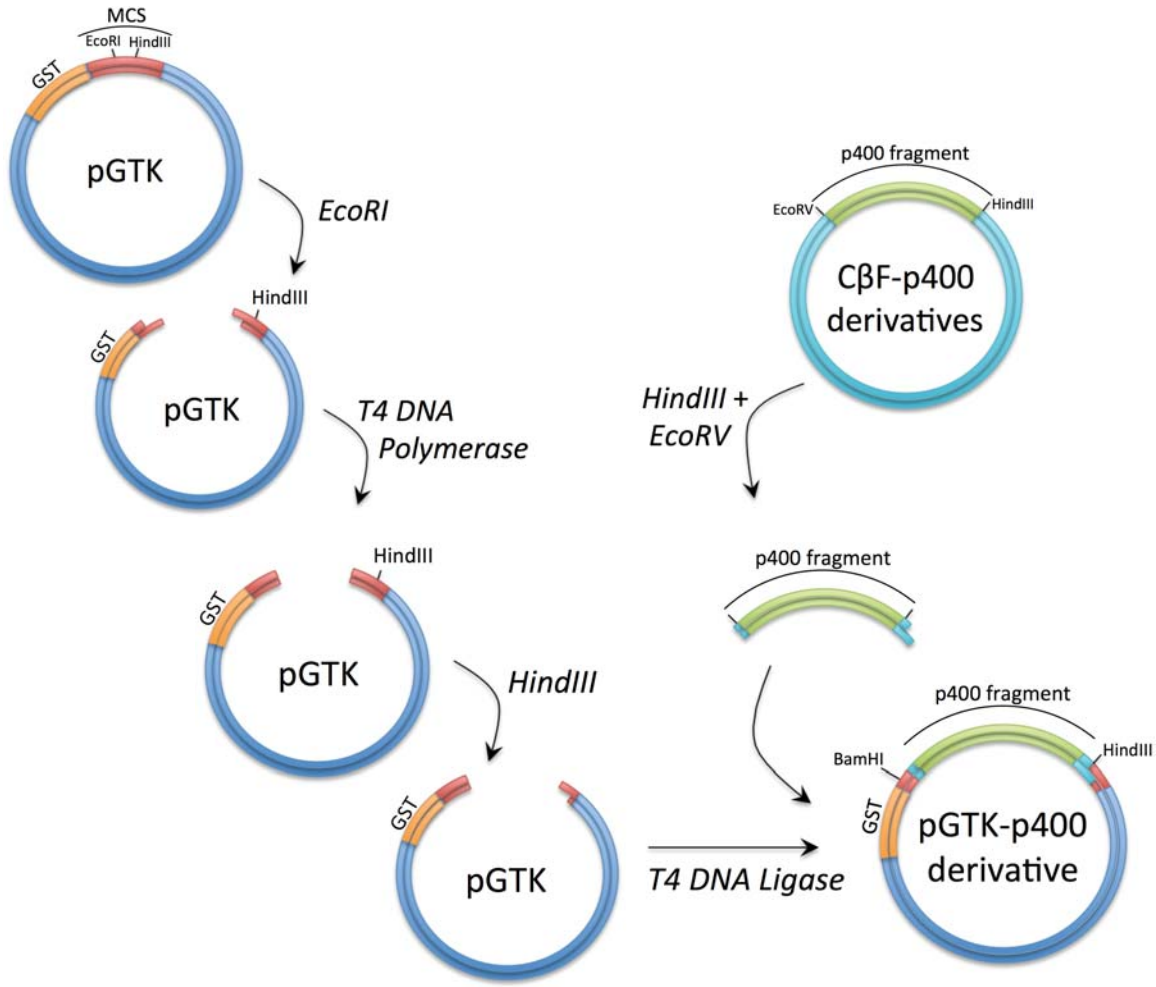

Figure 3.2 Cloning strategy for GST-p400 fragment fusion protein expression. Six p400 fragment inserts were digested from CβF vectors at the EcoRV and HindIII cut sites and inserted into pGTK vectors. pGTK vectors were prepared by digestion with EcoRI, T4 polymerase fill in of cohesive ends, a second digest with HindIII and subsequent CIP treatment. The p400 fragments were inserted in frame with the GST tag. The vector backbone is represented in blue while the open reading frames are indicated by the orange GST sequence and green p400 fragment sequence.

E. coli DH5α was transformed using the ligation reaction products according to section 2.2.9 and selected on LB agar plates containing ampicillin (amp). Candidate clones were screened via digestion with BamHI and HindIII to identify plasmids containing p400 fragments. BamHI cuts a few base pairs (bp) upstream from the EcoRV/EcoRI insertion region so fragments from a BamHI/HindIII digestion are of

comparable size to the purified fragments digested with EcoRV and HindIII from the CβF vector. Figure 3.2 shows the digestion of the pGTK vector as well as the pGTK-p400 fragment constructs. It is apparent from this gel that the fragments cut from CβF correlate with the fragments digested from the pGTK constructs isolated from D5Hα cells. The slight discrepancy between travel distances would be due to the salt content in the buffers used during gel purification versus restriction enzyme digestion [165].

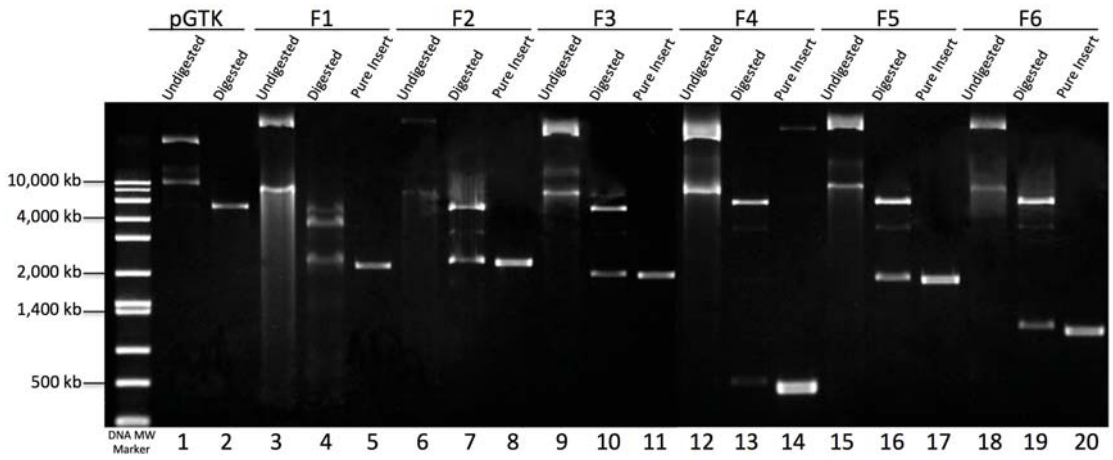

Figure 3.3 Cloning of pGTK-FLAG-p400 domain constructs. Restriction digests to cut and purify the FLAG-tagged-p400 fragment of interest from a CβF vector and insert into a pGTK vector with the GST preceding the N-terminus of the protein fragment. Plasmids were digested with BamHI and HindIII and resolved on a 1% (w/v) agarose gel in 1x TBE at 120 V for 1 h. Lane 1: pGTK control vector uncut, Lane 2: digested pGTK control vector, Lane 3: pGTK-p400-fragment 1 (pGTK-F1) uncut, Lane 4: digested pGTK-F1, Lane 5: F1 purified, Lane 6: pGTK-p400-fragment 2 (pGTK-F2) uncut, Lane 7: digested pGTK-F2, Lane 8: F2 purified, Lane 9: pGTK-p400-fragment 3 (pGTK-F3) uncut, Lane 10: digested pGTK-p400-F3, Lane 11: F3 purified, Lane 12: pGTK-p400-fragment 4 (pGTK-F4) uncut, Lane 13: digested pGTK-F4, Lane 14: F 4 purified, Lane 15: pGTK-p400-fragment 5 (pGTK-F5) uncut, Lane 16: digested pGTK-F5, Lane 17: F5 purified, Lane 18: pGTK-p400-fragment 6 (pGTK-F6) uncut, Lane 19: digested pGTK-F6, Lane 20: F6 purified.

The *E. coli* BL21 strain was used for expression of the GST-p400 derivative fusion proteins. BL21 cells are deficient in Lon and OmpT proteases, making them suitable for expression of non-toxic genes by reducing the potential for protein degradation due to native *E. coli* proteases. The constructs were transformed into *E. coli* BL21 and selected for according to section 2.2.9 and selected for on LB agar containing amp. Clones were screened for correct constructs by digestion with BamHI and HindIII. The results can be seen in Figure A1.1 of the appendix.

In order to express GST-p400 fragment recombinant proteins, individual colonies of transformed BL21 cells were grown as an overnight culture in LB broth and used the following day a 1% inoculation into 100mL of LB containing amp in accordance with section 2.3.1. Once an OD of 0.6 was achieved cells were cooled on ice and induced by the addition of isopropyl β-D-1-thiogalactopyranoside (IPTG), a molecular mimic of allolactose. ITPG was added at a concentration of 0.6 mM to the cooled cell cultures and cells were incubated at 25°C for 1 h. Tetracycline (5μg/mL) was added slow the production of proteins and allow time for proper folding and protein stability. The lower temperature was utilized in order to try and achieve full-length proteins with minimal fragmentation [166, 167]. Reducing temperature favors proper folding by slowing protein synthesis as well as limiting cellular protein concentration, two factors that influence the proper folding and stability of recombinant protein expression in *E. coli* cells.

Cells were harvested and proteins were extracted according to section 2.3.2. After centrifugation and sonication, the cell lysates were subjected to affinity chromatography (affinity purification) through use of glutathione sepharose 4B resins. The Glutathione Sepharose ™ 4B assay elutes proteins under mild, non-denaturing conditions in order to prevent loss of protein antigenicity and functionality. A solution of cell lysate was incubated with glutathione (GSH)-coupled agarose beads. Proteins capable of binding to GSH, such as GST, were retained with the beads while all other proteins washed through the column filter. Samples were eluted from the beads and transferred to semi-permeable membranes in order to concentrate the protein samples and to dilute out the GSH. Subsequently a Western blot analysis was performed to identify the purified fusion proteins using an α-GST antibody (Figures 3.3 and 3.4)

There was no production of GST in the absence of IPTG induction (Lane 1). It can be observed that a large amount of GTS was produced when induced by IPTG (Lane 2), indicating that the plasmid is functional. No significant amount of full-length

protein was produced in any of the GST-p400 fragment samples with only GST-F4 and GST-F6 producing any quantity of protein similar to the expected size (Lanes 6 and 8). Band representing proteins larger than the expected sizes could be indicative anything from contamination, a dimer association between two protein fragments as a result in the failure to denature, or simply as a reduction in the amount of SDS bound to the protein and ultimately a decreased negative charge and decrease its mobility [168].

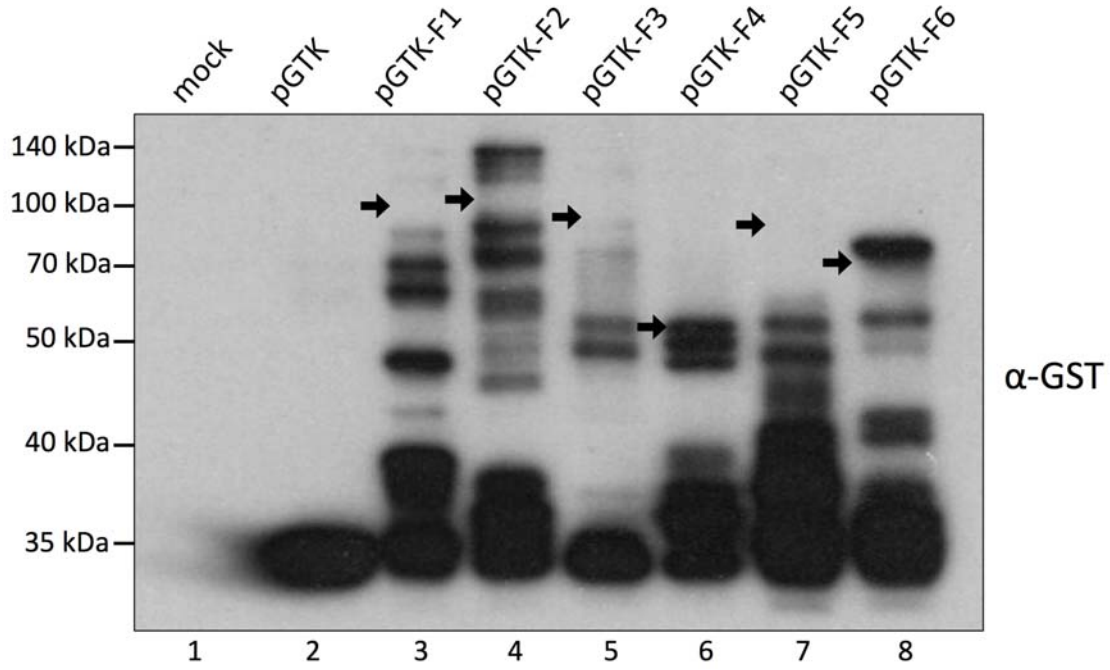

Figure 3.4 Expression and purification of GST-p400 fragment fusion proteins. BL21 cells transformed with pGTK-p400 derivatives were grown to an OD of 0.6 then induced with ITPG at a concentration of 0.6 mM for 1 h. Cells were harvested and cell lysate was prepared for α-GST IP. IP products were run on a 10% polyacrylamide gel by SDS-PAGE for 1 h at 30 mA. Proteins were transferred to a PVDF membrane for 2 h at 150 mA. Samples were examined with an α-GST antibody. Lane 1: pGTK with no ITPG induction, Lane 2: GST (empty pGTK vector), Lane 3: GST-F1 (107 kDa), Lane 4: GST-F2 (113 kDa), Lane 5: GST-F3 (100 kDa), Lane 6: GST-F4 (55 kDa), Lane 7: GST-F5 (92 kDa), Lane 8: GST-F6 (70 kDa). Theoretical protein sizes are indicated by the black arrows.

The coomassie stain of purified GST-p400 derivative recombinant proteins (figure 3.5) is representative of the same results observable by Figure 3.4.

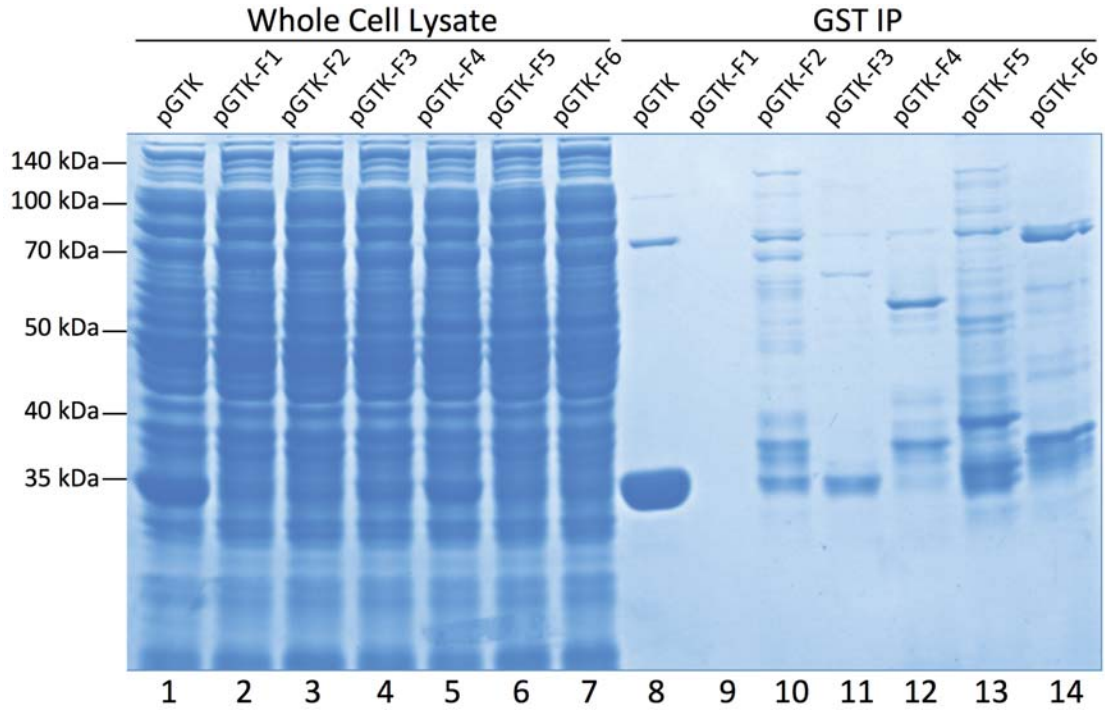

Figure 3.5 Expression of GST-p400 derivatives. BL21 cells transformed with pGTK-p400 derivatives were grown to an OD of 0.6 then induced with ITPG at a concentration of 0.6 mM for 1 hour. Cells were harvested and cell lysate was prepared for α-GST IP with 20 μL of cell lysate conserved as an input. The remainder of the cell lysate was used in an IP assay and the inputs, as well as IP products, were run on a 10% polyacrylamide gel by SDS-PAGE for 1 h at 30 mA. Proteins were transferred to a PVDF membrane for 2 h at 150 mA. Samples were examined with an α-GST antibody. Lane 1: input GST, Lane 2: input GST-F1, Lane 3: input GST-F2, Lane 4: input GST-F3, Lane 5: input GST-F4, Lane 6: input GST-F5, Lane 7: input GST-F6, Lane 8: GST, Lane 9: GST-F1, Lane 10: GST-F2, Lane 11: GST-F3, Lane 12: GST-F4, Lane 13: GST-F5, Lane 14: GST-F6.

Overall, the recombinant proteins could not be obtained as full-length proteins in any significant quantities under the conditions and parameters used. Their production was only marginally increased by the addition of tetracycline and a reduction in the

incubation temperature during induction with ITPG. By evidence of both the Western blot (figure 3.3) and the coomassie stain (figure 3.4) the empty pGTK vector can be successfully transformed into the BL21 cells and produces large quantities of GST indicating that some property the p400 derivative inserts is the reason for the protein break down.

3.3 Expression of ATM from Sf9 cells

Insect Sf9 cells were used to produce FLAG-ATM for a GST-pull-down assay to demonstrate a direct interaction between various p400 fragments and ATM. The Sf9 cells were infected with a P3 generation of baculovirus containing a construct for FLAG-ATM (obtained from Rebecca Smith) and cells were harvested after an optimized time of 48 h of incubation at 26°C for maximum protein production with reduced degradation products, as determined by Smith (2014) [77].

Cells were harvested and lysed using an F buffer (20 mM Tris-HCl, pH 7.9, 500 mM KCl, 4 mM $MgCl_2$, 20% (v/v) glycerol, 0.4 mM EDTA, 2 mM DDT) supplemented with a protease inhibitor cocktail and PMSF in order to prevent degradation of ATM and a dounce homogenizer. Then samples were run on an SDS-polyacrylamide gel and subjected to a Western analysis using an α-FLAG antibody to confirm the presence of FLAG-ATM. ATM was initially undetectable (data not shown). Figure 3.5 represents one of several attempts to extract ATM using an F buffer compared to an ATM control, which was extracted from Sf9 cells using an ATM lysis buffer (20 mM HEPES pH 7.4, 120 mM $NaCL_2$, 1.5 mM $MgCl_2$, 1 mM EGTA, 50 mM NaF, 0.2% Tween-20, 0.5 mM DTT, 1 mM PMSF). The ATM lysis buffer control extracted a much larger amount of ATM than the F buffer. Cell lysates needed to be obtained with F buffer as to be compatible with GST-F1 samples extracted from *E. coli* BL21 cells. It was necessary to visualize the proteins using a SuperSignal® West Femto Maximum Sensitivity Substrate, a stronger substrate than typically required, and it is apparent that the ATM band representing 60 μL cell lysate (Lane 4) does not contain a substantial amount of protein.

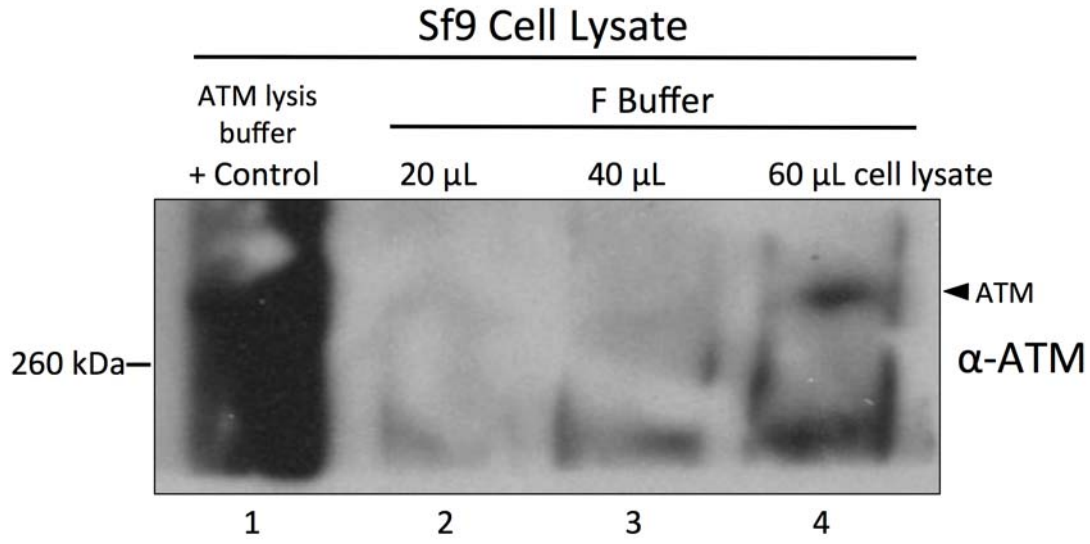

Figure 3.6 Expression of FLAG-ATM. Sf9 cells were infected with 500 µL P3 baculovirus containing FLAG-ATM. Samples were run on a 6% SDS polyacrylamide gel for 1 h at 30 mA then transferred to a PVDF membrane for 2 h at 150 mA. Lane 1 contains 20 µL a positive control sample of Sf9 cells lysed using an ATM lysis buffer while lanes 2-4 contain various volumes, 20 µL, 40 µL and 60 µL, respectively, of cell lysate from Sf9 cells lysed with F buffer.

After several attempts to express ATM through the Sf9 expression system it became evident that although ATM could be detected when the cells were lysed with ATM lysis buffer, the amount of detectable protein when cells were lysed with buffer F was dramatically lower.

3.4 GST Pull-Down Assay

Although there was no substantial amount of full-length GST-p400 derivative recombinant proteins produce or any significant quantity of ATM, it was decided that several attempts at a GST-pull-down assay should be performed in case the portions of the p400 fragments produced were able to interact with the minimal amount of ATM present in the Sf9 cell lysates. Samples collected from α-GST-pull-down assay were combined with glutathione-Sep4B agarose beads and allowed to incubate for 1 h at 4°C before the addition of cell lysate from FLAG-ATM expressing Sf9 cells. The two samples were incubated together overnight at 4°C before being resolved on a 4-12%

SDS-polyacrylamide gradient gel. Figure 3.6 represents one of several attempts at a GST-pull-down. Presence of ATM in the Sf9 samples was confirmed through a western blot (data not shown). No detectable amount of ATM could be pulled down by any of the samples. This could be due to the low levels of ATM in the Sf9 cell lysate samples, the truncated proteins produced from the BL21 expression, or a lack of ability of the p400 fragments to bind directly to ATM in this capacity.

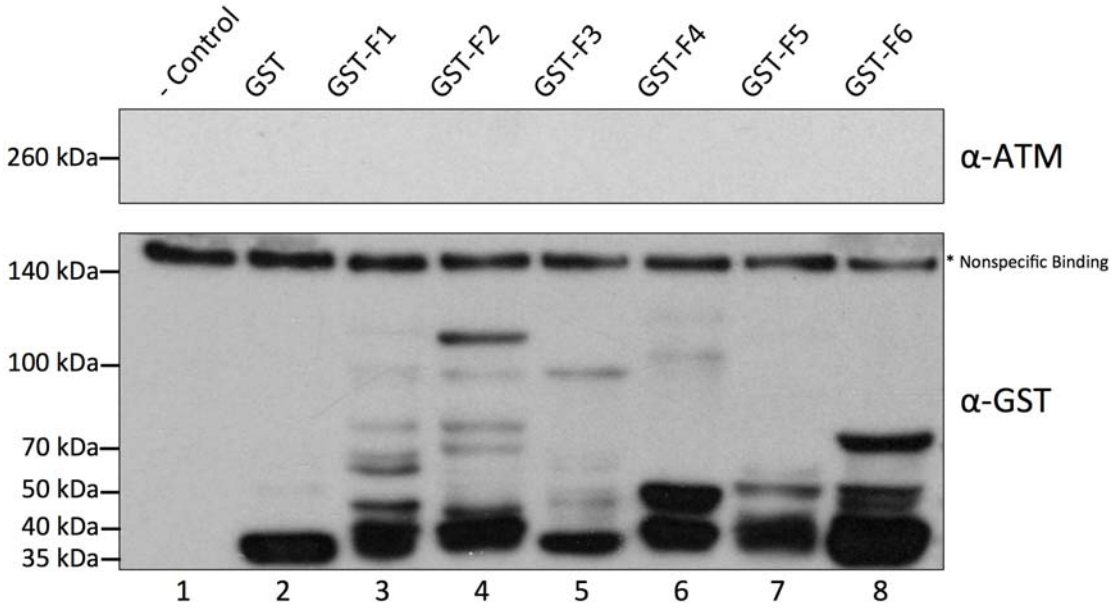

Figure 3.7 Co-immunoprecipitation between ATM and GST-p400 derivatives. A volume of 60 μL of each reaction was run on a 5-12% gradient SDS-polyacrylamide gel for 1 h at 30 mA. Proteins were transferred to a PVDF membrane for 2 h at 150 mA. Membranes were examined using α-GST and α-ATM antibodies. Lane 1: FLAG-ATM, Lane 2: empty pGTK vector, Lane 3: GST-F1 and FLAG-ATM, Lane 4: GST-F2 and FLAG-ATM, Lane 5: GST-F3 and FLAG-ATM, Lane 6: GST-F4 and FLAG-ATM, Lane 7: GST-F5 and FLAG-ATM, Lane 8: GST-F6 and FLAG-ATM.

3.5 Discussion

DSB repair requires a fluid cooperation and interaction between all of the machinery involved. Two of these proteins are ATM and p400. As previously mentioned, there are several lines of evidence suggesting that there could be a potential direct interaction between ATM and p400. This includes the commonality of phosphorylation substrates between members of the PIKK family such as the phosphorylation of H2AX by both ATM and ATR as well as the similarity between PIKK domains that hints at a prospective common binding partners [98]. TRRAP is a scaffolding subunit of the Tip60/p400 complex and binds directly to p400 implicating a potential interaction between p400 and ATM [141]. Lastly, the interaction between ATM and Tip60 as well as Tip60 and p400 gives cause to believe that ATM and p400 may play a role in the regulation of each other if not as evidence of a direct interaction between the two ATM [101, 118, 142]. A GST pull-down assay was used in order to determine the interaction between ATM and six p400 fragments (Figure 3.7). This assay was performed several times with each resulting in no ATM pull-down by any of the six p400 GST-fused protein fragments. However, this cannot be considered a negative result but rather an inconclusive one, as no significant quantities of either HA-ATM or GST-fused p400 fragments could be extracted.

In preparation for this experiment, BL21 *E. coli* was used to produce GST-fused p400 fragments with the GST tag located at the N terminus of the proteins. The protocol was optimized in order to attempt to obtain full-length proteins. This included reductions in the incubation temperatures during cell growth as well as ITPG induction and the addition of tetracycline in order to slow protein production and allow for proper polypeptide folding. These optimization techniques, although subtly successful, were not able to produce substantial quantities of full-length proteins for all of the p400 fragments. GST-F4 and GST-F6 were the only full-length p400 fragments produced at any noticeable levels and the amount was negligible compared to the quantity of degradation products (Figure 3.4). The rest of the p400 fragments, GST-F1, GST-F2, GST-F3, and GST-F5 did not give any bands representative of the theoretical expected size but each produced a large quantity of truncated proteins, mostly at the expected size for GST. The band pattern in each attempt was very similar, but not exact, to other attempts at purification. These same p400 fragment DNA sequences were used in a previous experiment in both human and SF9 insect cells [77]. The resulting protein fragments were expressed at their expected sizes with little to no degradation products.

This suggests that the inability to produce full-length proteins stems from the expression of these protein fragments in *E. coli* rather than the sequences of the p400 fragments themselves.

Several factors could be responsible for this outcome. First and foremost, the microenvironment in *E. coli* cells is different to that of eukaryotic cells, including the osmolarity, pH, Redox potentials, folding mechanisms, and cofactors [169, 170]. *E. coli* struggle to express proteins over 60 kDa in size and it has been estimated that less than 15% of non-bacterial proteins can be expressed in *E. coli* in a soluble form without the assistance of modifications [171]. These differences in the microenvironment can potentially be overcome by the use of molecular chaperones. These chaperones are able to help nascent polypeptides fold into their tertiary structures [172]. Another factor is codon bias: *E. coli* do not possess the same ratios of tRNA molecules as human cells, which can cause translational complications when the frequency of synonymous codons of the mRNA is different from that of the host [173]. Low levels of charged rare tRNA molecules have been shown to cause ribosome stalling and consequent detachment of ribosomes from the mRNA, resulting in the failure to produce full-length proteins [174, 175]. This can result in the misincorporation of amino acids or truncation of the polypeptide. One method to resolve this is to supply the cells with under represented tRNAs and the use of cell strains such as BL21(DE3)CodonPlus and Rosetta(DE3), which include plasmids that code for rare tRNAs. Another way to overcome translational difficulties is codons optimization of the mRNA where rare codons are replaced by commonly used *E. coli* codons. An analysis of the p400 fragment codon sequence using GeneScript® suggests that all of the sequences are below the level for good protein expression (Appendix Table A2.2). Codon optimization can also design mRNA sequences that contain “fast” codons in the 5’ end. This would clear the initiation site more quickly, allowing for new ribosomes to bind [176]. However, changing the codons may cause a reduction in the mRNA secondary sequence and produce unintentional Shine-Dalgarno-like structures, which can result in translational pausing [175]. Unfortunately, due to time constraints, it was not possible to explore any of these optimization mechanisms.

The processing of the extracted protein could also have influenced the presence of degradation products. Purifying the GST-fusion proteins took several days between the cell harvest and purified protein elution. Each step was performed on ice or in the cold room to reduce the likelihood of protein degradation. Protease inhibitor cocktails as well

as the protease inhibitor PMSF were employed to reduce the activity of proteases in the cell lysates. Glycerol was used as a stabilizing agent to help maintain the p400 fragments. However, all of these steps to prevent degradation were not enough to produce full-length product. Besides the potential translational complications another reason for the degradation could be due to inherent protein instabilities of the p400 protein fragments in an *E. coli* or in vitro environment. The Internet program Phyre2 was used to analyze the predicted structure of the GST-p400 fragments, while the ExPASy server analyzed stability of the protein products [177, 178]. Results can be seen in Appendix Figure A5.1 – A5.6. The results obtained indicate that the GST-fusion proteins are unstable and disorganized. As these are predictions are acquired by theoretical rules and associations and not determined by experimental evidence with the GST-p400 fragments it is unknown whether the instability of the proteins comes as a result of their production in E. coli or by their inherent instable nature.

Producing and purifying full-length HA-tagged ATM in Sf9 cells presented its own challenges. F buffer was used to lyse the Sf9 cells to create a cell lysate containing the full-length HA-ATM protein. This buffer was used in order for the lysate to be compatible with the GST-p400 fragments that were purified using F buffer. This is necessary for the GST pull-down assay. To determine if the buffer was the cause of the difference in protein levels, a solution of Sf9 cells infected with P3 baculovirus was divided into two samples and harvested with ATM lysis buffer or F buffer, with all other aspects remaining the same. It can be seen in Figure 3.7 that lysing the cells with ATM-lysis buffer produced significantly more ATM that cells lysed with F buffer. This could be due to the pH requirements of ATM or due to the additives used in the F buffer. One suggestion was the ATM is bound to the chromatin in Sf9 cells and requires a more stringent buffer to extract the cells [77]. Another hypothesis is that ATM requires a gentler buffer as ATM lysis buffer has a much lower salt concentration than the F buffer used to extract ATM from the Sf9 cells. Alternative protease inhibitors for insect cells such as Leupeptin and Pepstatin A could have been used in conjunction with the EDTA and PMSF contained in the F buffer.

Although significant quantities of HA-ATM and GST-p400 proteins could not be produced, a GST pull-down assay was performed. The results in Figure 3.7 indicate that there was no ATM pulled down with the GST-p400 fragments. There is however non-specific binding of an insect protein larger than 140 kDa believed to interact with the glutathione (GSH) Sep4 beads (Figure 3.7). These results can neither argue for or

against the potential binding interaction of p400 and ATM, as the experiment could not be conducted due to the inability to produce sufficient quantities of the desired proteins. Time restrains prevented the exploration into alternative means of producing protein products.

4 Functional analysis of interaction between p400 and ATM

4.1 Effect of p400 fragment expression on ATM function and DNA repair

4.1.1 Introduction

Although a direct interaction *in vitro* could not be established, it was determined that the examination of the functional implication of ectopically expressing N-terminal derivatives would continue due to the evidence provided by the previous study [77]. ATM and p400 both function within the DNA repair system to ensure efficient restoration of damaged DNA. ATM is responsible for the phosphorylation of a number of vital repair proteins required for DNA repair and checkpoint control [119, 124, 128]. One of these substrates is H2AX. The phosphorylation of H2AX at serine 139 by activated ATM is arguably the most important function of ATM, as it induces the formation of the nuclear foci around the DSB site. Effective repair also requires the relaxation of chromatin around the DSB site. This appears to be independent of ATM activity but has been shown to require the Tip60/p400 complex, which contains the chromatin remodeler p400, the histone acetyltransferase Tip60, and the PIKK family member TRRAP. All three of these subunits are essential for DNA-damage induced chromatin decondensation [179]. The p400 subunit in particular is responsible for the exchange of canonical histone H2A for the histone variant H2AZ at promoters, resulting in a relaxed state allowing access to the DNA [143, 145]. It has been postulated that the chromatin remodeling functions of p400 are also employed during DSB repair. Currently, the exact mechanism by which p400 is recruited to the break site is unknown but it has been speculated that DNA repair proteins such as TRRAP, MDC1 or Rad51 may play a role [158]. Although ATM and TRRAP are responsible for the recruitment of different repair proteins to the nuclear foci, the similarities between them as well as their modular FATC domain suggests that they may share more binding partners than originally speculated. One such potential partner is p400, which directly associates with TRRAP in the Tip60/p400 complex. As mentioned previously, p400 has been shown to co-immunoprecipitate with ATM *in vivo*, suggesting a potential functional interaction between the two proteins [77].

4.1.2 Cloning and isolation of FLAG-p400 fragments

Previous analysis of the six p400 fragments identified the three N-terminal fragments (F1, F2, and F3) as the most promising candidates for a functional interaction with ATM. The sixth fragment, F6, was chosen to act a negative control as previous studies had eliminated it as a direct binding partner of ATM [77]. F1, F2, F3 and F6 contained in the CβF vector from the previous section were used in the generation of four lentiviral constructs using the pCDH1-MCS1-EF1-Puro lentiviral vector (pCDH1). This vector is commonly used for production of lentivirus particles and constitutive expression of the inserted therapeutic gene in a wide variety of mammalian cell lines after infection. Key traits of this vector include the CMV promoter, multiple cloning site (MCS), WPRE element, SV40 polyadenylation signal, hybrid RSV-5LTR promoter, genetic elements such as cPPT, GAG, and LTRs, as well as the SV40 origin, pUC origin, and the ampicillin resistance gene. Cloning the vector in *E. coli* DH5α took advantage of the pUC origin, which enables high copy replication and maintenance of the construct in *E. coli*; the ampicillin resistance gene, used for selection; as well as the MCS, specifically the NotI and BamHI restriction sites.

The cloning strategy (Figure 4.1) implemented the use of the FLAG-p400 fragment-containing CβF vectors previously constructed by Rebecca Smith as described in section 3.2. In preparation for the insertion of the FLAG-p400 fragments into the pCDH1 vector, the CβF-p400 derivative vectors were first digested with the restriction enzyme ClaI. This was followed by a T4 DNA polymerase step to fill in the cohesive ends of the ClaI cut site in order to create a blunt end for future ligation reactions (section 2.2.2). The FLAG-p400 fragments were then excised from the CβF vector through digestion with BamHI and gel purified (section 2.2.6). A similar process was used to prepare the pCHD1 vector. The pCDH1 vector was digested with NotI (section 2.2.1) followed by incubation with T4 DNA polymerase to fill in the cohesive ends of the NotI cut site (section 2.2.2). This created a blunt end for future ligation reactions. The vector was then digested with BamHI and processed with CIP digestion to remove 5’ phosphate groups on digested plasmid DNA (section 2.2.4). This serves to reduce the potential for religation of empty vector DNA. The digested pCDH1 vector DNA was then gel purified. Ligation reactions between the pCDH1 vector and the p400 fragments described above were carried out according to section 2.2.7.

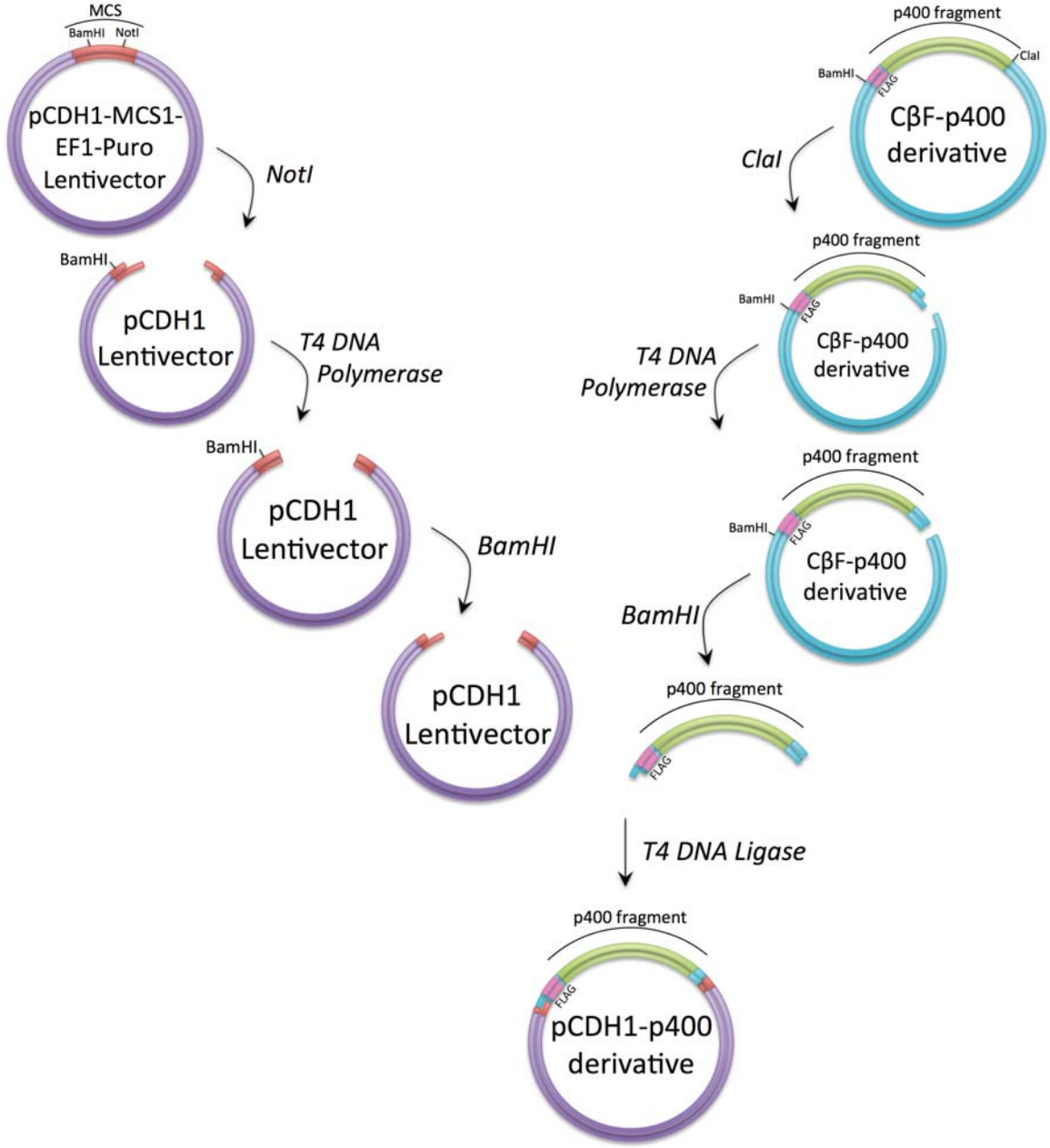

Figure 4.1 Cloning strategy for lentiviral vector containing FLAG-p400 derivatives. Four FLAG-p400 fragment inserts (F1, F2, F3, and F6) were digested from CβF vectors [77] at the ClaI and BamHI cut sites and inserted into the CDH1-MSC1-EF1-Puro lentiviral vector (pCDH1) utilizing the NotI and BamHI cut sites. The pCDH1 vector was prepared by RE digestion with NotI, T4 polymerase fill in of cohesive ends, RE digest with BamHI and subsequent CIP treatment. The p400 fragments were prepared by RE digestion with ClaI, T4 DNA polymerase fill in of cohesive ends, followed by RE digestion with BamHI. The p400 fragments were inserted in frame with the FLAG tag. The vector backbones are represented by blue and purple while the open reading frames are indicated by the pink FLAG tag sequence and green p400 fragment sequence.

The ligation reaction products were used to transform *E. coli* DH5α according to section 2.2.9 and selected for on LB agar plates containing ampicillin (amp). Plasmid DNA from candidate clones was extracted using small-scale high quality plasmid isolation (section 2.2.10.2) and screened via digestion with BamHI and HindIII in order to identify constructs containing FLAG-p400 fragments. BamHI has one restriction site in the pCDH1 vector and is located at the recovered restriction site between the FLAG-p400 insert and the pCDH1 vector. HindIII however, has five restriction sites within the pCDH1 vector and none within the FLAG-p400 fragment insert. This created a band pattern where, in the absence of an insert, six bands were present after digestion and in the inclusion of an insert seven bands were observed with the seventh band being a comparable size to the expected purified FLAG-p400-fragment insert prior to ligation. Figure 4.2 shows both digested and undigested constructs as well as the purified p400-fragments used in the ligation reaction. From this gel, it is apparent that the p400-derivatives cut from CβF are comparable to the fragments digested from the pCDH1 constructs isolated from transformed DH5α cells. The slight discrepancy between travel distances is due to the differences between the salt content of the buffers used for gel purification versus the buffers used in the restriction enzyme digestion [165].

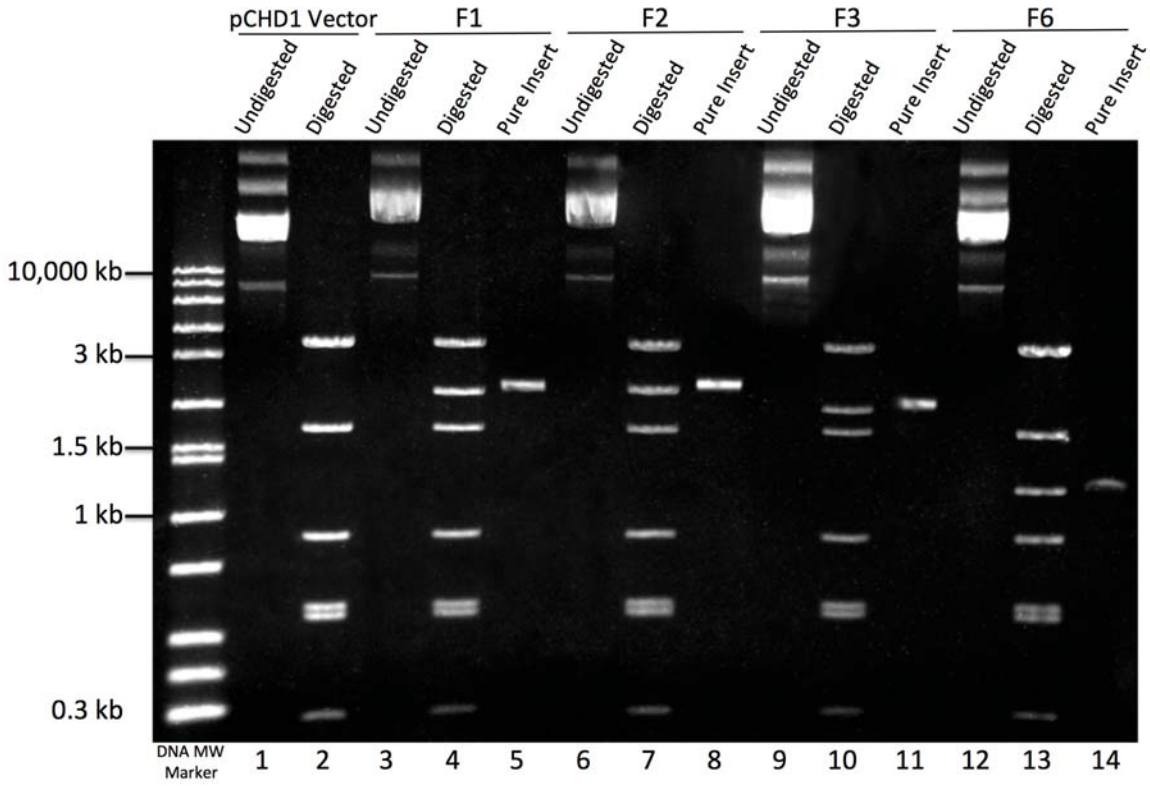

Figure 4.2 Cloning of pCDH1-p400 domain constructs. Restriction digests of plasmid DNA extracted from amp selected DH5α cells were performed using BamHI and HindIII (section 2.2.1) to confirm the correct insertion of FLAG-p400 fragments into a pCDH1-viral vector. Lane 1: undigested pCDH1 lentiviral vector, Lane 2: digested pCDH1, Lane 3: undigested pCDH1-p400-fragment 1, Lane 4: digested pCDH1-p400-fragment 1, Lane 5: purified p400-fragment 1, Lane 6: undigested pCDH1-p400-fragment 2, Lane 7: digested pCDH1-p400-fragment 2, Lane 8: purified p400-fragment 2, Lane 9: undigested pCDH1-p400-fragment 3, Lane 10: digested pCDH1-p400-fragment 3, Lane 11: purified p400-fragment 3, Lane 12: undigested pCDH1-p400-fragment 6, Lane 13: digested pCDH1-p400-fragment 6, Lane 14: purified p400-fragment 6. Plasmid digests were analyzed on a 1% agarose gel in 1x TBE for 1 h at 120 V.

After the preliminary screening and confirmation of FLAG-p400-fragment insertion into pCDH1, samples of the extracted constructs were sent for DNA sequencing (section 2.2.11). The resulting data confirmed that the fragments were in the correct orientation within the pCDH1 vector and contained no errors in their DNA sequence (data not shown). Upon this verification, large quantities of the constructs were produced. This was accomplished by inoculating 100 mL of LB broth with DH5α

cells containing the pCDH1-p400 fragment constructs in order to obtain a large quantity of construct DNA. The plasmid DNA was extracted using large-scale high quality plasmid isolation (section 2.2.10.3).

4.1.3 Production of lentivirus containing FLAG-p400 fragments

The isolated pCDH1-p400 fragment constructs were used in the production of lentivirus (section 4.1.2). The lentiviral system is a well-established mechanism for incorporating DNA into a host cell genome. A few key features of the pCDH1 vector help to ensure high-volume production of lentiviral particles in Human Embryonic Kidney (HEK) 293T producer cells. The first is the hybrid RSV-5LTR promoter, which ensures large quantities of expression of the full-length pCDH1-p400 fragment transcript. The vector also includes genetic elements such as cPPT, GAG, and LTRs. These elements are essential for the packaging, transduction, and stable integration of the pCDH1-p400 viral expression construct into the genome of the human osteocarcinoma U2OS target cells. Lastly, the SV40 origin allows for the steady reproduction of pCDH1-p400 derivative constructs in HEK 293T cells.

Before transfection, the solutions of pCDH1-p400 derivatives were quantified using the DNA quantification method described in section 2.2.12. HEK293T cells were then transfected with 5 μg pCDH1-p400 lentivirus plasmid DNA and 3 μg packaging plasmid mix in order to generate lentiviral particles (Figure 4.3). The lentiviral-containing growth media from the HEK293T plates was pipetted out of the tissue culture plate and dispensed into 50 mL Falcon™ tubes 41 h and 65 h after transfection (section 2.4.5). The solutions were then concentrated as described in section 2.4.6. Concentrated lentivirus solutions underwent an RT-qPCR titration (section 2.2.13), which exploited the woodchuck hepatitis virus (WHP) posttranscriptional regulatory element (WPRE) in order to estimate the viral titer. This both confirmed the production of virus and provided a rough approximation of volume needed for infection (data not shown).

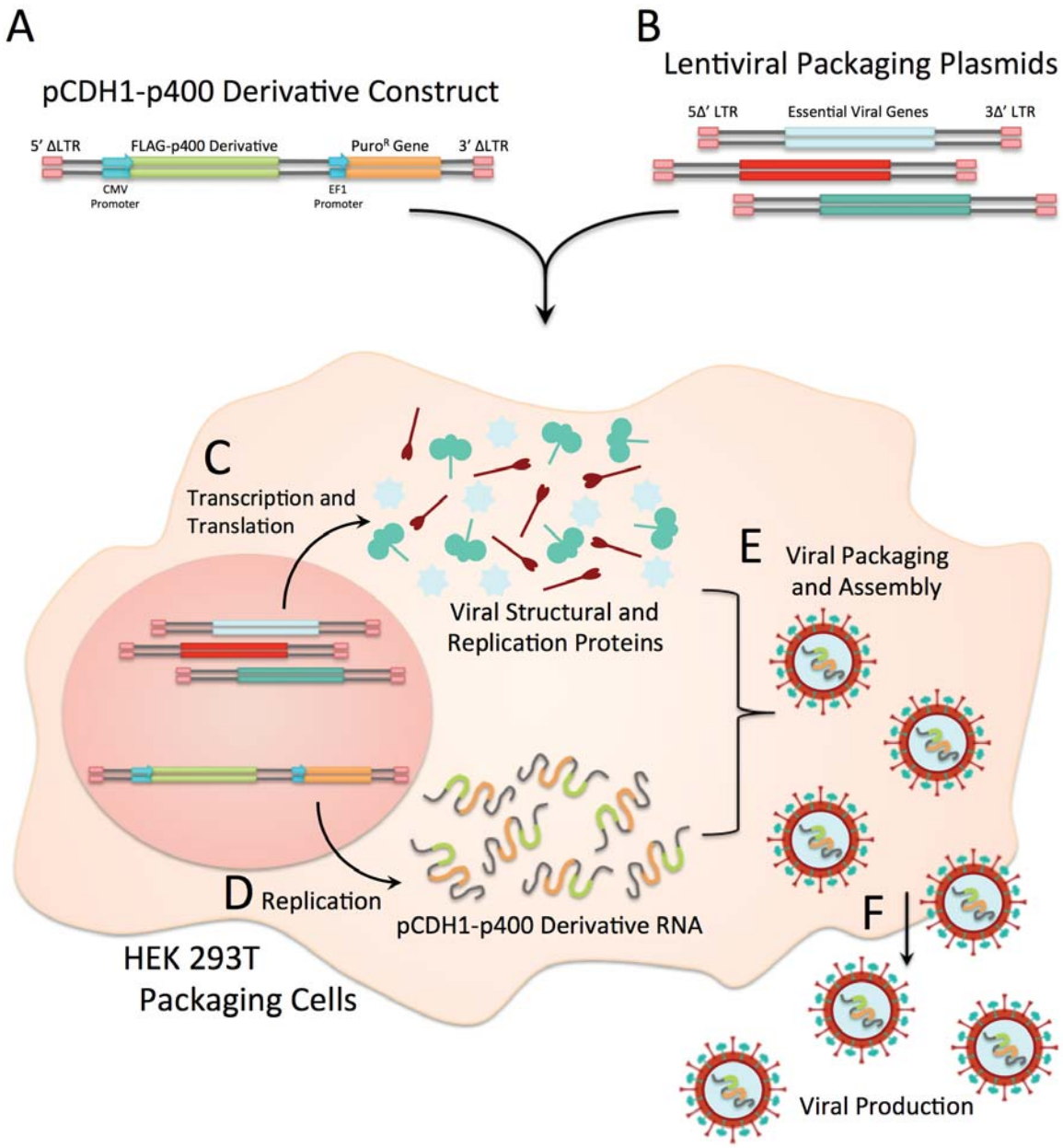

Figure 4.3 Schematic diagram for production of lentiviral particles in HEK293t cells. HEK293T packaging cells were transfected with (A) a lentiviral vector (pCDH1-MCS1-EF1-Puro) containing an insert of p400 derivative DNA flanked by long terminal repeats (LTRs) as well as several (B) lentiviral packaging plasmids. (D) The pCDH1-p400 DNA is replicated via transcription into RNA. (C) The packaging plasmid DNA is transcribed then translated into viral packaging proteins that (E) assemble with the pCDH1-p400 RNA into functional viral particles. (F) These particles are secreted out of the HEK293T packaging cells and into the medium. (Adapted from Goverdhana et al., 2005) [180]

Several aspects of the pCDH1 vector help to ensure efficient infection and insertion of lentiviral pCDH1-p400 fragment DNA into the genome of the U2OS target cell line. The cytomegalovirus (CMV) promoter of pCDH1 encourages a high level of expression of the inserted gene of interest. This is aided by the WPRE element, which enhances stability and translation of the CMV-driven transcripts. Efficient termination and processing of recombinant transcripts is facilitated by the SV40 polyadenylation signal. The elongation factor 1 (EF1) promoter allows for the expression of the puromycin resistance gene, which provides a means for the selection of cells that have successfully integrated the pCDH1-p400 fragment construct into their genome. The lentiviral system employs a method of random DNA insertion into the genome of the host cell rather than targeted integration. Thus, copy number and location of the inserts is unknown and uncontrollable.

Concentrated solution of lentivirus containing pCDH1-p400 derivative constructs in a volume of 0.5 mL was added to U2OS cells (section 2.4.7). These cells were incubated with the lentivirus for 24 h before selection with puromycin (1.5 μg/mL). Cells were harvested after a 4-day puromycin selection period and lysed in a volume of 500 μL according to section 2.4.10. Whole cell extracts were normalized after analysis by a BCA assay then resolved by SDS-PAGE. Samples were then subjected to Western analysis using antibodies raised against FLAG. U2OS cells infected with lentivirus containing pCDH1-p1 and pCDH1-F6 showed expression of F1 and F6. However, samples from cells infected with pCDH1-F2 or pCDH1-F3 constructs did not show any protein product. Therefore, to verify the presence of the p400 protein fragments the samples were immunoprecipitated with M2 agarose beads (section 2.3.9) to concentrate the FLAG-tagged p400 fragments. Samples before and after immunoprecipitation (IP) were resolved by SDS-PAGE and examined with Western blotting using an α-FLAG antibody (Figure 4.4). The IP showed that all FLAG-p400 fragment proteins were being expressed successfully. Samples of FLAG-F2 could be clearly visualized after IP with FLAG-F3 observed at significantly lower quantities. FLAG-F1 and FLAG-F6 were produced in substantial quantities and could be visualized by Western blotting in both the input as well as the IP. The lentiviral expression system inserts the desired DNA randomly into the genome, potentially causing a difference in expression level if the gene is inserted into a non-transcribed region of the genome. However, this same difference in protein content was observed in

every attempt to demonstrate expression and was similar to the pattern of expression in previous studies using transient transfection of HEK293T cells [77]. It was therefore speculated that some other property of the protein fragments, such as toxicity, caused this difference in expression level.

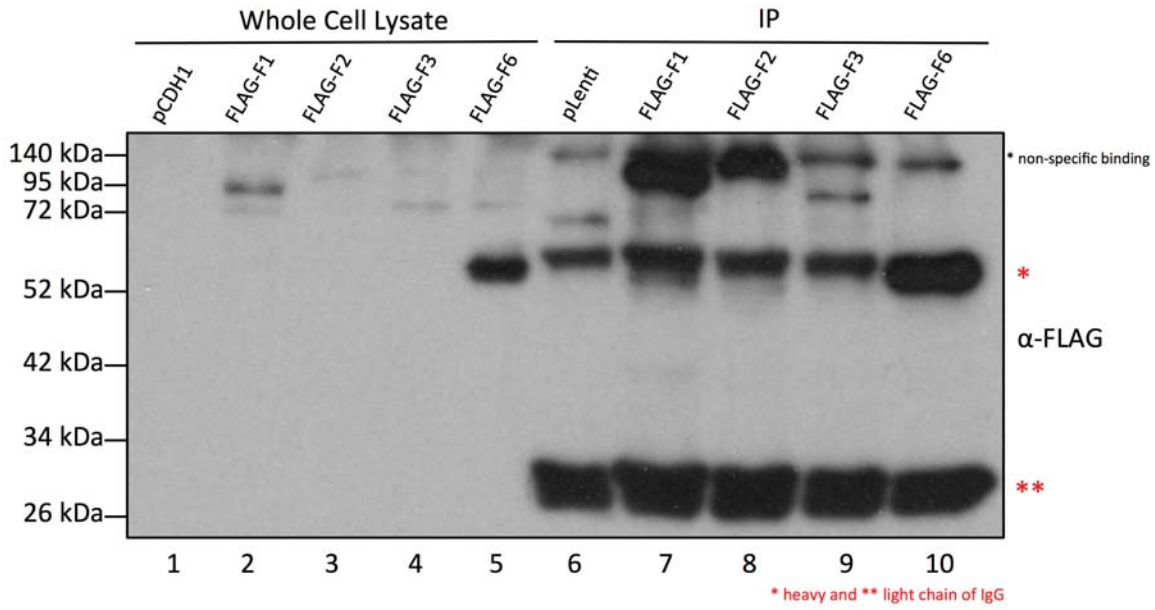

Figure 4.4 Expression of FLAG-p400 from pCDH1 lentivirally infected U2OS cells. U2OS cells with a 60% confluence were infected with lentivirus containing either empty pCDH1 vector or pCDH1 vector containing one of the p400 fragments F1, F2, F3, or F6. Extracts were resolved on a 10% polyacrylamide gel for 1 hour at 30 mA. The proteins were transferred to a PVDF membrane for 2 hours at 150 mA. The membrane was examined using antibodies raised against FLAG (α-FLAG) to visualized FLAG-p400 fragments. Lane 1: whole cell lysate pCDH1 lentiviral vector, Lane 2: whole cell lysate FLAG-F1, Lane: 3 whole cell lysate FLAG-F2, Lane 4: whole cell lysate FLAG-F3, Lane 5: whole cell lysate FLAG-F6: Lane 6: IP empty pCDH1 lentiviral vector, Lane 7: IP FLAG-F1, Lane 8: IP FLAG-F2, Lane 9: IP FLAG-F3, Lane 10: IP FLAG-F6.

4.1.4 Examination of p400 N-terminal fragment expression on ATM activity

U2OS cell lines infected with pCD1-F1, pCDH1-F2, and pCDH1-F3 were used in this assay. The effect of constitutively expressed p400 fragments on ATM activity during DNA damage recovery was investigated through the use of DSB induction by bleomycin. Bleomycin is a chemotherapeutic drug used in cancer treatment for its ability to induce DSBs, although its exact mechanism of action is unknown. U2OS cells stably expressing p400 fragment proteins were incubated with bleomycin (10 μg/mL) for 1 h followed by a recovery period of 0, 1, 3, or 7 h (section 2.4.9). Control samples for the three U2OS cell lines were examined in the absence of bleomycin. Following the harvesting, the samples were processed into soluble and insoluble fractions containing ATM and H2AX respectively (section 2.4.10 and 2.4.11). Thirty percent (v/v) of the soluble fraction and 100% (v/v) of the insoluble fraction were resolved by SDS-PAGE. Samples were examined by immunoblotting (section 2.3.7) in a sequential manner using antibodies raised against ATM, ATM phosphorylated at serine 1981 (P-ATM), and β-actin (loading control) for samples containing the soluble fraction. The insoluble fraction was analyzed with antibodies raised against H2AX and H2AX phosphorylated at serine 139 (γH2AX) (Figure 4.5). The β-actin in all lanes is present in equal intensities indicating even loading for each sample. In all lanes the quantity of total ATM remains the same, which is expected. Control samples for each cell line indicate a basal level of phosphorylated ATM (Figure 4.5 lanes 1, 6, 11, and 16). Immediately following the removal of bleomycin all cell lines showed an increase in the amount of P-ATM (Figure 4.5 lanes 2, 7, 12, and 17) while returning to basal levels after 3 h of recovery (Figure 4.5 lanes 4, 9, 14, and 19). This is suggests that ectopic expression of p400 fragments does not alter the activation process of ATM or the autophosphorylation of ATM.

In the insoluble fraction, the quantity of total H2AX is comparable in most lanes except 14, 16, and 17 where the level is marginally reduced. Control samples of each cell line show basal levels of γH2AX are almost undetectable (lanes 1, 6, 11, and 16). In all cell lines γH2AX levels are at their peak immediately after bleomycin removal (lanes 2, 7, 12, and 17). Cells infected with control lentivirus (pCDH1 vector) or lentivirus-containing pCDH1-F3 exhibited a rapid clearance of γH2AX during the recovery period with the quantity of γH2AX returning to near basal levels after 7 h of recovery. Cells infected with lentivirus containing pCDH1-F1 demonstrated a persistence of γH2AX

during the recovery period, indicating that the expression of F1 alters the ability of the cell to clear γH2AX during DSB repair. Stable U2OS cells ectopically expressing F2 also gave an indication of persistent γH2AX but due to slightly uneven loading, represented by total H2AX levels, no conclusive results can be drawn regarding the functional effect of F2 on γH2AX clearance.

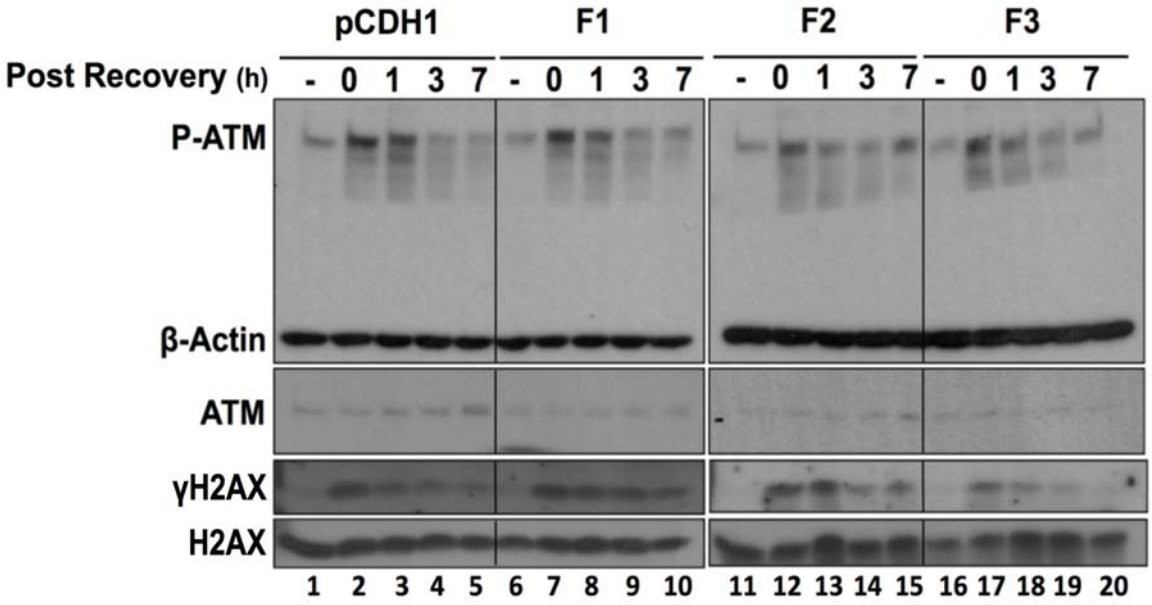

Figure 4.5 ATM activity assay. U2OS cells with a 60% confluence were infected with lentivirus containing either empty pCDH1 lentiviral vector or pCDH1 lentiviral vector containing one of the p400 fragments. After 4 days of puromycin selection the cells were treated with bleomycin (10 μg/mL) for 1 h then allowed to recover in bleomycin free media for 0, 1, 3, or 7 hours. A control with no bleomycin addition was also used in the assay. Whole cell extracts were loaded on 8-12% gradient polyacrylamide gels and resolved by electrophoresis for 1 h at 30 mA. Proteins were transferred to PVDF membranes for 2 h at 150 mA. Histones were extracted using HCl then loaded on a 5% polyacrylamide gel and resolved by electrophoresis for 1 h at 30 mA. Proteins were transferred to PVDF membranes for 2 h at 150 mA. The membranes were examined with α-ATM-P, α-β-actin, α-ATM, α-P-H2AX, and α-H2AX.

4.1.5 Examination of F1 expression on cell survival after DNA damage

The examination of p400 fragment expression on cell survival after induction of DNA damage was originally designed to study cell lines ectopically expressing pCDH1, F1, F2, F3 or F6 but after several trials it was determined that only pCDH1, F1, and F6 would be tested further due to the low level of F2 and F3 expression. After infection with lentivirus containing pCDH1, pCDH1-F1, or pCDH1-F6 and a 4-day selection period with puromycin, stable U2OS cells lines were subcultured onto two plates and maintained in puromycin (0.5 μg/mL) until a cell density of approximately 60%. One of the two plates was incubated with bleomycin (10 μg/mL) for 12 h before the replacement of the bleomycin-containing media with fresh growth media. Control and bleomycin treated cell lines were counted with a hemocytometer and plated in triplicate onto seven 96-well plates according to section 2.4.12. Each recovery day, one plate was harvested and processed. All plates were analyzed using CyQUANT® Cell Proliferation Assay Kit (section 2.4.12) on the seventh recovery day. Raw data obtained from the BMG LABTECH POLARstar® Omega microplate reader were converted into percent growth quantities to normalize the data and graphed with standard deviation bars calculated using Microsoft Excel (Figure 4.6). A one-way ANOVA analysis was performed using the StatPlus application in order to determine any significant variance within the percentage of proliferation of the three cell lines for each recovery day. Once significant variance was established within the three samples, a two-tailed t-test was performed to compare two cell lines at a time in order to determine which of the three cell lines expressed the alteration in percent growth. The growth curves of the samples maintained under standard conditions demonstrated no pattern of significant variance within the cell lines. The ANOVA analysis for variations between the percent growth rates of U2OS cell lines exposed to bleomycin divulged that from day 1-3 there was no variance in cell proliferation but from day 4-7 there is a steady increase in the statistically significant variance within the cell lines. A t-test established that pCDH1 and F6 had no statistically significant difference between each other. However, the t-test found that U2OS cells expressing F1 showed a marked difference to the growth percentages of pCDH1 and F6. This indicates that the ectopic expression of F1 has an inhibitory effect on cell proliferation after induction of DSBs with the chemotherapeutic drug bleomycin. ANOVA and t-test result are located in Appendix Table A2.3 – A2.12.

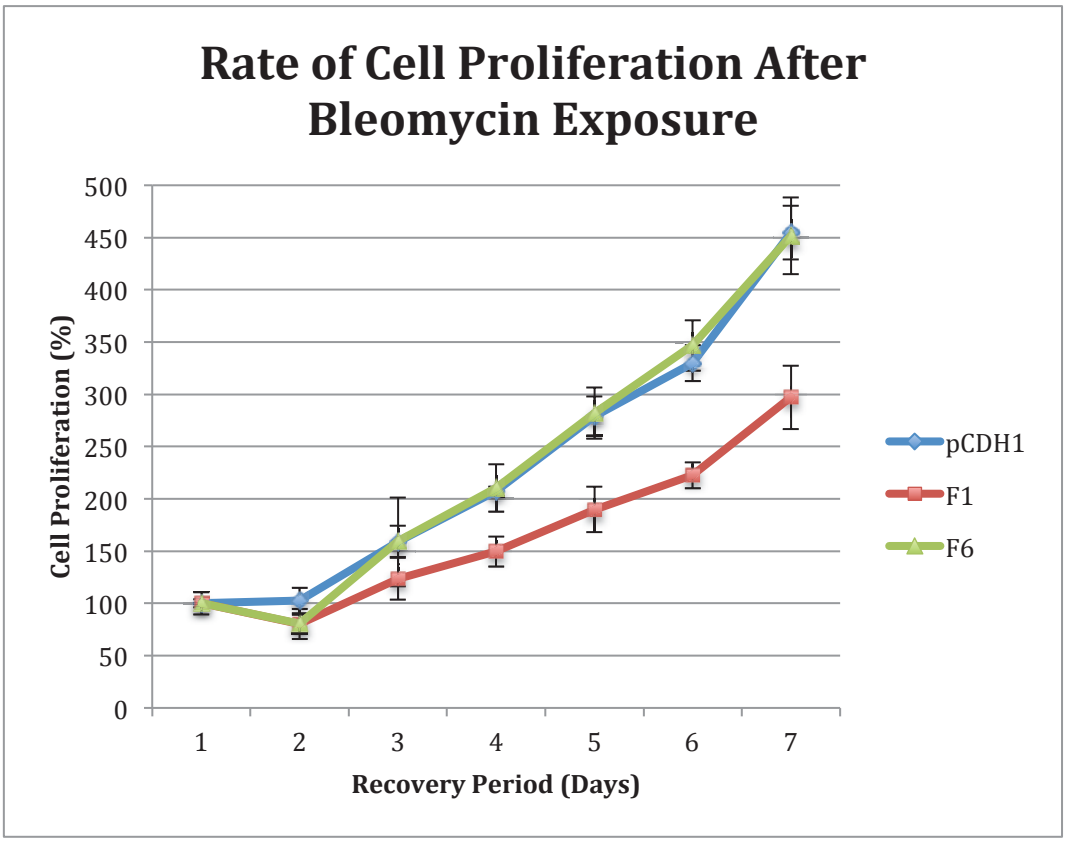
Rate of Cell Proliferation After Bleomycin Exposure
Cell Proliferation (%)
500
450
400
350
300
250
200
150
100
50
0
1
2
3
4
5
6
7
Recovery Period (Days)
pCDH1
F1
F6

A

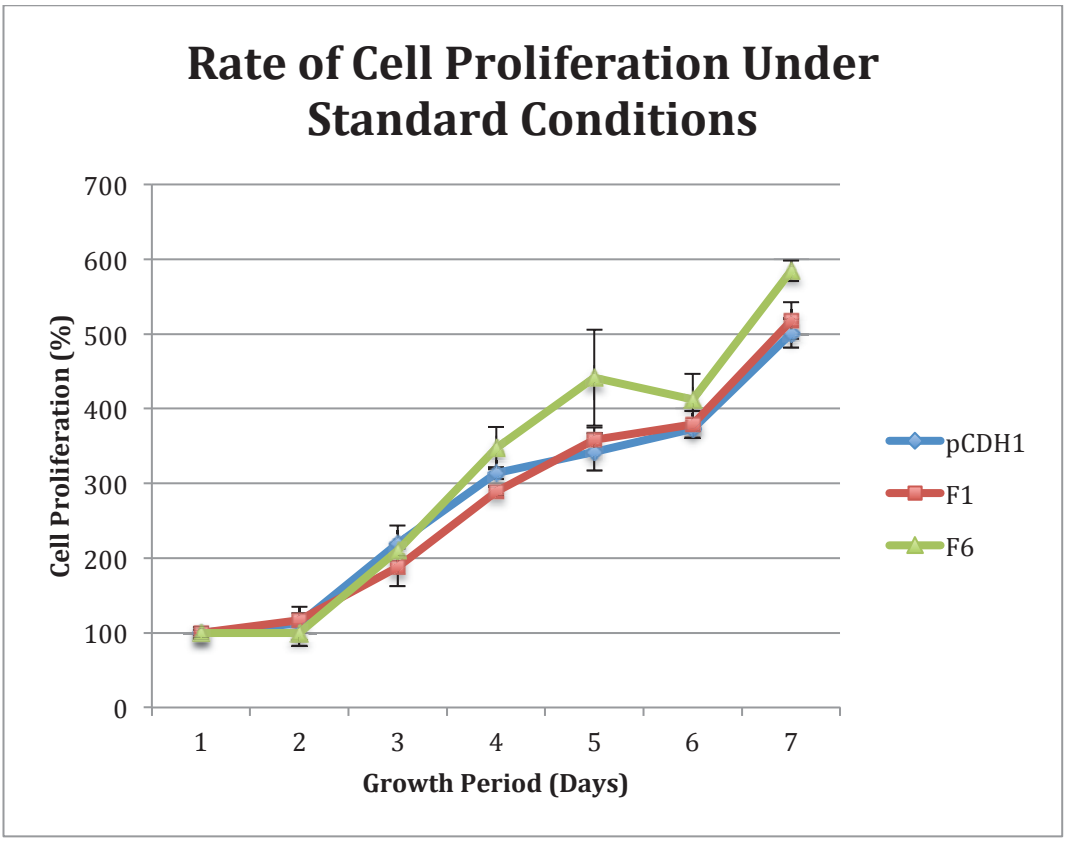
Rate of Cell Proliferation Under Standard Conditions
Cell Proliferation (%)
700
600
500
400
300
200
100
0
1
2
3
4
5
6
7
Growth Period (Days)
pCDH1
F1
F6

B

Figure 4.6 Rate of cell proliferation of U2OS stable cell lines expressing pCDH1 empty vector, F1, or F6. Three stable U2OS cell lines previously infected with lentivirus containing either pCDH1, pCDH1-F1, or pCDH1-F6 were analyzed for a seven day recovery period either after a treatment with bleomycin (10 μg/mL) or under standard conditions. Fluorescence data was normalized as a percentage of fluorescence from day 1 to the remaining days of recovery. The measurement of fluorescence is directly correlated to the amount of DNA present in a sample and thus, the percentage difference can be used as a value to determine percent growth. All samples for the first day were considered to be at 100% survival and the following days were calculated according to that pretense. Error bars represent ±SD. A) U2OS cell lines that were exposed to bleomycin before the seven-day recovery showed a statistically significant difference between cells expressing F1 when compared to pCDH1 and F6. B) There was no great statistical difference between any of the cell lines when grown under standard conditions with no bleomycin treatment with no trend to indicate one cell line grew more efficiently or poorly than another.

4.2 Discussion

The PIKK family members ATM and TRRAP share many conserved structural features. This insinuates that there is potential for a functional interaction between p400 and ATM similar to that between p400 and TRRAP. Previous work demonstrated a direct association between p400 and ATM with the N-terminus of p400 demonstrating the most robust ability to bind and co-immunoprecipitate ATM.

4.2.1 Effect of N-terminal p400 fragments on ATM activity and γH2AX phosphorylation

In order to deduce if the expression of the N-terminal fragments of p400 (F1, F2, and F3) have any functional effect on the activation of ATM or its phosphorylation of H2AX during DNA repair, an ATM activation assay was designed. Stable U2OS cell lines produced through infection with lentiviral particles containing pCDH1, pCDH1-F1, pCDH1-F2 or pCDH1-F3 constructs were incubated with the chemotherapeutic drug bleomycin for 1 h and allowed a recovery period of 0, 1, 3, or 7 h. A control sample of each cell line was also investigated in order to elucidate basal phosphorylation states of both ATM and H2AX. Analysis of P-ATM, an indicator of ATM activation, revealed that the phosphorylation state of ATM during DNA damage and repair is not altered by the ectopic expression of any of the p400 fragments examined or by the presence of the empty vector pCDH1. This was shown by the

concentration pattern of the bands representing P-ATM, where the phosphorylation level of ATM at time points over the recovery period was comparable between all four stable U2OS cell lines, F1, F2, F3 and empty pCDH1 (Figure 4.5). As a result, it can be inferred that F1, F2, and F3 do not affect the activation of ATM. However, there was an observed difference between the ability of some cell lines to clear γH2AX, a substrate of ATM. U2OS cell line expressing F1 exhibited the most notable difference when compared to the other cell lines. F1-expressing cells continued to display persistent levels of γH2AX after 7 h of recovery while γH2AX in pCDH1 and F3 cell lines had returned to near-basal levels by that time point. Levels of γH2AX are expected to decrease fairly rapidly over the recovery period presumably because the DNA damage is being efficiently repaired. As a biomarker of DSBs, the persistent phosphorylation of H2Ax in the F1 U2OS cell line may indicate that the p400 fragment F1 is acting as an inhibitor of the DSB repair. Observations regarding F2 were inconclusive.

With the obtained data, the specific mechanism of the effect F1 has on DNA repair cannot be determined. The protocol was designed to use the phosphorylation of H2AX as an indicator of ATM activity with and expected reduction γH2AX of levels if ATM was impaired. However, persistence of yH2AX in cells ectopically expressing F1 was observed instead. It is also possible that ATM activity is being modified through interference of F1 and the phosphorylation of H2AX is a result the activity of other PIKK family members such as ATR and DNA-PKcs, which are able to phosphorylate H2AX during DSBs. Although this data is encouraging, conclusive results cannot be determined with confidence as this data could not be replicated. The assay was performed more than ten times with each trial demonstrating various complications. The first few attempts were spent optimizing the protocol and determining effective ways of normalizing the amount of total protein in the insoluble fraction. The number of samples also presented a challenge. The samples could not be run and transferred using the same SDS-PAGE and Western transfer apparatus, which encouraged differences in transference of proteins from the gel to the membranes due to disparities between the machines. Another complication came from the quantity of p400 protein fragments being expressed in the U2OS cell lines. The amount of F2 and F3 produced was so minimal that it is not possible to draw any conclusions as to whether these p400 protein fragments are able to alter ATM activity or phosphorylation of H2AX. This encourages the speculation that the low levels of expression may result in the false negative results.

Due to time constraints, it was determined that more attention should be focused on the other functional assays being examined concurrently.

4.2.2 Effect F1 ectopic expression on cell proliferation after induction of DSBs

It was of interest to the study to determine any potential increase in sensitivity to DNA damage in stable U2OS cell lines expressing F1, F2, F3, or F6. However, during the trials it was decided that only p400 fragments F1 and F6 would be examined. This was due to several factors: the first being the extremely low levels of expression of F2 and F3 and another determining aspect was the inferior growth rate detected during the subculturing of cell lines expressing F2 and F3 when compared to all other cell lines. This observation was supported in the preliminary cell proliferation assays of cell lines examined under standard conditions (data not shown for F2 and F3). It was postulated that the low expression and the inhibited growth rate could be due to toxic effects of the F2 and F3 protein fragments. If true, it is reasonable to assume that cells containing a high number of F2 or F3 DNA inserts would die while cells with fewer inserts or cells capable of inhibiting the CMV promoter would be favored for survival. Obstructing the CMV promoter and terminating F2 or F3 production would not alter puromycin resistance as this gene is under the influence of the EF1 promoter, allowing cell survival during selection and maintenance with puromycin. This would account for both the low expression levels as well as the inhibited cell growth immediately after selection with puromycin. This obstruction could potentially be eliminated through the use of an inducible switch. Protein expression could be reserved for the experimentation period rather than during puromycin selection and maintenance, reducing the potentially toxic effects of F2 and F3. Another influence was the results of the ATM activity assay. Neither F2 nor F3 showed any significant influence on the phosphorylation of H2AX, whether due to low expression or potentially their inability to alter DNA repair. As such, experimentation with these fragments was terminated. The assay became structured around F1 as a potential influencer of cell sensitivity to DNA damage with pCDH1 and F6 acting as control cell lines.

The bleomycin sensitivity assay was executed with freshly prepared stable U2OS cell lines (section 2.4.7) grown to a 60% confluence and incubated with bleomycin (10 μg/mL) for 12 h (section 2.4.12) before the replacement with bleomycin-free media. Samples were collected over a seven-day period and analyzed using the

CyQUANT® Cell Proliferation Assay Kit (section 2.4.12), which measures the quantity of cells through the detection of fluorescence. This is accomplished through the properties of the dye, which exhibits strong fluorescence enrichment when it is bound to DNA. Figure 4.6 represents one of two assays that revealed the most reliable data achieved from the sensitivity assay. In these data sets it was observed that cells ectopically expressing F1 demonstrated a reduced proliferation rate when compared to the control cell lines pCDH1 and F6 indicating that this cell line displays an increase in sensitivity to DNA damage presumably due to an inhibition of the DNA repair mechanism. This data was found to possess statistically variance through a one-way ANOVA analysis followed by a two tailed t-test where it was determined that F1 was statistically different from both pCDH1 and F6 with no statistically significant difference between pCDH1 and F6. A functional effect of F1 expression on cell growth rate after recovery from DNA damage with bleomycin suggests that the F1 fragment of p400 may be a novel means to explore the inner workings of DNA repair. However, no conclusive remarks can be made regarding the potential functional implications of p400 fragment F1, as the data obtained was not fully reproducible.

The majority of the assays were not comparable to each other due to the many necessary alterations to the protocol before a final method was established (Appendix 3). This included changes to the length of the recovery period, number of samples during the recovery period, number of cell lines used, and concentration of bleomycin during treatments. Another consequence of the protocol was the large propensity for uncontrollable variables and human error. The CyQUANT assay is a single endpoint fluorescence microscopy, meaning cells had to be terminated in order to determine the quantity in each sample. This required plating seven individual plates with triplicates of each cell line for both control and bleomycin-treated cells on each plate. Although a technique for plating even numbers of cells was developed and the standard deviation between triplicate samples vastly reduced, it was difficult to ensure that the cells in each plate were comparable to the cells in other plates. These potential differences between cell populations could have risen from slight variations during pipetting or as a consequence of microenvironments, in which each plate possesses unique variations compared to the other plates. This could potentially alter cell recovery and proliferation. Additionally, during the plate-harvesting step, the PBS rinse could dislodge cells unequally encouraging a reduction in the expected cell numbers. Furthermore, the CyQUANT assay also does not differentiate between healthy, senescent, or dead cells

as the CyQUANT dye binds to the DNA of all cells that have adhered to the surface of the well. This eliminates potential nuances regarding the state of the cells that could be paramount to elucidating the full functional effect of F1.

Modifications were made in order to reduce these sources of error but it is apparent from some trials that the chance for uncontrollable variables remained high, resulting in very few reliable data sets. In one example, the control U2OS cell line pCDH1 grows normally from day 1 to day 2 but then begins to decrease over the rest of the growth period while cells expressing F1 and F6 proliferate in an expected manner. Another example, possibly demonstrating microenvironments, shows the exact same spikes and dips in growth rate for the control cell line pCDH1 in both the bleomycin treated cells and the cells grown under standard conditions, which is not shown in any other data sets. It is highly unlikely that this pattern would be mirrored in both bleomycin treated cells and bleomycin-free cells as both of these populations were plated from different stocks of cells. From this same data set, F1 and F6 cells also seem to mirror a pattern of increased and decreased growth rate between cells incubated with bleomycin versus control cells although not as apparent as pCDH1.

An ulterior method to perform a sensitivity assay by measuring the rate of cell proliferation could be accomplished through the xCELLigence system by ACEA Biosciences, Inc. This methodology allows for dynamic, real-time monitoring of cell proliferation and viability of adherent cells without the use of labels such as fluorescent dyes. This technique uses an electronic readout termed “impedance to non-invasively quantify adherent cell proliferation and viability in real time”. The cells are seeded onto standard microplates fitted with microelectronic sensor arrays. When the cells interact with the electronic biosensors, a cell-electrode impedance response is generated. This correlates to cell viability as well as the number of cells in the well. Through continuous, real-time monitoring, an kinetic record of the cells can provide information regarding the biological state of the cell, such as enhanced cell growth, cell quiescence, morphological changes, or cell death [181].

Although no conclusive remarks can be made regarding the result from either assay individually, a trend emerges in regards to the functional effect of p400 fragment F1 on DNA repair when the two are evaluated together. F1 causes persistence in γH2AX after DSB induction by bleomycin, indicating that the cells are unable to repair the damage efficiently and clear γH2AX from the break site. At the same time, ectopically expressed F1 causes a reduction in the proliferation rate after an onslaught

of DSB by bleomycin with no apparent growth retardation observed in control samples free from bleomycin treatment. This was speculated to be a consequence of impaired DNA repair functions. F1 was shown to have no effect on the activation of ATM, however a direct association of F1 with ATM could result in inhibition of other aspects of ATM function. This includes, but is not limited to, the potential role of ATM as a recruiter of p400 to the break site. ATM is one of the first responders to DNA damage, an association between ATM and p400 would allow for rapid and early recruitment of p400 activity to the break site. This is supported a previous observation where loss of ATM reduces or postpones histone loss at sites of DSBs [182]. Examination of the literature indicates that the interaction of F1 with ATM could also interfere with protein-protein associations with other repair proteins such as Rad51, a repair protein with several roles during HR repair, indicated in two separate studies. ATM knockout cells showed a decrease in the formation of Rad51 foci while p400 depletion resulted in Rad51 foci formation delay [158, 183]. A clear functional role for F1 during DNA repair remains elusive but with further work F1 may prove to be a potential target for study.

5 Summary and Future Directions

5.1 Summary

DNA double strand breaks are one of the most cytotoxic lesions to DNA. A cell's ability to effectively repair this damage and avoid genetic instability involves the orchestration of a plethora of repair proteins. These proteins have a variety of functions in the DNA repair mechanism and any disruption to one or more of the proteins or their roles can instigate catastrophic consequences. This study aimed to examine two key proteins of DNA repair; ATM, a serine/threonine kinase of the PIKK family, and p400, an ATPase chromatin remodeler.

In a previous study, ATM was shown to interact with full-length p400 as well as constructed N-terminal derivatives of p400 *in vivo*. In order to eliminate the possibility of an interaction due to mammalian bridging proteins, a GST pull-down assay was performed using the six GST-FLAG-tagged p400 derivatives expressed using *E. coli* BL21 cells and whole cell lysate from insect Sf9 cells expressing ATM. The majority of GST-p400 fragment protein produced seemed to be degraded and therefore no which sufficient quantities could be obtained for the GST pull-down assay. That impediment was compounded with the inability to produce adequate quantities of ATM. Nonetheless, the GST pull-down assay was executed with the samples obtained, but failed to elucidate a direct interaction between ATM and any of the six p400 derivatives. This could be due to the low quantities of protein produced and thus, no conclusive results can be drawn.

With support from previous studies, functional analysis of these proteins was performed. These analyses were executed in order to investigate if stable expression of any of the p400 derivatives in human U2OS cells is able to instigate a functional effect during DNA damage repair. In both assays, DSBs were induced through exposure to bleomycin. To determine possible alterations to ATM activation or ATM kinase activity, samples were examined for changes in the phosphorylation status of ATM and its substrate H2AX, a biomarker of DNA damage. None of the fragments appeared to be capable of interfering with the autophosphorylation activation of ATM. The N-terminal p400-fragment F1, however, caused persistence of γH2AX during the recovery period after DSB induction. This persistence is indicative of either an inability to clear γH2AX

from break sites or an inhibition of the DNA repair mechanism. Additionally, U2OS cells ectopically expressing F1 showed a reduction in proliferation rate post-bleomycin incubation with no alterations in the growth rate of cells maintained in standard conditions when compared to control cell lines. This is suggestive of an inability to efficiently repair damaged DNA. Taken together, it is reasonable to insinuate that F1 is acting as an inhibitor in some process of DNA repair, potentially as an interferer of essential protein-protein interactions.

Review of the literature indicates that F1 may be interfering with efficient recruitment of repair proteins by occupying a protein-protein interaction domain of ATM. The FATC domain of the PIKK family members ATR, DNA-PKcs, and TRRAP can replace the homologous domain in ATM and sufficiently retain ATM functionality [98]. This domain is known to be critical for protein-protein interactions. The structural similarity between ATM and TRRAP, as well as the described association between TRRAP and p400, indicates that F1 contains a potential binding region. ATM is responsible for the recruitment of many repair proteins to DSBs. When ATM is depleted, the formation of the Rad51 repair protein foci is decreased [183]. The persistence of γH2AX implies that an interference with ATM protein-protein interactions may effect the shuttling of chromatin remodelers such as p400 by ATM. While no conclusive discoveries can be made by this study, trends have emerged with the p400 fragment F1 as a potential inhibitor of DNA repair.

5.2 Limitations

There were several limitations encountered during this study. Time was by far the most limiting factor confronted. Production of the lentivirus used to infect U2OS cells and develop stable cell lines expressing p400 fragments came to a sudden halt during the functional assays. After troubleshooting lentivirus could be produced again. A mycoplasma infection was discovered in the U2OS cell lines. An infection with mycoplasma can alter protein expression and cellular functions, making any results obtained from assays with cells potentially infected with mycoplasma unreliable. When this was discovered, HEK239T packaging cells were replaced with HEK293T cells from another lab and U2OS cells were treated with Plasmocin^{TM} an antimycoplasma reagent that combines a macrolide and a quinolone. Electroporation could have been

used as an alternate mechanism by which to integrate the pCDH1-p400 derivative constructs into the U2OS cells.

The passage number and age of cells used varied due to the time interval between trials. These variations can cause differences in protein composition and genetic homogeneity [184]. Continuous culture of cell lines can create a propensity for genetic drift. This can produce inconsistent results between assays, preventing a confident comparison between data obtained.

Repair of DNA damage requires a multitude of pathways and mechanisms that often contain redundancies within each other. In particular to this study, the phosphorylation of H2AX is a marker for DSB sites and is accomplished through the kinase activity of ATM, ATR, and DNA-PKcs [51, 185]. Thus, enzymes other than ATM may have been responsible for the phosphorylation of H2AX in the examination of ATM activity rather than ATM itself, potentially concealing an inhibition of ATM activity.

5.3 Future Directions

Further work should be performed in order to establish conclusive evidence supporting the role of F1 as an inhibitor of ATM protein-protein interactions and DNA repair mechanism. In addition, the assays executed in this study should be attempted with the modifications suggested.

5.3.1 Confirmation of in vitro interaction between ATM and p400 derivatives

This study aimed to confirm the direct association of the N-terminal fragments of p400 and ATM. This was attempted in an *in vitro* environment through the use of a GST pull-down assay. Unfortunately, the GST-fused p400 derivatives could not be produced in significant quantities. Levels of ATM in Sf9 cell lysates were also lower than the applicable amount needed for a GST pull-down assay. Modifications to the protocol mentioned in section 3.5 could potentially be sufficient to increase the obtained quantities and allow the successful performance of this assay. Furthermore, the production of ATM could be improved by various means. ATM cannot be expressed as a full size protein in *E. coli* BL21 cells due to its large size so insect Sf9 cells were used to produce ATM. Whole Sf9 cell lysates were used in the GST pull down assay. This whole cell lysate could potentially contain proteins able to act as bridging proteins

between p400 and ATM. Isolating ATM from the solution rather than using a whole cell lysate may achieve more reliable results.

This study was based off of previous work that investigated the interaction of p400 and ATM through their overexpression in human HEK293T and insect Sf9 cells. Over-expressing proteins can often cause false interactions due to the large quantities of protein being produced. This research project was unable to confirm a direct association between p400 fragments and ATM *in vitro* due to several confounding factors. As a result, there is chance that p400 and ATM may not truly exhibit and interaction. Thus, it is essential to be able to conclusively demonstrate a direct binding between the p400 N-terminal fragments and ATP. Due to the size of ATM and apparent instability of the p400 fragments, an *in vivo* examination may be the only was in which to show direct interaction. This would involve immunoprecipitation of endogenously expressed proteins with each other. Currently there are no suitable antibodies to perform this analysis.

5.3.2 Confocal imaging to elucidate γH2AX phosphorylation and protein localization

Examination of γH2AX persistence via immunofluorescence microscopy via immunofluorescence with U2OS cells infected with pCDH1 had commenced towards the end of this study (Figure A1.2). Continuation of this analysis would have proceeded with U2OS cells ectopically expressing F1 and F6 once the protocol had been optimized.

The pCDH1 stable cell line was seeded onto coverslips according to section 2.4.15.1 and processed as per section 2.4.15.2. A control sample with no bleomycin exposure was used to detect basal levels of γH2AX. Optimization of cell processing as well as concentration and administration of primary and secondary antibodies were underway when the argon (488 nm) laser of the confocal microscope became non-operational. Before this malfunction, several attempts with the control cell line were examined, with no apparent alteration in the phosphorylation of H2AX after induction of DSBs through bleomycin exposure (data not shown). Although the examination was not complete, confocal microscopy to elucidate the phosphorylation state of H2AX in stable cell lines after exposure to bleomycin is a promising mechanism in which to visualize the effect of F1 expression on DNA repair within a cellular system.

Additionally, examination of γH2AX can be tested in conjunction with observations regarding the localization of ATM as well as other potential ATM binding partners with the used of specific antibodies. This could potentially identify discrepancies between cell lines regarding the localization of key proteins during the DNA damage in response to F1 expression response. Some potential candidate protein targets would include p400, Rad51, and MDC1, which are all either knows or suspected binding partners of ATM and the current literature supports a prospective role of ATM as a shuttle to bring these proteins to DSB foci [77, 123, 183].

5.3.3 Examination of F1 functional effect on ATM in other human cell lines

The original purpose for this study was to examine the effect of N-terminal p400 fragments on ATM activity in order to elucidate a potential pharmacological target for development of a novel cancer therapy. It was theorized that expression of one of the N-terminal derivatives in cancer cells could inhibit the DNA repair mechanism by altering the activity of ATM. Although derived from osteosarcoma cancer cells, the U2OS cell line contains minimal alterations to both the metabolic pathways and DNA repair mechanisms of the cell, making them very similar to normal human cells and the reason behind why this cell line was chosen for examination. However, it would be of interest to determine if the inhibition of DNA repair observed during the ectopic expression of F1 is maintained in other cancer cell lines that may contain more dramatic alterations to DNA repair system and its machinery. Expressing a sensitization to DNA damage by the ectopic expression of F1 across multiple cell lines could help to establish F1 as a promising contender for the inhibition of cancer cell proliferation and potentially useful as a means to further explore the inner workings of the DNA damage repair system.

5.3.4 Competition assay between p400 and p400 N-terminal derivatives for ATM

The findings of this study imply a potential role for the p400 fragment F1 as an inhibitor of ATM protein-protein interactions, with the ATM-p400 association of particular interest. A competition assay testing the ability of p400 to co-immunoprecipitate ATM during the ectopic expression of F1 compared to control cells could demonstrate the proposed interference ability of F1. Control cell lines and stable cell lines expressing F1 could be transiently transfected with HA-p400 and subjected to immunoprecipitation using α-HA antibody-conjugated beads. Reduced levels of ATM

co-immunoprecipitated from F1 expressing cells compared to control cells would be indicative of F1 interference of the ATM-p400 protein-protein interaction and γH2AX clearance process, which would also support the notion of ATM as a potential shuttle for p400 to the break site. Investigation of the potential interference of F1 to other ATM binding proteins such as Rad51 could also help elucidate the full effect F1 has on ATM and the DNA repair mechanism. As previously mentioned, formation of the Rad51 foci is deterred when either ATM or p400 is knocked down [158, 183]. A reduction in the formation of the Rad51 foci may be causative of γH2AX persistence, as the DNA will not be repaired efficiently. Elucidating if F1 expression interferes with the ATM-Rad51 association could shed light on other potential means by which F1 alters DNA repair through blocking protein-protein interactions of ATM. The same assay can also be used to elucidate if F1 inhibits TRRAP association with p400. The structural similarities between ATM and TRRAP, an identified binding partner of p400, imply F1 expression may also affect the TRRAP-p400 interaction and the functional activities of the Tip60/p400 complex during DNA repair.

5.3.5 Examination of F2 and F3 under inducible promoters

Expression levels of F2 and F3 were significantly lower than that of the other p400 protein fragments. U2OS cells ectopically expressing these two protein derivatives showed a marked decrease in cellular proliferation under standard conditions, indicating a probable toxic effect of these fragments. F1, F2 and F3 were all shown to have a strong interaction with ATM in a co-immunoprecipitation assay [77]. It was also observed that F2 and F3 levels of expression during transient transfection were far greater than during long-term stable expression, arguing for a preferential selection for cells expressing lower levels of these derivatives. One way in which to examine these fragments further with expression levels comparable to that of F1 and F6 is to regulate their expression through the use of an inducible switch. This would allow for the controlled expression of these fragments during the trail period.

Another interesting application of an inducible promoter would be an examination of expressing F2 and F3 on cell proliferation through the use of the xCELLigence real-time and dynamic monitoring system. Control cell lines and cell lines infected with lentiviral constructs carrying F2 or F3 under the control of an inducible promoter could be monitored in real time either under induction or suppression conditions, giving a

comparison of the rate of cell proliferation and biological states such as cell quiescence, morphological deviations, and cell death. Induction of the promoter could also take place during the first or last half of the trial period in order to determine how quickly alterations to the cellular systems can be recovered from or stimulated. F2 and F3 appear to have a significant effect on cellular mechanisms when ectopically expressed and could be potential targets for future study.

5.4 Conclusion

Although this study failed to produce conclusive results, a potential role for the p400 N-terminal derivative F1 as an inhibitor of DNA repair has been revealed. Both p400 and ATM have been shown to play critical roles in DNA damage repair and other cellular functions. The understanding of the inner workings of p400 and ATM in response to one another and identification of key domains of p400 in which ATM has a direct association may help to elucidate the mechanisms behind DNA repair. In addition, further research into the N-terminal fragments of p400 may provide for a novel target in the pursuit of innovative pharmacological treatments for cancer therapies in order to develop a more precise and efficient cancer therapy treatment.

6 References

1. Hoeijmakers , J.H.J., *DNA Damage, Aging, and Cancer.* New England Journal of Medicine, 2009. **361**(15): p. 1475-1485.
2. Ciccia, A. and S.J. Elledge, *The DNA damage response: making it safe to play with knives.* Mol Cell, 2010. **40**(2): p. 179-204.
3. Eriksson, D. and T. Stigbrand, *Radiation-induced cell death mechanisms.* Tumour Biol, 2010. **31**(4): p. 363-72.
4. Kuroda, S., Y. Urata, and T. Fujiwara, *Ataxia-telangiectasia mutated and the Mre11-Rad50-NBS1 complex: promising targets for radiosensitization.* Acta Med Okayama, 2012. **66**(2): p. 83-92.
5. Campos, E.I. and D. Reinberg, *Histones: annotating chromatin.* Annu Rev Genet, 2009. **43**: p. 559-99.
6. Luger, K., et al., *Crystal structure of the nucleosome core particle at 2.8 A resolution.* Nature, 1997. **389**(6648): p. 251-60.
7. Robinson, P.J.J., et al., *EM measurements define the dimensions of the "30-nm" chromatin fiber: Evidence for a compact, interdigitated structure.* Proceedings of the National Academy of Sciences, 2006. **103**(17): p. 6506-6511.
8. Canzio, D., et al., *Chromodomain-mediated oligomerization of HP1 suggests a nucleosome-bridging mechanism for heterochromatin assembly.* Mol Cell, 2011. **41**(1): p. 67-81.
9. Luger, K., M.L. Dechassa, and D.J. Tremethick, *New insights into nucleosome and chromatin structure: an ordered state or a disordered affair?* Nat Rev Mol Cell Biol, 2012. **13**(7): p. 436-447.
10. Weber, C.M. and S. Henikoff, *Histone variants: dynamic punctuation in transcription.* Genes & Development, 2014. **28**(7): p. 672-682.
11. Kouzarides, T., *Chromatin modifications and their function.* Cell, 2007. **128**(4): p. 693-705.
12. Li, B., M. Carey, and J.L. Workman, *The role of chromatin during transcription.* Cell, 2007. **128**(4): p. 707-19.
13. Barski, A., et al., *High-resolution profiling of histone methylations in the human genome.* Cell, 2007. **129**(4): p. 823-37.
14. Guenther, M.G., et al., *A chromatin landmark and transcription initiation at most promoters in human cells.* Cell, 2007. **130**(1): p. 77-88.
15. Robinson, P.J., et al., *30 nm chromatin fibre decompaction requires both H4-K16 acetylation and linker histone eviction.* J Mol Biol, 2008. **381**(4): p. 816-25.
16. Shogren-Knaak, M., et al., *Histone H4-K16 acetylation controls chromatin structure and protein interactions.* Science, 2006. **311**(5762): p. 844-7.
17. de Wit, E., F. Greil, and B. van Steensel, *High-resolution mapping reveals links of HP1 with active and inactive chromatin components.* PLoS Genet, 2007. **3**(3): p. e38.
18. Fischle, W., et al., *Regulation of HP1-chromatin binding by histone H3 methylation and phosphorylation.* Nature, 2005. **438**(7071): p. 1116-22.
19. Peng, J.C. and G.H. Karpen, *Epigenetic regulation of heterochromatic DNA stability.* Curr Opin Genet Dev, 2008. **18**(2): p. 204-11.
20. Pokholok, D.K., et al., *Genome-wide map of nucleosome acetylation and methylation in yeast.* Cell, 2005. **122**(4): p. 517-27.

21. Sarcinella, E., et al., *Monoubiquitylation of H2A.Z distinguishes its association with euchromatin or facultative heterochromatin.* Mol Cell Biol, 2007. **27**(18): p. 6457-68.
22. Draker, R., E. Sarcinella, and P. Cheung, *USP10 deubiquitylates the histone variant H2A.Z and both are required for androgen receptor-mediated gene activation.* Nucleic Acids Res, 2011. **39**(9): p. 3529-42.
23. Eberharter, A. and P.B. Becker, *ATP-dependent nucleosome remodelling: factors and functions.* J Cell Sci, 2004. **117**(Pt 17): p. 3707-11.
24. Eisen, J.A., K.S. Sweder, and P.C. Hanawalt, *Evolution of the SNF2 family of proteins: subfamilies with distinct sequences and functions.* Nucleic Acids Res, 1995. **23**(14): p. 2715-23.
25. Cairns, B.R., *Chromatin remodeling: insights and intrigue from single-molecule studies.* Nat Struct Mol Biol, 2007. **14**(11): p. 989-96.
26. Fan, H.Y., et al., *Distinct strategies to make nucleosomal DNA accessible.* Mol Cell, 2003. **11**(5): p. 1311-22.
27. Saha, A., J. Wittmeyer, and B.R. Cairns, *Chromatin remodelling: the industrial revolution of DNA around histones.* Nat Rev Mol Cell Biol, 2006. **7**(6): p. 437-447.
28. Clapier, C.R. and B.R. Cairns, *The biology of chromatin remodeling complexes.* Annu Rev Biochem, 2009. **78**: p. 273-304.
29. Jin, J., et al., *In and out: histone variant exchange in chromatin.* Trends Biochem Sci, 2005. **30**(12): p. 680-7.
30. Talbert, P.B. and S. Henikoff, *Histone variants--ancient wrap artists of the epigenome.* Nat Rev Mol Cell Biol, 2010. **11**(4): p. 264-75.
31. Chan, H.M., et al., *The p400 E1A-associated protein is a novel component of the p53 --> p21 senescence pathway.* Genes Dev, 2005. **19**(2): p. 196-201.
32. West, M.H. and W.M. Bonner, *Histone 2A, a heteromorphous family of eight protein species.* Biochemistry, 1980. **19**(14): p. 3238-45.
33. Hardy, S., et al., *The euchromatic and heterochromatic landscapes are shaped by antagonizing effects of transcription on H2A.Z deposition.* PLoS Genet, 2009. **5**(10): p. e1000687.
34. Wong, M.M., L.K. Cox, and J.C. Chrivia, *The chromatin remodeling protein, SRCAP, is critical for deposition of the histone variant H2A.Z at promoters.* J Biol Chem, 2007. **282**(36): p. 26132-9.
35. Goldman, J.A., J.D. Garlick, and R.E. Kingston, *Chromatin remodeling by imitation switch (ISWI) class ATP-dependent remodelers is stimulated by histone variant H2A.Z.* J Biol Chem, 2010. **285**(7): p. 4645-51.
36. Suto, R.K., et al., *Crystal structure of a nucleosome core particle containing the variant histone H2A.Z.* Nat Struct Biol, 2000. **7**(12): p. 1121-4.
37. Luk, E., et al., *Stepwise histone replacement by SWR1 requires dual activation with histone H2A.Z and canonical nucleosome.* Cell, 2010. **143**(5): p. 725-36.
38. Viens, A., et al., *Analysis of human histone H2AZ deposition in vivo argues against its direct role in epigenetic templating mechanisms.* Mol Cell Biol, 2006. **26**(14): p. 5325-35.
39. Valdes-Mora, F., et al., *Acetylation of H2A.Z is a key epigenetic modification associated with gene deregulation and epigenetic remodeling in cancer.* Genome Res, 2012. **22**(2): p. 307-21.
40. Dryhurst, D., et al., *Characterization of the histone H2A.Z-1 and H2A.Z-2 isoforms in vertebrates.* BMC Biol, 2009. **7**: p. 86.

41. Binda, O., et al., *SETD6 monomethylates H2AZ on lysine 7 and is required for the maintenance of embryonic stem cell self-renewal.* Epigenetics, 2013. **8**(2): p. 177-83.
42. Pinto, D.M. and A. Flaus, *Structure and function of histone H2AX.* Subcell Biochem, 2010. **50**: p. 55-78.
43. Stucki, M., et al., *MDC1 directly binds phosphorylated histone H2AX to regulate cellular responses to DNA double-strand breaks.* Cell, 2005. **123**(7): p. 1213-26.
44. Yuan, J., R. Adamski, and J. Chen, *Focus on histone variant H2AX: to be or not to be.* FEBS Lett, 2010. **584**(17): p. 3717-24.
45. Downs, J.A., et al., *Binding of chromatin-modifying activities to phosphorylated histone H2A at DNA damage sites.* Mol Cell, 2004. **16**(6): p. 979-90.
46. Shroff, R., et al., *Distribution and dynamics of chromatin modification induced by a defined DNA double-strand break.* Curr Biol, 2004. **14**(19): p. 1703-11.
47. Xu, Y., et al., *The p400 ATPase regulates nucleosome stability and chromatin ubiquitination during DNA repair.* The Journal of Cell Biology, 2010. **191**(1): p. 31-43.
48. Bassing, C.H., et al., *Increased ionizing radiation sensitivity and genomic instability in the absence of histone H2AX.* Proc Natl Acad Sci U S A, 2002. **99**(12): p. 8173-8.
49. Celeste, A., et al., *H2AX haploinsufficiency modifies genomic stability and tumor susceptibility.* Cell, 2003. **114**(3): p. 371-83.
50. Kao, J., et al., *gamma-H2AX as a therapeutic target for improving the efficacy of radiation therapy.* Curr Cancer Drug Targets, 2006. **6**(3): p. 197-205.
51. Burma, S., et al., *ATM phosphorylates histone H2AX in response to DNA double-strand breaks.* J Biol Chem, 2001. **276**(45): p. 42462-7.
52. Rogakou, E.P., et al., *DNA double-stranded breaks induce histone H2AX phosphorylation on serine 139.* J Biol Chem, 1998. **273**(10): p. 5858-68.
53. Ward, I.M. and J. Chen, *Histone H2AX Is Phosphorylated in an ATR-dependent Manner in Response to Replicational Stress.* Journal of Biological Chemistry, 2001. **276**(51): p. 47759-47762.
54. Jiang, X., Y. Xu, and B.D. Price, *Acetylation of H2AX on lysine 36 plays a key role in the DNA double-strand break repair pathway.* FEBS Lett, 2010. **584**(13): p. 2926-30.
55. Stratton, M.R., P.J. Campbell, and P.A. Futreal, *The cancer genome.* Nature, 2009. **458**(7239): p. 719-24.
56. Halazonetis, T.D., V.G. Gorgoulis, and J. Bartek, *An oncogene-induced DNA damage model for cancer development.* Science, 2008. **319**(5868): p. 1352-5.
57. Bekker-Jensen, S., et al., *HERC2 coordinates ubiquitin-dependent assembly of DNA repair factors on damaged chromosomes.* Nat Cell Biol, 2010. **12**(1): p. 80-6; sup pp 1-12.
58. Stracker, T.H. and J.H. Petrini, *The MRE11 complex: starting from the ends.* Nat Rev Mol Cell Biol, 2011. **12**(2): p. 90-103.
59. de Jager, M., et al., *DNA-binding and strand-annealing activities of human Mre11: implications for its roles in DNA double-strand break repair pathways.* Nucleic Acids Research, 2001. **29**(6): p. 1317-1325.
60. Hopfner, K.P., et al., *Structural biochemistry and interaction architecture of the DNA double-strand break repair Mre11 nuclease and Rad50-ATPase.* Cell, 2001. **105**(4): p. 473-85.

61. Williams, R.S., et al., *Nbs1 flexibly tethers Ctp1 and Mre11-Rad50 to coordinate DNA double-strand break processing and repair.* Cell, 2009. **139**(1): p. 87-99.
62. Difilippantonio, S., et al., *Distinct domains in Nbs1 regulate irradiation-induced checkpoints and apoptosis.* J Exp Med, 2007. **204**(5): p. 1003-11.
63. Difilippantonio, S. and A. Nussenzweig, *The NBS1-ATM connection revisited.* Cell Cycle, 2007. **6**(19): p. 2366-70.
64. Falck, J., J. Coates, and S.P. Jackson, *Conserved modes of recruitment of ATM, ATR and DNA-PKcs to sites of DNA damage.* Nature, 2005. **434**(7033): p. 605-11.
65. Lee, J.H. and T.T. Paull, *ATM activation by DNA double-strand breaks through the Mre11-Rad50-Nbs1 complex.* Science, 2005. **308**(5721): p. 551-4.
66. Stracker, T.H., et al., *The carboxy terminus of NBS1 is required for induction of apoptosis by the MRE11 complex.* Nature, 2007. **447**(7141): p. 218-21.
67. Bhaskara, V., et al., *Rad50 adenylate kinase activity regulates DNA tethering by Mre11/Rad50 complexes.* Mol Cell, 2007. **25**(5): p. 647-61.
68. Derheimer, F.A. and M.B. Kastan, *Multiple roles of ATM in monitoring and maintaining DNA integrity.* FEBS Lett, 2010. **584**(17): p. 3675-81.
69. Uziel, T., et al., *Requirement of the MRN complex for ATM activation by DNA damage.* The EMBO Journal, 2003. **22**(20): p. 5612-5621.
70. Lee, J.H. and T.T. Paull, *Direct activation of the ATM protein kinase by the Mre11/Rad50/Nbs1 complex.* Science, 2004. **304**(5667): p. 93-6.
71. Bensimon, A., et al., *ATM-dependent and -independent dynamics of the nuclear phosphoproteome after DNA damage.* Sci Signal, 2010. **3**(151): p. rs3.
72. Matsuoka, S., et al., *ATM and ATR substrate analysis reveals extensive protein networks responsive to DNA damage.* Science, 2007. **316**(5828): p. 1160-6.
73. Mu, J.J., et al., *A proteomic analysis of ataxia telangiectasia-mutated (ATM)/ATM-Rad3-related (ATR) substrates identifies the ubiquitin-proteasome system as a regulator for DNA damage checkpoints.* J Biol Chem, 2007. **282**(24): p. 17330-4.
74. Stiff, T., et al., *ATM and DNA-PK function redundantly to phosphorylate H2AX after exposure to ionizing radiation.* Cancer Res, 2004. **64**(7): p. 2390-6.
75. Kobor, M.S., et al., *A protein complex containing the conserved Swi2/Snf2-related ATPase Swr1p deposits histone variant H2A.Z into euchromatin.* PLoS Biol, 2004. **2**(5): p. E131.
76. Kusch, T., et al., *Acetylation by Tip60 is required for selective histone variant exchange at DNA lesions.* Science, 2004. **306**(5704): p. 2084-7.
77. Smith, R.J., *ATM and p400: Charaterisation of a novel interaction between a DNA repair enzyme and a chromatin remodeler.* Massey Univeristy, Palmerston North, New Zealand, 2014. **Doctor of Philosophy in Biochemistry Thesis**.
78. Shrivastav, M., L.P. De Haro, and J.A. Nickoloff, *Regulation of DNA double-strand break repair pathway choice.* Cell Res, 2008. **18**(1): p. 134-47.
79. Takata, M., et al., *Homologous recombination and non-homologous end-joining pathways of DNA double-strand break repair have overlapping roles in the maintenance of chromosomal integrity in vertebrate cells.* The EMBO Journal, 1998. **17**(18): p. 5497-5508.
80. Lieber, M.R., *The mechanism of human nonhomologous DNA end joining.* J Biol Chem, 2008. **283**(1): p. 1-5.

81. Shinohara, A., H. Ogawa, and T. Ogawa, *Rad51 protein involved in repair and recombination in S. cerevisiae is a RecA-like protein.* Cell, 1992. **69**(3): p. 457-70.
82. Filippo, J.S., P. Sung, and H. Klein, *Mechanism of Eukaryotic Homologous Recombination.* Annual Review of Biochemistry, 2008. **77**(1): p. 229-257.
83. Li, X. and W.-D. Heyer, *Homologous recombination in DNA repair and DNA damage tolerance.* Cell Res, 2008. **18**(1): p. 99-113.
84. Perlman, S.L., et al., *Ataxia-telangiectasia.* Handb Clin Neurol, 2012. **103**: p. 307-32.
85. Lavin, M.F. and Y. Shiloh, *The genetic defect in ataxia-telangiectasia.* Annu Rev Immunol, 1997. **15**: p. 177-202.
86. Shiloh, Y., *ATM and related protein kinases: safeguarding genome integrity.* Nat Rev Cancer, 2003. **3**(3): p. 155-68.
87. Morrell, D., E. Cromartie, and M. Swift, *Mortality and cancer incidence in 263 patients with ataxia-telangiectasia.* J Natl Cancer Inst, 1986. **77**(1): p. 89-92.
88. Yuille, M.A. and L.J. Coignet, *The ataxia telangiectasia gene in familial and sporadic cancer.* Recent Results Cancer Res, 1998. **154**: p. 156-73.
89. Swift, M., et al., *Incidence of cancer in 161 families affected by ataxia-telangiectasia.* N Engl J Med, 1991. **325**(26): p. 1831-6.
90. Barlow, C., et al., *Atm-deficient mice: a paradigm of ataxia telangiectasia.* Cell, 1996. **86**(1): p. 159-71.
91. Elson, A., et al., *Pleiotropic defects in ataxia-telangiectasia protein-deficient mice.* Proc Natl Acad Sci U S A, 1996. **93**(23): p. 13084-9.
92. Xu, Y., et al., *Targeted disruption of ATM leads to growth retardation, chromosomal fragmentation during meiosis, immune defects, and thymic lymphoma.* Genes Dev, 1996. **10**(19): p. 2411-22.
93. Gao, Y., et al., *DNA repair gene polymorphisms and tobacco smoking in the risk for colorectal adenomas.* Carcinogenesis, 2011. **32**(6): p. 882-7.
94. Goldgar, D.E., et al., *Rare variants in the ATM gene and risk of breast cancer.* Breast Cancer Res, 2011. **13**(4): p. R73.
95. Prokopcova, J., et al., *The role of ATM in breast cancer development.* Breast Cancer Res Treat, 2007. **104**(2): p. 121-8.
96. Umesako, S., et al., *Atm heterozygous deficiency enhances development of mammary carcinomas in p53 heterozygous knockout mice.* Breast Cancer Res, 2005. **7**(1): p. R164-70.
97. Lovejoy, C.A. and D. Cortez, *Common mechanisms of PIKK regulation.* DNA Repair (Amst), 2009. **8**(9): p. 1004-8.
98. Jiang, X., et al., *The FATC domains of PIKK proteins are functionally equivalent and participate in the Tip60-dependent activation of DNA-PKcs and ATM.* J Biol Chem, 2006. **281**(23): p. 15741-6.
99. Young, D.B., et al., *Identification of domains of ataxia-telangiectasia mutated required for nuclear localization and chromatin association.* J Biol Chem, 2005. **280**(30): p. 27587-94.
100. Smith, J., et al., *The ATM-Chk2 and ATR-Chk1 pathways in DNA damage signaling and cancer.* Adv Cancer Res, 2010. **108**: p. 73-112.
101. Bakkenist, C.J. and M.B. Kastan, *DNA damage activates ATM through intermolecular autophosphorylation and dimer dissociation.* Nature, 2003. **421**(6922): p. 499-506.

102. Dupre, A., L. Boyer-Chatenet, and J. Gautier, *Two-step activation of ATM by DNA and the Mre11-Rad50-Nbs1 complex.* Nat Struct Mol Biol, 2006. **13**(5): p. 451-7.
103. Sun, Y., et al., *A role for the Tip60 histone acetyltransferase in the acetylation and activation of ATM.* Proc Natl Acad Sci U S A, 2005. **102**(37): p. 13182-7.
104. Sun, Y., et al., *Histone H3 methylation links DNA damage detection to activation of the tumour suppressor Tip60.* Nat Cell Biol, 2009. **11**(11): p. 1376-82.
105. Brown, K.D., et al., *The ataxia-telangiectasia gene product, a constitutively expressed nuclear protein that is not up-regulated following genome damage.* Proceedings of the National Academy of Sciences of the United States of America, 1997. **94**(5): p. 1840-1845.
106. Andegeko, Y., et al., *Nuclear retention of ATM at sites of DNA double strand breaks.* J Biol Chem, 2001. **276**(41): p. 38224-30.
107. Dar, I., et al., *Analysis of the ataxia telangiectasia mutated-mediated DNA damage response in murine cerebellar neurons.* J Neurosci, 2006. **26**(29): p. 7767-74.
108. Gately, D.P., et al., *Characterization of ATM expression, localization, and associated DNA-dependent protein kinase activity.* Mol Biol Cell, 1998. **9**(9): p. 2361-74.
109. Watters, D., et al., *Cellular localisation of the ataxia-telangiectasia (ATM) gene product and discrimination between mutated and normal forms.* Oncogene, 1997. **14**(16): p. 1911-21.
110. Shiotani, B. and L. Zou, *Single-stranded DNA orchestrates an ATM-to-ATR switch at DNA breaks.* Mol Cell, 2009. **33**(5): p. 547-58.
111. You, Z., et al., *Rapid activation of ATM on DNA flanking double-strand breaks.* Nat Cell Biol, 2007. **9**(11): p. 1311-8.
112. Richard, D.J., et al., *Single-stranded DNA-binding protein hSSB1 is critical for genomic stability.* Nature, 2008. **453**(7195): p. 677-81.
113. Jazayeri, A., et al., *Mre11-Rad50-Nbs1-dependent processing of DNA breaks generates oligonucleotides that stimulate ATM activity.* EMBO J, 2008. **27**(14): p. 1953-62.
114. Mazur, D.J. and F.W. Perrino, *Excision of 3' termini by the Trex1 and TREX2 3'->5' exonucleases. Characterization of the recombinant proteins.* J Biol Chem, 2001. **276**(20): p. 17022-9.
115. Yang, Y.G., T. Lindahl, and D.E. Barnes, *Trex1 exonuclease degrades ssDNA to prevent chronic checkpoint activation and autoimmune disease.* Cell, 2007. **131**(5): p. 873-86.
116. Thurn, K.T., et al., *Histone deacetylase regulation of ATM-mediated DNA damage signaling.* Mol Cancer Ther, 2013. **12**(10): p. 2078-87.
117. Soutoglou, E. and T. Misteli, *Activation of the cellular DNA damage response in the absence of DNA lesions.* Science, 2008. **320**(5882): p. 1507-10.
118. Kaidi, A. and S.P. Jackson, *KAT5 tyrosine phosphorylation couples chromatin sensing to ATM signalling.* Nature, 2013. **498**(7452): p. 70-4.
119. Canman, C.E., et al., *Activation of the ATM kinase by ionizing radiation and phosphorylation of p53.* Science, 1998. **281**(5383): p. 1677-9.
120. Jungmichel, S., et al., *The molecular basis of ATM-dependent dimerization of the Mdc1 DNA damage checkpoint mediator.* Nucleic Acids Res, 2012. **40**(9): p. 3913-28.

121. Liu, J., et al., *Structural mechanism of the phosphorylation-dependent dimerization of the MDC1 forkhead-associated domain.* Nucleic Acids Res, 2012. **40**(9): p. 3898-912.
122. Luo, K., J. Yuan, and Z. Lou, *Oligomerization of MDC1 protein is important for proper DNA damage response.* J Biol Chem, 2011. **286**(32): p. 28192-9.
123. Lou, Z., et al., *MDC1 maintains genomic stability by participating in the amplification of ATM-dependent DNA damage signals.* Mol Cell, 2006. **21**(2): p. 187-200.
124. Gatei, M., et al., *ATM protein-dependent phosphorylation of Rad50 protein regulates DNA repair and cell cycle control.* J Biol Chem, 2011. **286**(36): p. 31542-56.
125. Lim, D.S., et al., *ATM phosphorylates p95/nbs1 in an S-phase checkpoint pathway.* Nature, 2000. **404**(6778): p. 613-7.
126. Yuan, S.S., et al., *Neocarzinostatin induces Mre11 phosphorylation and focus formation through an ATM- and NBS1-dependent mechanism.* Toxicology, 2002. **177**(2-3): p. 123-30.
127. Bhatti, S., et al., *ATM protein kinase: the linchpin of cellular defenses to stress.* Cell Mol Life Sci, 2011. **68**(18): p. 2977-3006.
128. Geng, L., et al., *Artemis Links ATM to G(2)/M Checkpoint Recovery via Regulation of Cdk1-Cyclin B.* Molecular and Cellular Biology, 2007. **27**(7): p. 2625-2635.
129. Kastan, M.B. and D.S. Lim, *The many substrates and functions of ATM.* Nat Rev Mol Cell Biol, 2000. **1**(3): p. 179-86.
130. Xu, B., et al., *Two molecularly distinct G(2)/M checkpoints are induced by ionizing irradiation.* Mol Cell Biol, 2002. **22**(4): p. 1049-59.
131. Rashi-Elkeles, S., et al., *Transcriptional modulation induced by ionizing radiation: p53 remains a central player.* Mol Oncol, 2011. **5**(4): p. 336-48.
132. Reinhardt, H.C. and B. Schumacher, *The p53 network: cellular and systemic DNA damage responses in aging and cancer.* Trends Genet, 2012. **28**(3): p. 128-36.
133. Choi, M., et al., *Attractor landscape analysis reveals feedback loops in the p53 network that control the cellular response to DNA damage.* Sci Signal, 2012. **5**(251): p. ra83.
134. Sullivan, K.D., et al., *The p53 circuit board.* Biochim Biophys Acta, 2012. **1825**(2): p. 229-44.
135. Nakagawa, K., et al., *Requirement of ATM in phosphorylation of the human p53 protein at serine 15 following DNA double-strand breaks.* Mol Cell Biol, 1999. **19**(4): p. 2828-34.
136. Fuchs, M., et al., *The p400 complex is an essential E1A transformation target.* Cell, 2001. **106**(3): p. 297-307.
137. Ruhf, M.L., et al., *The domino gene of Drosophila encodes novel members of the SWI2/SNF2 family of DNA-dependent ATPases, which contribute to the silencing of homeotic genes.* Development, 2001. **128**(8): p. 1429-41.
138. Krogan, N.J., et al., *A Snf2 family ATPase complex required for recruitment of the histone H2A variant Htz1.* Mol Cell, 2003. **12**(6): p. 1565-76.
139. Mizuguchi, G., et al., *ATP-driven exchange of histone H2AZ variant catalyzed by SWR1 chromatin remodeling complex.* Science, 2004. **303**(5656): p. 343-8.
140. Aasland, R., A. Francis Stewart, and T. Gibson, *The SANT domain: a putative DNA-binding domain in the SWI-SNF and ADA complexes, the transcriptional*

corepressor N-CoR and TFIIIB. Trends in Biochemical Sciences. **21**(3): p. 87-88.
141. Ikura, T., et al., *Involvement of the TIP60 histone acetylase complex in DNA repair and apoptosis.* Cell, 2000. **102**(4): p. 463-73.
142. Park, J.H., X.-J. Sun, and R.G. Roeder, *The SANT Domain of p400 ATPase Represses Acetyltransferase Activity and Coactivator Function of TIP60 in Basal p21 Gene Expression.* Molecular and Cellular Biology, 2010. **30**(11): p. 2750-2761.
143. Doyon, Y., et al., *Structural and functional conservation of the NuA4 histone acetyltransferase complex from yeast to humans.* Mol Cell Biol, 2004. **24**(5): p. 1884-96.
144. Doyon, Y. and J. Cote, *The highly conserved and multifunctional NuA4 HAT complex.* Curr Opin Genet Dev, 2004. **14**(2): p. 147-54.
145. van Attikum, H., O. Fritsch, and S.M. Gasser, *Distinct roles for SWR1 and INO80 chromatin remodeling complexes at chromosomal double-strand breaks.* EMBO J, 2007. **26**(18): p. 4113-25.
146. Krogan, N.J., et al., *Regulation of chromosome stability by the histone H2A variant Htz1, the Swr1 chromatin remodeling complex, and the histone acetyltransferase NuA4.* Proc Natl Acad Sci U S A, 2004. **101**(37): p. 13513-8.
147. Gevry, N., et al., *p21 transcription is regulated by differential localization of histone H2A.Z.* Genes Dev, 2007. **21**(15): p. 1869-81.
148. Frank, S.R., et al., *MYC recruits the TIP60 histone acetyltransferase complex to chromatin.* EMBO Rep, 2003. **4**(6): p. 575-80.
149. Lu, J., et al., *A genome-wide RNA interference screen identifies putative chromatin regulators essential for E2F repression.* Proc Natl Acad Sci U S A, 2007. **104**(22): p. 9381-6.
150. Taubert, S., et al., *E2F-dependent histone acetylation and recruitment of the Tip60 acetyltransferase complex to chromatin in late G1.* Mol Cell Biol, 2004. **24**(10): p. 4546-56.
151. Gevry, N., et al., *Histone H2A.Z is essential for estrogen receptor signaling.* Genes Dev, 2009. **23**(13): p. 1522-33.
152. Tyteca, S., et al., *Tip60 and p400 are both required for UV-induced apoptosis but play antagonistic roles in cell cycle progression.* EMBO J, 2006. **25**(8): p. 1680-9.
153. Svotelis, A., N. Gevry, and L. Gaudreau, *Regulation of gene expression and cellular proliferation by histone H2A.Z.* Biochem Cell Biol, 2009. **87**(1): p. 179-88.
154. Toth, K., N. Brun, and J. Langowski, *Chromatin compaction at the mononucleosome level.* Biochemistry, 2006. **45**(6): p. 1591-8.
155. Ferreira, H., et al., *Histone tails and the H3 alphaN helix regulate nucleosome mobility and stability.* Mol Cell Biol, 2007. **27**(11): p. 4037-48.
156. Murr, R., et al., *Histone acetylation by Trrap-Tip60 modulates loading of repair proteins and repair of DNA double-strand breaks.* Nat Cell Biol, 2006. **8**(1): p. 91-9.
157. Bird, A.W., et al., *Acetylation of histone H4 by Esa1 is required for DNA double-strand break repair.* Nature, 2002. **419**(6905): p. 411-5.
158. Courilleau, C., et al., *The chromatin remodeler p400 ATPase facilitates Rad51-mediated repair of DNA double-strand breaks.* J Cell Biol, 2012. **199**(7): p. 1067-81.

159. Mattera, L., et al., *The p400/Tip60 ratio is critical for colorectal cancer cell proliferation through DNA damage response pathways.* Oncogene, 2009. **28**(12): p. 1506-17.
160. Mattera, L., et al., *The E1A-Associated p400 Protein Modulates Cell Fate Decisions by the Regulation of ROS Homeostasis.* PLoS Genet, 2010. **6**(6): p. e1000983.
161. Ueda, T., et al., *Critical role of the p400/mDomino chromatin-remodeling ATPase in embryonic hematopoiesis.* Genes Cells, 2007. **12**(5): p. 581-92.
162. Holmes, D.S. and M. Quigley, *A rapid boiling method for the preparation of bacterial plasmids.* Anal Biochem, 1981. **114**(1): p. 193-7.
163. Smith, D.B. and K.S. Johnson, *Single-step purification of polypeptides expressed in Escherichia coli as fusions with glutathione S-transferase.* Gene, 1988. **67**(1): p. 31-40.
164. Harper, S. and D.W. Speicher, *Purification of proteins fused to glutathione S-tranferase.* Methods in molecular biology (Clifton, N.J.), 2011. **681**: p. 259-280.
165. Loening, U.E., *The determinination of the molecular weight of ribonucleic acid by polyacrylamide-gel electrophoresis. The effects of changes in conformation.* Biochemical Journal, 1969. **113**(1): p. 131-138.
166. San-Miguel, T., P. Pérez-Bermúdez, and I. Gavidia, *Production of soluble eukaryotic recombinant proteins in E. coli is favoured in early log-phase cultures induced at low temperature.* SpringerPlus, 2013. **2**: p. 89.
167. Schein, C.H. and M.H.M. Noteborn, *Formation of Soluble Recombinant Proteins in Escherichia Coli is Favored by Lower Growth Temperature.* Nat Biotech, 1988. **6**(3): p. 291-294.
168. Hjelmeland, L.M., et al., *Electrophoresis in gels containing zwitterionic groups.* ELECTROPHORESIS, 1981. **2**(2): p. 82-90.
169. Carrio, M.M. and A. Villaverde, *Construction and deconstruction of bacterial inclusion bodies.* J Biotechnol, 2002. **96**(1): p. 3-12.
170. Hartley, D.L. and J.F. Kane, *Properties of inclusion bodies from recombinant Escherichia coli.* Biochem Soc Trans, 1988. **16**(2): p. 101-2.
171. Braun, P. and J. LaBaer, *High throughput protein production for functional proteomics.* Trends Biotechnol, 2003. **21**(9): p. 383-8.
172. Hartl, F.U. and M. Hayer-Hartl, *Molecular chaperones in the cytosol: from nascent chain to folded protein.* Science, 2002. **295**(5561): p. 1852-8.
173. Sorensen, H.P. and K.K. Mortensen, *Advanced genetic strategies for recombinant protein expression in Escherichia coli.* J Biotechnol, 2005. **115**(2): p. 113-28.
174. Buchan, J.R. and I. Stansfield, *Halting a cellular production line: responses to ribosomal pausing during translation.* Biol Cell, 2007. **99**(9): p. 475-87.
175. Li, G.-W., E. Oh, and J.S. Weissman, *The anti-Shine-Dalgarno sequence drives translational pausing and codon choice in bacteria.* Nature, 2012. **484**(7395): p. 538-541.
176. Chu, D., et al., *Translation elongation can control translation initiation on eukaryotic mRNAs.* EMBO J, 2014. **33**(1): p. 21-34.
177. Gasteiger, E.H., C.; Gattiker, A.; Duvaud, S.; Wilkins, M.R.; Appel, R.D.; Bairoch, A., *Protein Identification and Analysis Tools on the ExPASy Server.* John M. Walker (ed): The Proteomics Protocols Handbook, Human Press (2005), 2005: p. 571-607.
178. Kelley, L.A., et al., *The Phyre2 web portal for protein modeling, prediction and analysis.* Nat. Protocols, 2015. **10**(6): p. 845-858.

179. Lee, K., et al., *Decrease of p400 ATPase complex and loss of H2A.Z within the p21 promoter occur in senescent IMR-90 human fibroblasts.* Mechanisms of Ageing and Development, 2012. **133**(11–12): p. 686-694.
180. Goverdhana, S., et al., *Regulatable gene expression systems for gene therapy applications: progress and future challenges.* Mol Ther, 2005. **12**(2): p. 189-211.
181. Ke, N., et al., *The xCELLigence System for Real-Time and Label-Free Monitoring of Cell Viability*, in *Mammalian Cell Viability: Methods and Protocols*, J.M. Stoddart, Editor. 2011, Humana Press: Totowa, NJ. p. 33-43.
182. Berkovich, E., R.J. Monnat, Jr., and M.B. Kastan, *Roles of ATM and NBS1 in chromatin structure modulation and DNA double-strand break repair.* Nat Cell Biol, 2007. **9**(6): p. 683-90.
183. Chen, G., et al., *Radiation-induced assembly of Rad51 and Rad52 recombination complex requires ATM and c-Abl.* J Biol Chem, 1999. **274**(18): p. 12748-52.
184. Geraghty, R.J., et al., *Guidelines for the use of cell lines in biomedical research.* Br J Cancer, 2014. **111**(6): p. 1021-1046.
185. Heo, K., et al., *FACT-mediated exchange of histone variant H2AX regulated by phosphorylation of H2AX and ADP-ribosylation of Spt16.* Mol Cell, 2008. **30**(1): p. 86-97.

Appendix 1 Supplementary Figures

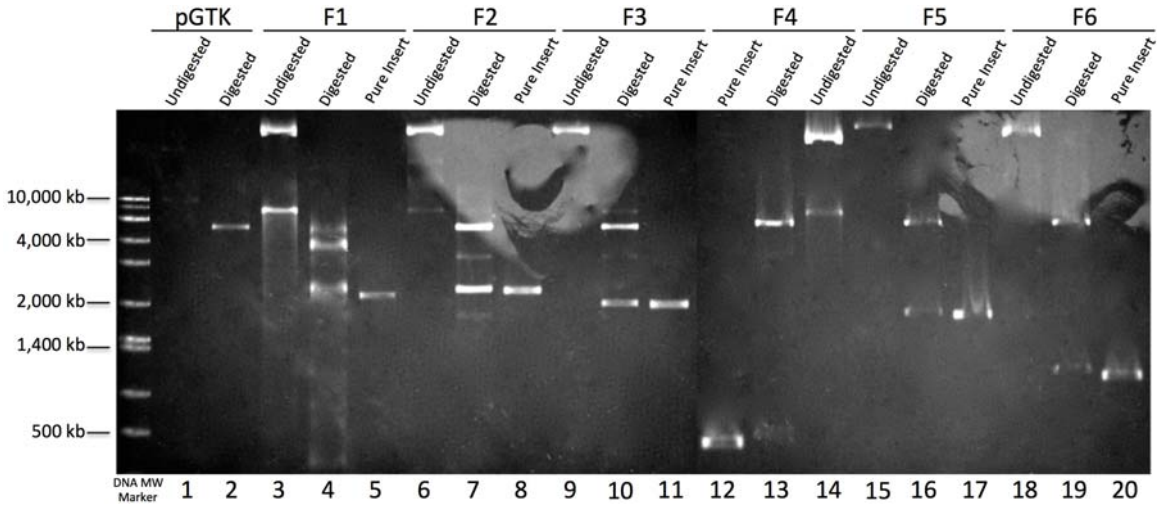

Figure A1.1 Confirmation digest of *E. coli* BL21 plasmids Restriction digests to cut and purify the FLAG-tagged-p400 fragment of interest from a CβF vector and insert into a pGTK vector with the GST preceding the N-terminus of the protein fragment. Plasmids were digested with BamHI and HindIII and resolved on a 1% (w/v) agarose gel in 1x TBE at 120 V for 1 h. Lane 1: pGTK control vector uncut, Lane 2: digested pGTK control vector, Lane 3: pGTK-p400-fragment 1 (pGTK-F1) uncut, Lane 4: digested pGTK-F1, Lane 5: F1 purified, Lane 6: pGTK-p400-fragment 2 (pGTK-F2) uncut, Lane 7: digested pGTK-F2, Lane 8: F2 purified, Lane 9: pGTK-p400-fragment 3 (pGTK-F3) uncut, Lane 10: digested pGTK-p400-F3, Lane 11: F3 purified, Lane 12: pGTK-p400-fragment 4 (pGTK-F4) uncut, Lane 13: digested pGTK-F4, Lane 14: F 4 purified, Lane 15: pGTK-p400-fragment 5 (pGTK-F5) uncut, Lane 16: digested pGTK-F5, Lane 17: F5 purified, Lane 18: pGTK-p400-fragment 6 (pGTK-F6) uncut, Lane 19: digested pGTK-F6, Lane 20: F6 purified.

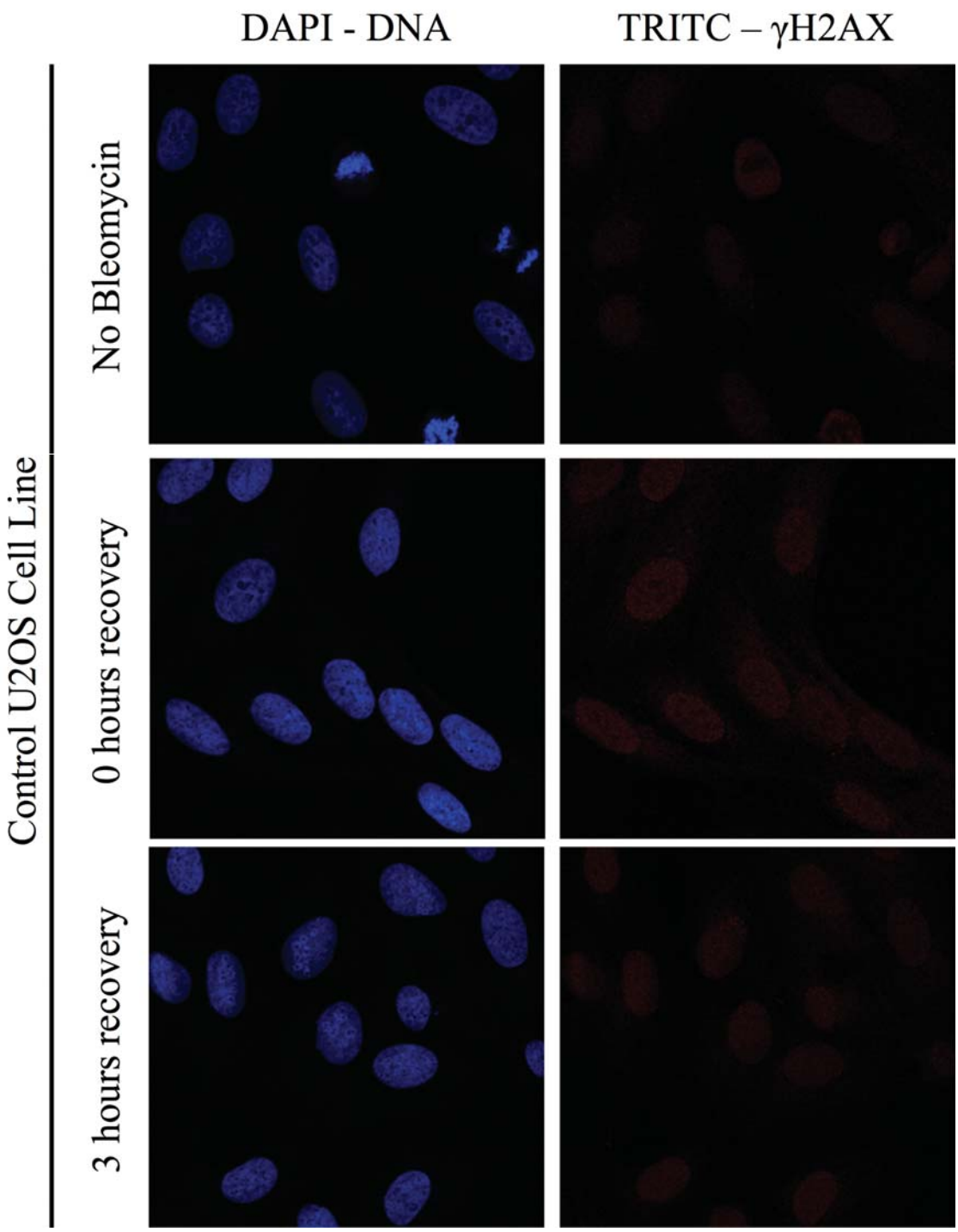

Figure A1.2 Confocal imaging of control U2OS cells before bleomycin exposure and during recovery after bleomycin exposure. Control U2OS cells were grown on 2x2 cm glass slides. Cells were either exposed to bleomycin and allowed to recover for 0 or 3 hours or were not exposed to bleomycin. Cells were fixed to the slides using paraformaldehyde and immunostained with TRITC and Dapi. The first row represents control cells with no exposure to bleomycin. The second row shows U2OS cells with no recovery after exposure to bleomycin. Row three indicates cells exposed to bleomycin and allowed to recover in normal growth medium for 3 hours. The first column represents the Dapi fluorescent stain, which stains DNA. The second column represents TRITC, which binds to the γ-H2AX antibody and is indicative of the presence of γ-H2AX in the cells. The brighter the cells, the more γ-H2AX which indicates the amount of ATM action.

Appendix 2 Supplementary Tables

Table A2.2 Primary and Secondary Antibodies

Antibody	Company	Catalogue Number	Initial Concentration	Immunoblot concentration	Species
α-ATM	Calbiochem	819844	0.1mg/mL	1 μg/mL	Rabbit
α-P-ATM	Abcam	ab36810	1 mg/mL	1 μg/mL	Mouse
α-β-actin	Sigma	A5316	1 mg/mL	1 μg/mL	Mouse
α-H2AX	Milipore	07-627	1 mg/mL	4 μg/mL	Rabbit
α-γH2AX	Milipore	07-164	1 mg/mL	4 μg/mL	Rabbit
α-FLAG	Sigma	F3165	1 mg/mL	2 μg/mL	Mouse
DAPI	Thermo	P36931	N/A	N/A	N/A
TRITC	Abcam	Ab6718	2 mg/mL	4 μg/mL	Goat anti-rabbit

Table A2.2 p400 codon analysis for expression in E. coli.

p400 Fragment Sequence	Codon Adaptation Index (CAI)	GC content (%)	Percentage of low frequency codons
F1	0.61	63.08%	13%
F2	0.60	55.96%	13%
F3	0.61	61.29%	13%
F4	0.61	53.49%	9%
F5	0.69	65.42%	7%
F6	0.70	65.86%	8%

A Codon Adaptation Index (CAI) score of 1.0 is considered ideal expression where as a CAI of >0.8 represents good expression. Low CAI scores indicate a higher chance of poor expression. The scores of the p400 fragments suggest that their expression would be less than what is considered good expression. The ideal percentage range of GC content for a sequence as determined by GeneScript® is between 30-70%. All of the p400 sequences lie within this range. GeneScript® evaluates the percentage of low frequency codons through computed codon quality groups. Codons that fall in groups with values lower than 30 are considered to be likely to encumber the efficiency of expression. The p400 fragments contain low frequency codon percentages between 7-13%. The GeneScript® codon analysis suggests that tandem rare codons within the sequences have the potential to reduce translation efficiency or, more severely, cause the disengasement of the translational machinery. (GeneScript® http://www.genscript.com/cgi-bin/tools/rare_codon_analysis)

Table A2.3 Protein stabilities of GST-p400 protein fragments using ExPASy.

Protein fragment	Molecular Weight (kDa)	Instability Index	Half life mammalian reticulocytes (in vitro) in hours	Half life E. coli (in vivo) in hours
GST-F1	107.394	68.98 (un)	30	>10
GST-F2	112.928	56.04	30	>10
GST-F3	100.751	52.23	30	>10
GST-F4	55.257	44.77	30	>10
GST-F5	92.497	56.85	30	>10
GST-F6	69.705	48.77	30	>10

The instability index indicated the estimated stability of the protein in a test tube. This has been determined through the analysis of stable and unstable proteins and the occurrence of particular dipeptides that appear to influence stability. A protein with an instability index of less than 40 is predicted as stable where as a value above 40 indicates potential instability. The half-life is defined by the predicted amount of time it takes for half of the total protein content to disappear after its synthesis. Each of the fusion proteins demonstrates a potential unstable form with a half-life of less than 10 hours in *E. coli*.

Table A2.4 Descriptive Statistics – Day 7 Samples after Bleomycin Exposure

Summary					
Group	**Sample Size**	**Sum**	**Mean**	**Variance**	**Standard Deviation**
pCDH1	3	1,502.457	500.819	366.311	19.139
F1	3	1,553.991	517.997	596.665	24.427
F6	3	1,753.171	584.390	195.976	13.999

Table A2.5 Analysis of Variance (ANOVA) One-Way – Day 7 Samples after Bleomycin Exposure

Analysis of Variance (ANOVA) One-Way – Day 7 Samples after Bleomycin Exposure						
Source of Variation	**SS**	**df**	**MS**	**F**	**p-level**	**F critical**
Between Groups	11,687.310	2	5,843.655	15.127	0.00453	5.14325
Within Groups	2,317.906	6	386.318			
Total		8				

Table A2.6 T-Test – Day 7 pCDH1 and F1 Samples after Bleomycin Exposure

T-Test Assuming Equal Variance (homoscendastic)	
Degrees of Freedom	4
Hypothesized Mean Difference	0
Pooled Variance	789.91616
Test Statistics	6.86277
Two-Tailed Distribution	
p-level	0.00236

Table A2.7 T-Test – Day 7 pCDH1 and F6 Samples after Bleomycin Exposure

T-Test Assuming Equal Variance (homoscendastic)	
Degrees of Freedom	4
Hypothesized Mean Difference	0
Pooled Variance	996.75450
Test Statistics	0.12023
Two-Tailed Distribution	
p-level	0.91010

Table A2.8 T-Test – Day 7 F1 and F6 Samples after Bleomycin Exposure

T-Test Assuming Equal Variance (homoscendastic)	
Degrees of Freedom	4
Hypothesized Mean Difference	0
Pooled Variance	1,131.07203
Test Statistics	5.62229
Two-Tailed Distribution	
p-level	0.00492

Table A2.9 ANOVA of pCDH1, F1, and F6 Samples under Standard Conditions

		F-critical = 5.14325
	p-level	**F**
Day 1	1.000	0.000
Day 2	0.47765	0.838
Day 3	0.23415	1.867
Day 4	0.01884	8.275
Day 5	0.05001	5.143
Day 6	0.15312	2.608
Day 7	0.00453	15.127

Table A2.10 ANOVA of pCDH1, F1, and F6 Samples after Exposure to Bleomycin

		F-critical = 5.14325
	p-level	F
Day 1	1.000	0.000
Day 2	0.10367	3.386
Day 3	0.28706	1.548
Day 4	0.00539	14.112
Day 5	0.00326	17.224
Day 6	0.00036	39.273
Day 7	0.00123	25.009

Table A2.11 T-test – pCDH1, F1, and F6 Samples after Bleomycin Exposure

Two-tailed distribution	Critical Value (5%) 2.776
Day 1	**p-level**
pCDH1 : F1	1.000
pCDH1 : F6	1.000
F1 : F6	1.000
Day 2	
pCDH1 : F1	0.11095
pCDH1 : F6	0.06366
F1 : F6	0.98836
Day 3	
pCDH1 : F1	0.13290
pCDH1 : F6	0.97890
F1 : F6	0.06934
Day 4	
pCDH1 : F1	0.00274
pCDH1 : F6	0.82705
F1 : F6	0.01741
Day 5	
pCDH1 : F1	0.00571
pCDH1 : F6	0.88114
F1 : F6	0.00833
Day 6	
pCDH1 : F1	0.00099
pCDH1 : F6	0.38046
F1 : F6	0.00137
Day 7	
pCDH1 : F1	0.00236
pCDH1 : F6	0.91010
F1 : F6	0.00492

Table A2.12 T-test – pCDH1, F1, and F6 Samples under Standard Conditions

T-test – pCDH1, F1, and F6 Samples under Standard Conditions	
Two-tailed distribution	Critical Value (5%) 2.776
Day 1	**p-level**
pCDH1 : F1	1.000
pCDH1 : F6	1.000
F1 : F6	1.000
Day 2	
pCDH1 : F1	0.7663
pCDH1 : F6	0.47135
F1 : F6	0.19323
Day 3	
pCDH1 : F1	0.19175
pCDH1 : F6	0.53909
F1 : F6	0.22012
Day 4	
pCDH1 : F1	0.01405
pCDH1 : F6	0.12068
F1 : F6	0.02665
Day 5	
pCDH1 : F1	0.37723
pCDH1 : F6	0.06622
F1 : F6	0.09558
Day 6	
pCDH1 : F1	0.60411
pCDH1 : F6	0.06191
F1 : F6	0.21440
Day 7	
pCDH1 : F1	0.39196
pCDH1 : F6	0.00364
F1 : F6	0.01504

Appendix 3 Bleomycin Sensitivity Assay Graphs

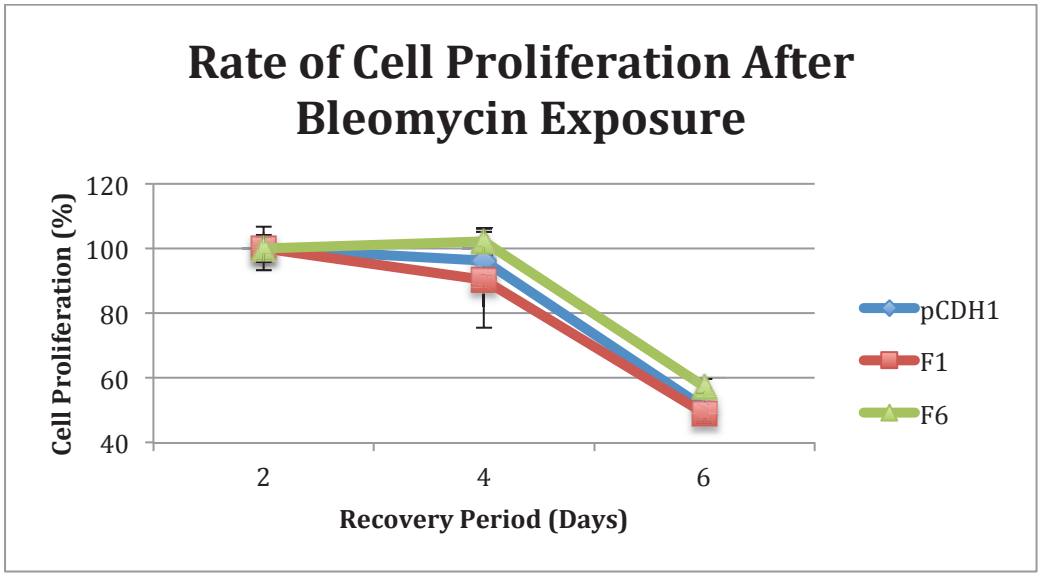

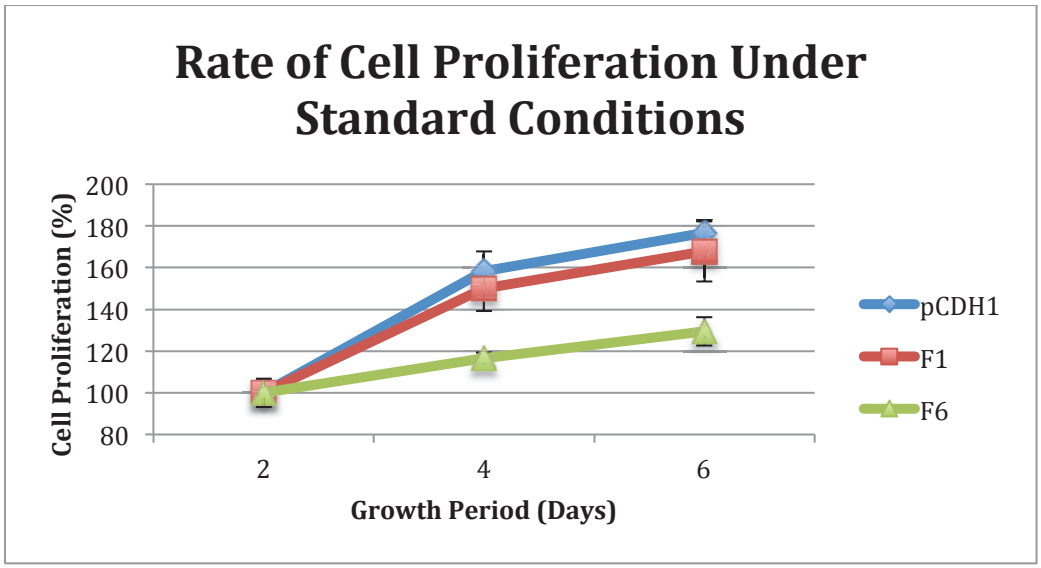

Figure A3.1 Rate of cell proliferation of U2OS stable cell lines expressing pCDH1 empty vector, F1, or F6 August 17. Three stable U2OS cell lines previously infected with lentivirus containing either pCDH1, pCDH1-F1, or pCDH1-F6 were analyzed for a seven day recovery period either after a treatment with bleomycin (10 μg/mL) or under standard conditions. Fluorescence data was normalized as a percentage of fluorescence from day 1 to the remaining days of recovery. The measurement of fluorescence is directly correlated to the amount of DNA present in a sample and thus, the percentage difference can be used as a value to determine percent growth. All samples for the first day were considered to be at 100% survival and the following days were calculated according to that pretense. Error bars represent ±SD. A) U2OS cell lines that were exposed to bleomycin before the seven-day recovery showed a statistically significant difference between cells expressing F1 when compared to pCDH1 and F6. B) There was no great statistical difference between any of the cell lines when grown under standard conditions with no bleomycin treatment with no trend to indicate one cell line grew more efficiently or poorly than another.

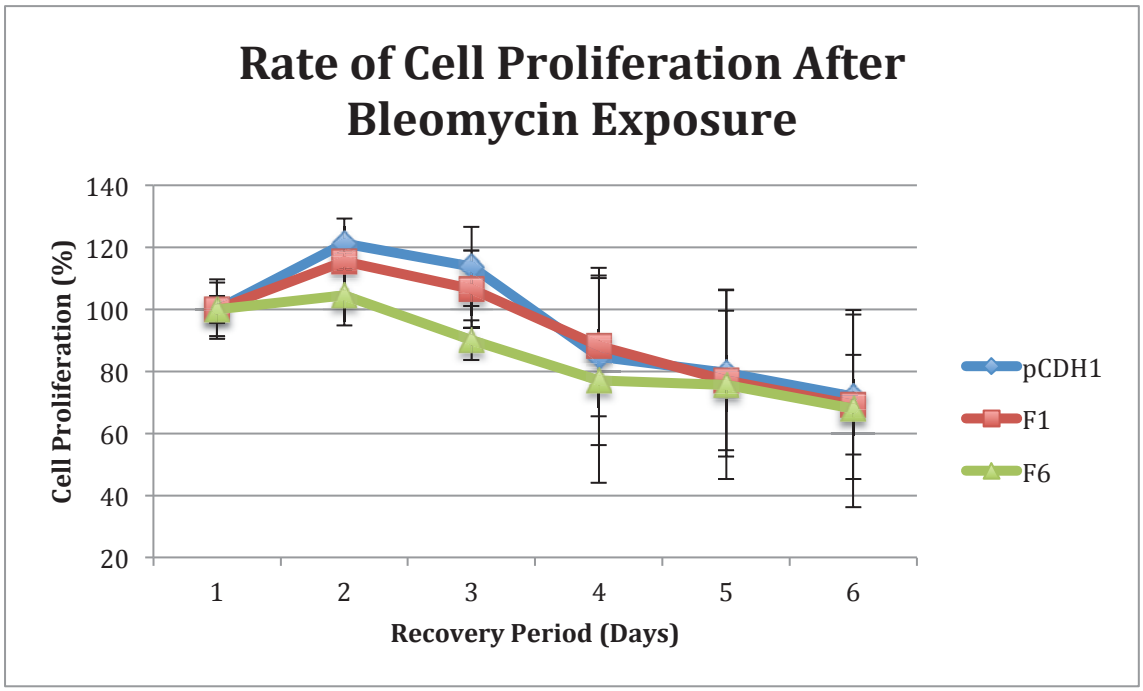

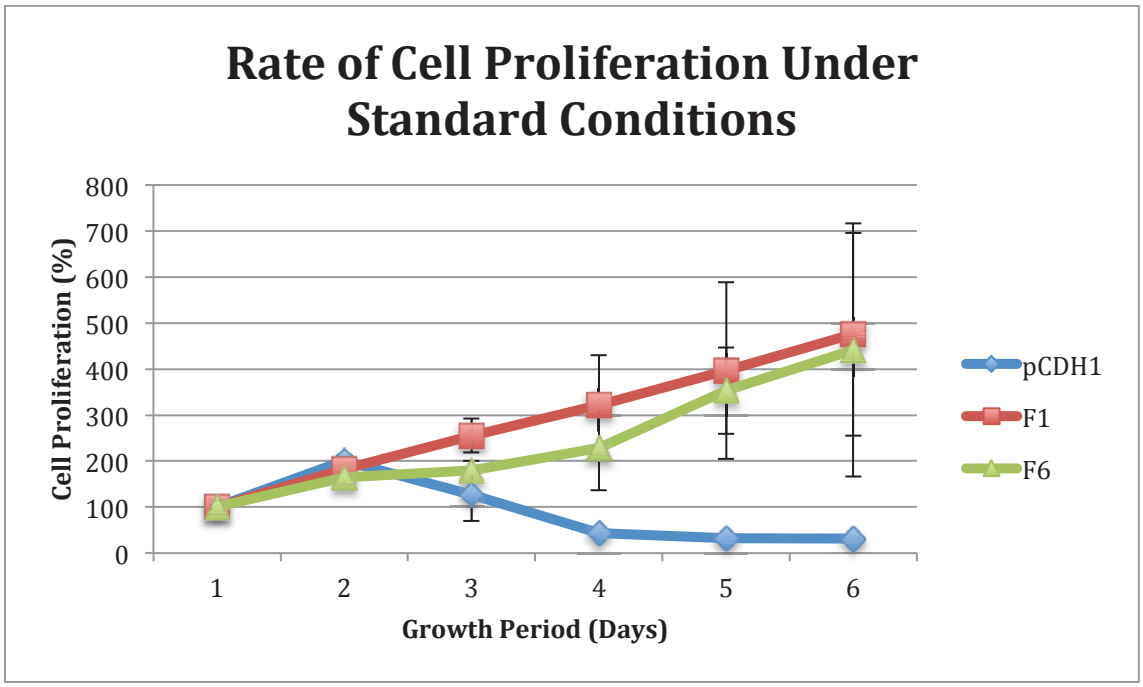

Figure A3.2 Rate of cell proliferation of U2OS stable cell lines expressing pCDH1 empty vector, F1, or F6 September 14. Three stable U2OS cell lines previously infected with lentivirus containing either pCDH1, pCDH1-F1, or pCDH1-F6 were analyzed for a seven day recovery period either after a treatment with bleomycin (10 μg/mL) or under standard conditions. Fluorescence data was normalized as a percentage of fluorescence from day 1 to the remaining days of recovery. The measurement of fluorescence is directly correlated to the amount of DNA present in a sample and thus, the percentage difference can be used as a value to determine percent growth. All samples for the first day were considered to be at 100% survival and the following days were calculated according to that pretense. Error bars represent ±SD. A) U2OS cell lines that were exposed to bleomycin before the seven-day recovery showed a statistically significant difference between cells expressing F1 when compared to pCDH1 and F6. B) There was no great statistical difference between any of the cell lines when grown under standard conditions with no bleomycin treatment with no trend to indicate one cell line grew more efficiently or poorly than another.

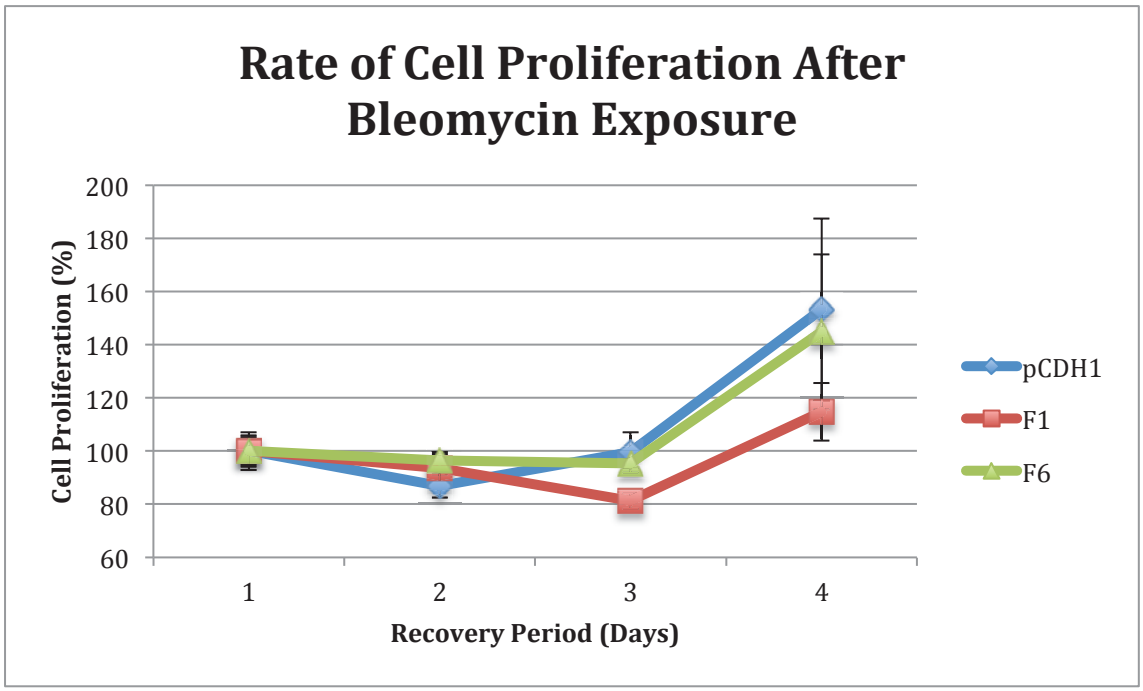

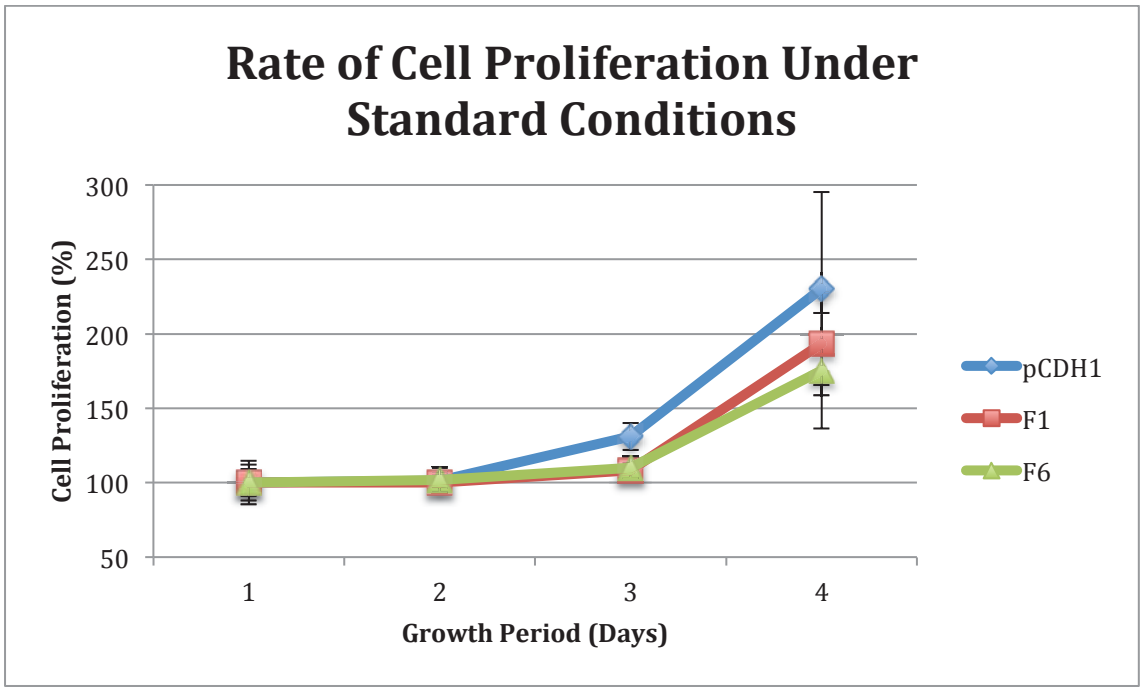

Figure A3.3 Rate of cell proliferation of U2OS stable cell lines expressing pCDH1 empty vector, F1, or F6 November 24. Three stable U2OS cell lines previously infected with lentivirus containing either pCDH1, pCDH1-F1, or pCDH1-F6 were analyzed for a seven day recovery period either after a treatment with bleomycin (10 μg/mL) or under standard conditions. Fluorescence data was normalized as a percentage of fluorescence from day 1 to the remaining days of recovery. The measurement of fluorescence is directly correlated to the amount of DNA present in a sample and thus, the percentage difference can be used as a value to determine percent growth. All samples for the first day were considered to be at 100% survival and the following days were calculated according to that pretense. Error bars represent ±SD. A) U2OS cell lines that were exposed to bleomycin before the seven-day recovery showed a statistically significant difference between cells expressing F1 when compared to pCDH1 and F6. B) There was no great statistical difference between any of the cell lines when grown under standard conditions with no bleomycin treatment with no trend to indicate one cell line grew more efficiently or poorly than another.

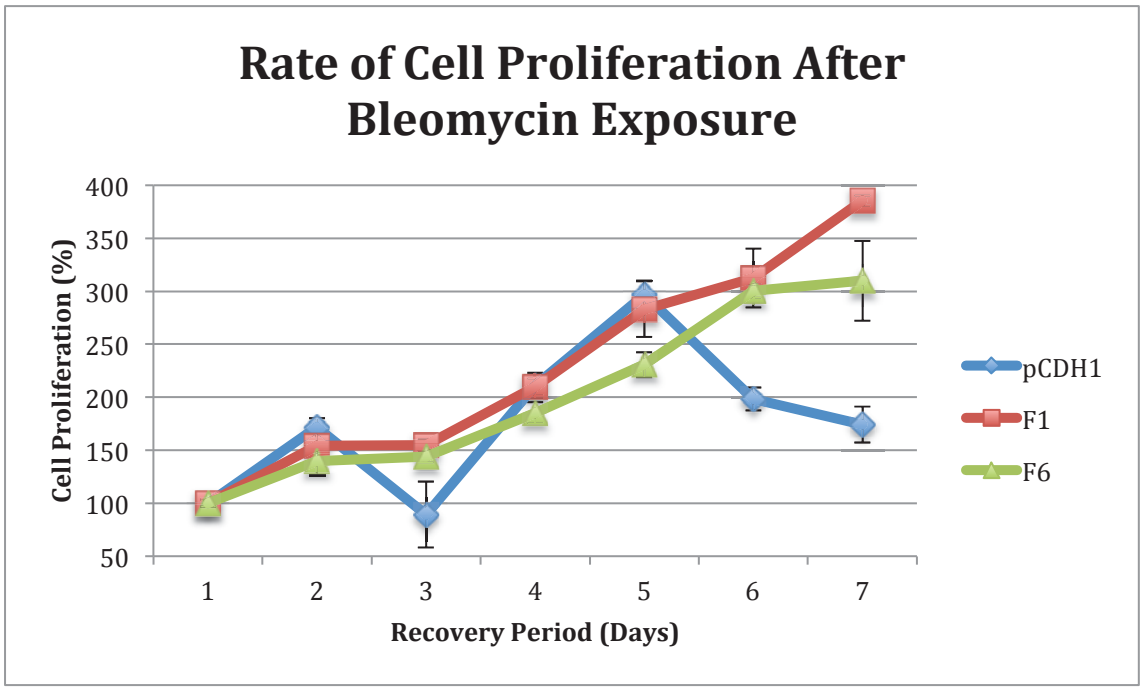

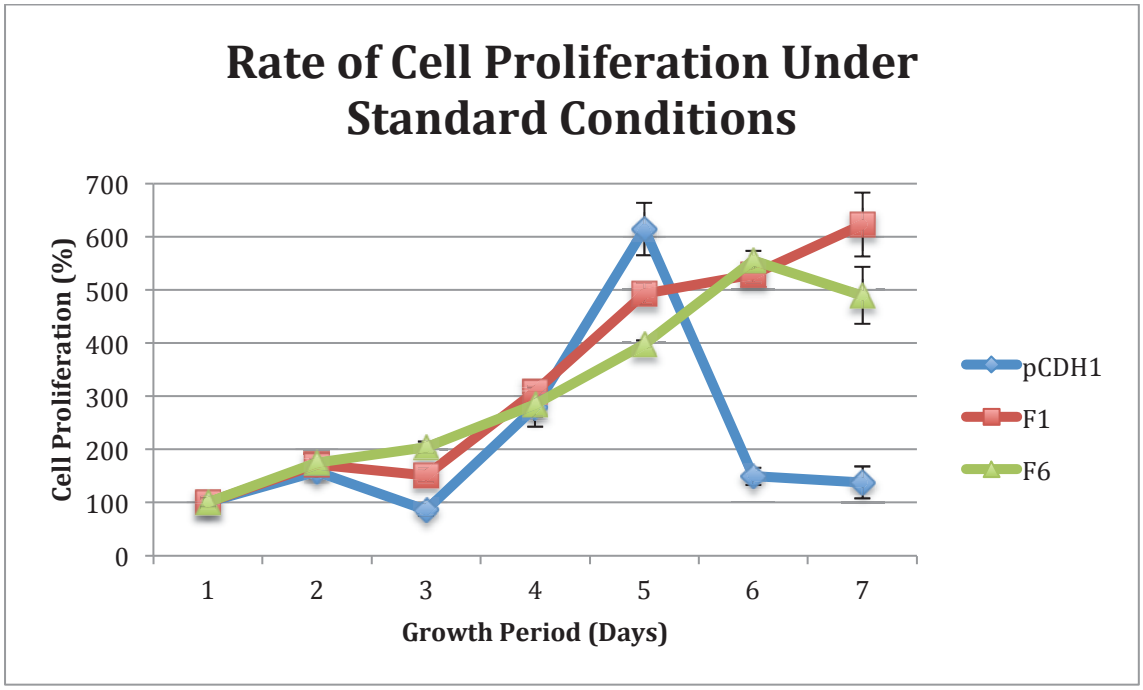

Figure A3.4 Rate of cell proliferation of U2OS stable cell lines expressing pCDH1 empty vector, F1, or F6 December 8. Three stable U2OS cell lines previously infected with lentivirus containing either pCDH1, pCDH1-F1, or pCDH1-F6 were analyzed for a seven day recovery period either after a treatment with bleomycin (10 μg/mL) or under standard conditions. Fluorescence data was normalized as a percentage of fluorescence from day 1 to the remaining days of recovery. The measurement of fluorescence is directly correlated to the amount of DNA present in a sample and thus, the percentage difference can be used as a value to determine percent growth. All samples for the first day were considered to be at 100% survival and the following days were calculated according to that pretense. Error bars represent ±SD. A) U2OS cell lines that were exposed to bleomycin before the seven-day recovery showed a statistically significant difference between cells expressing F1 when compared to pCDH1 and F6. B) There was no great statistical difference between any of the cell lines when grown under standard conditions with no bleomycin treatment with no trend to indicate one cell line grew more efficiently or poorly than another.

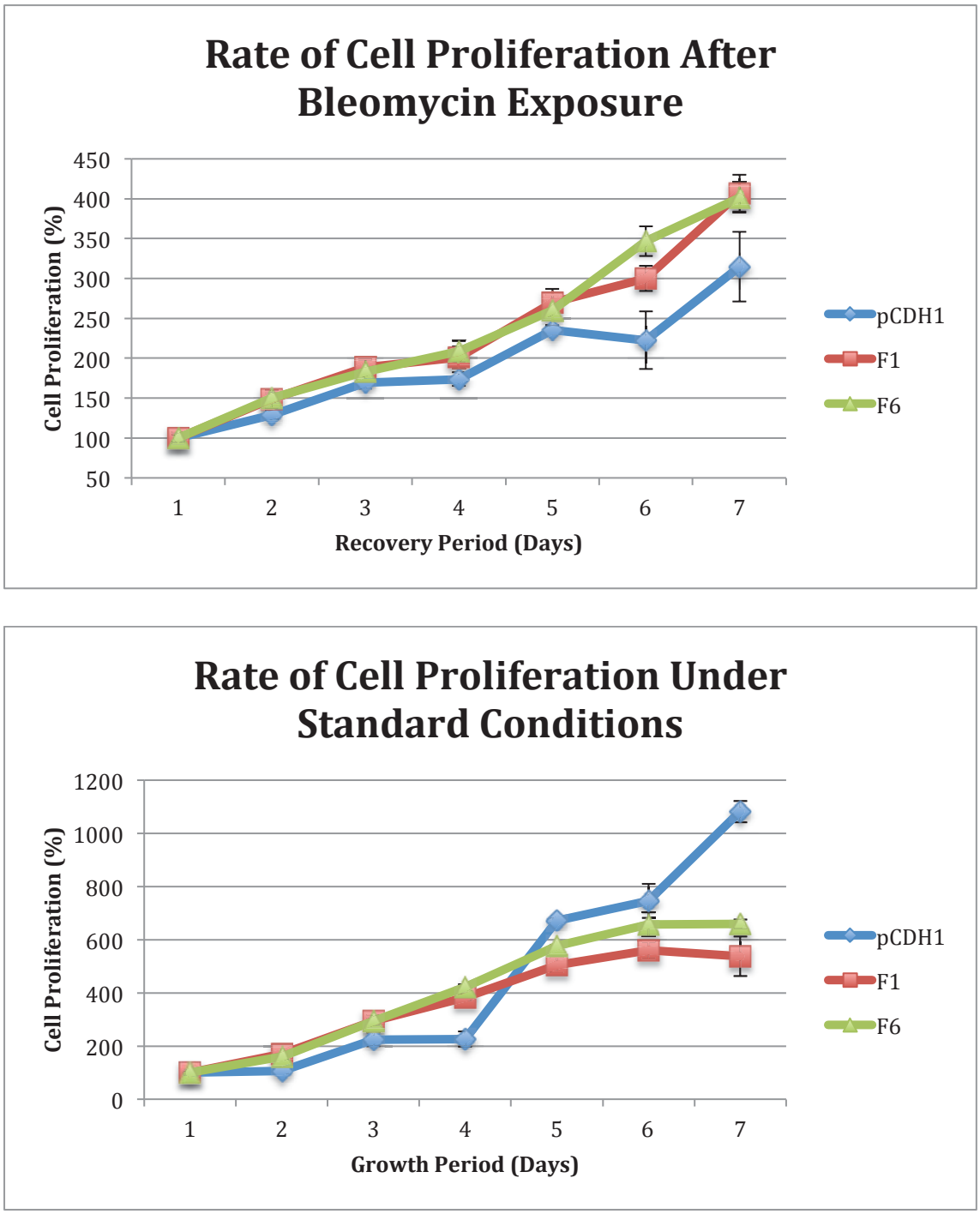

Figure A3.5 Rate of cell proliferation of U2OS stable cell lines expressing pCDH1 empty vector, F1, or F6 January 15. Three stable U2OS cell lines previously infected with lentivirus containing either pCDH1, pCDH1-F1, or pCDH1-F6 were analyzed for a seven day recovery period either after a treatment with bleomycin (10 μg/mL) or under standard conditions. Fluorescence data was normalized as a percentage of fluorescence from day 1 to the remaining days of recovery. The measurement of fluorescence is directly correlated to the amount of DNA present in a sample and thus, the percentage difference can be used as a value to determine percent growth. All samples for the first day were considered to be at 100% survival and the following days were calculated according to that pretense. Error bars represent ±SD. A) U2OS cell lines that were exposed to bleomycin before the seven-day recovery showed a statistically significant difference between cells expressing F1 when compared to pCDH1 and F6. B) There was no great statistical difference between any of the cell lines when grown under standard conditions with no bleomycin treatment with no trend to indicate one cell line grew more efficiently or poorly than another.

Appendix 4 Plasmid Maps

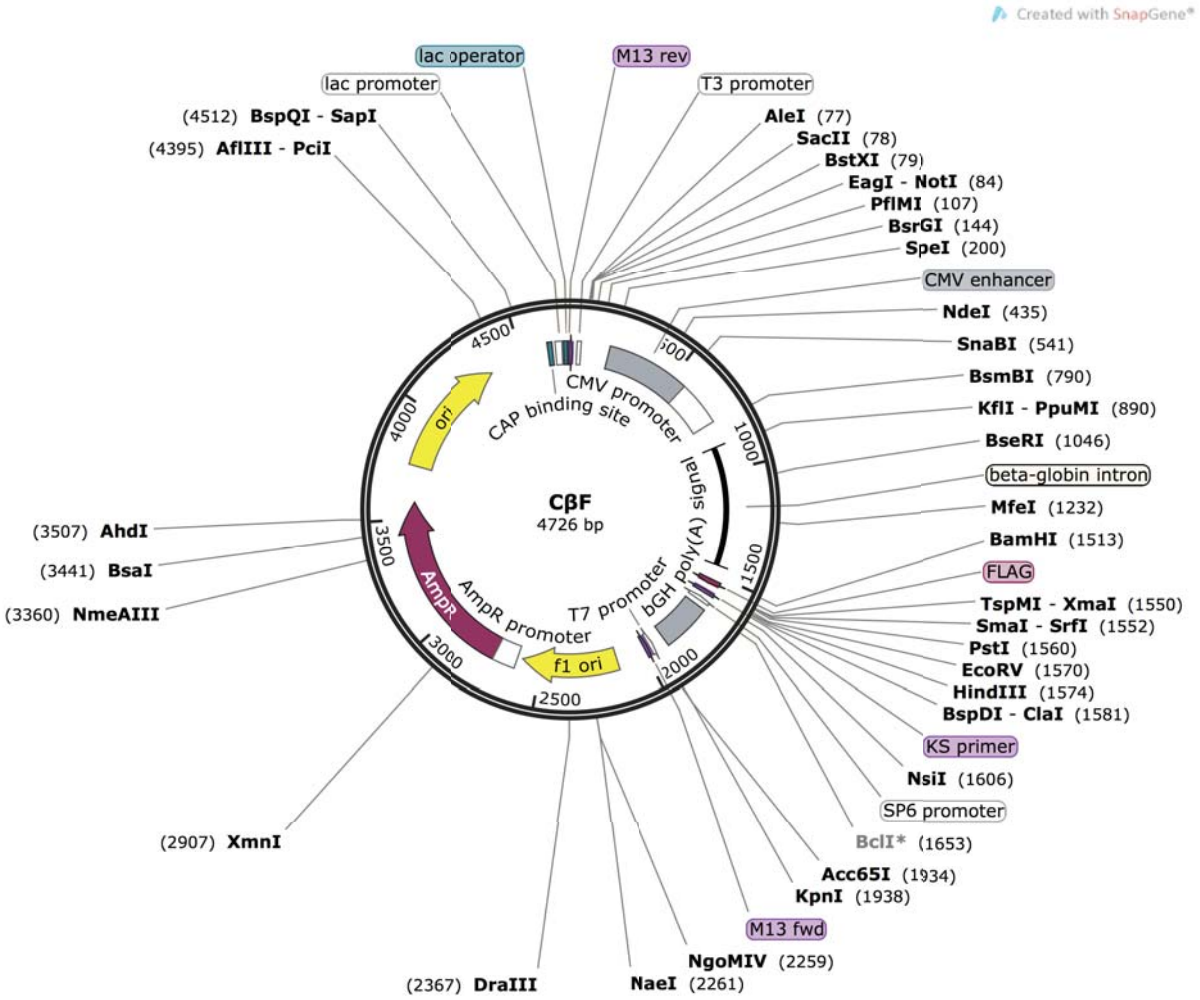

Figure A4.1 CβF Plasmid Map

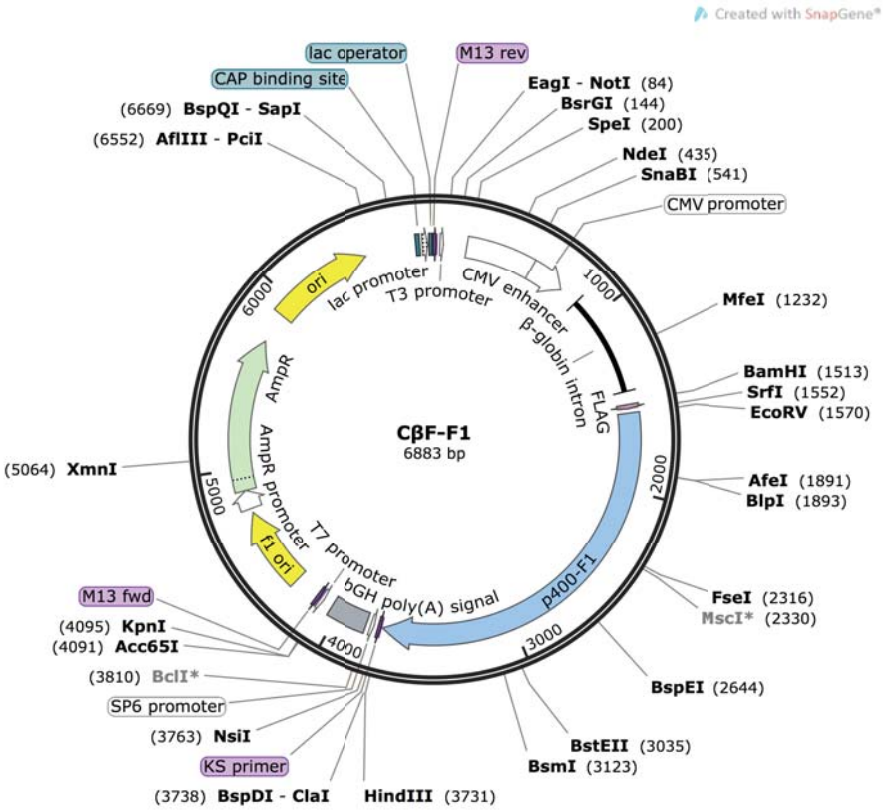

Figure A4.2 CβF-F1 Plasmid Map

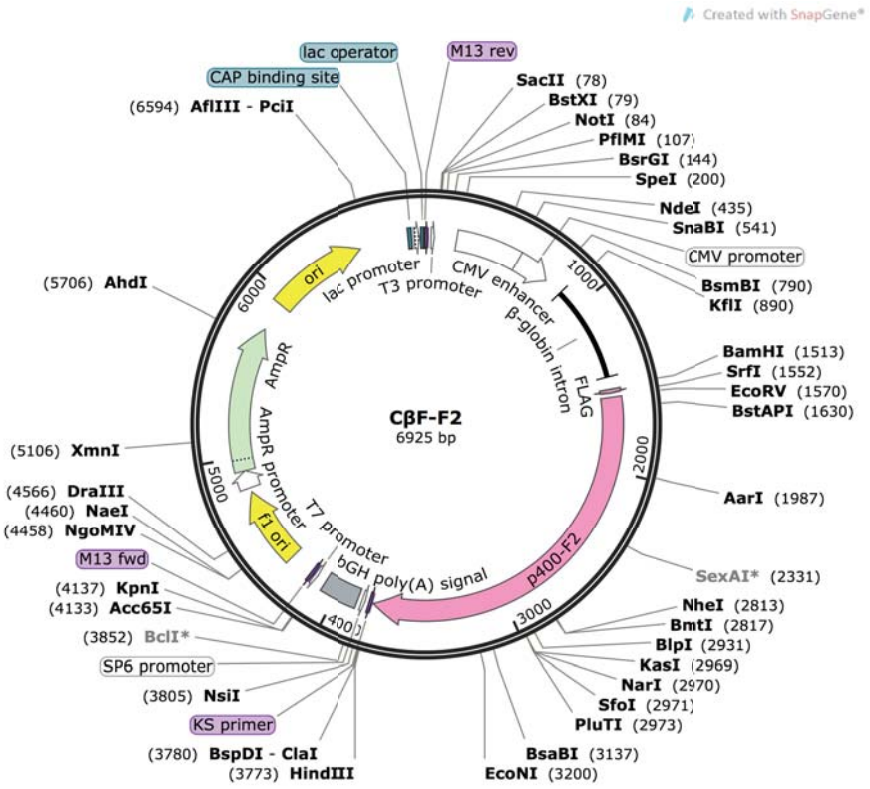

Figure A4.3 CβF-F2 Plasmid Map

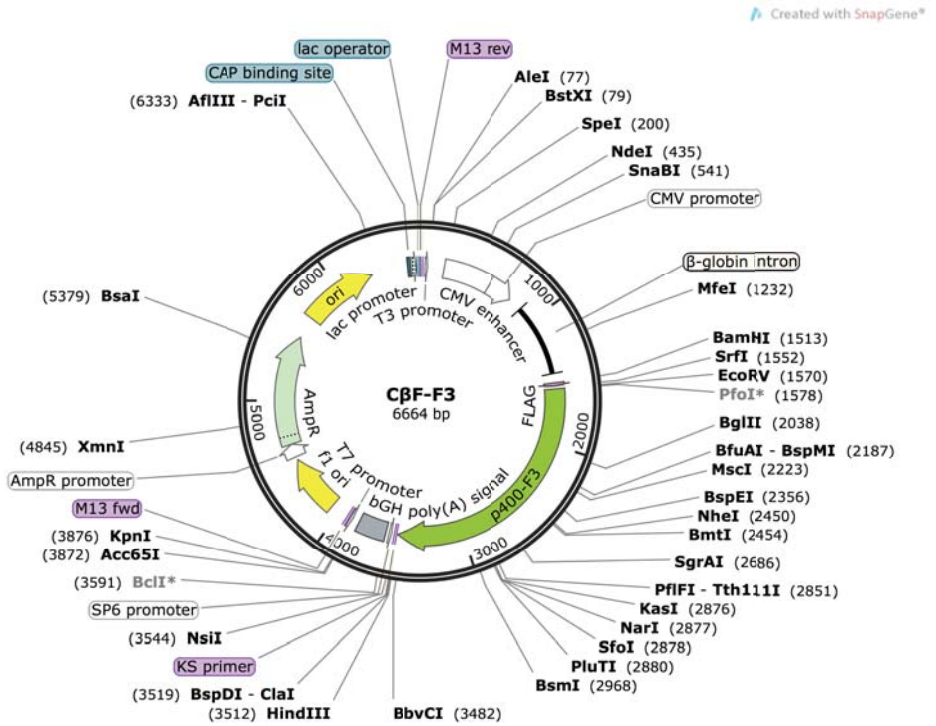

Figure A4.4 CβF-F3 Plasmid Map

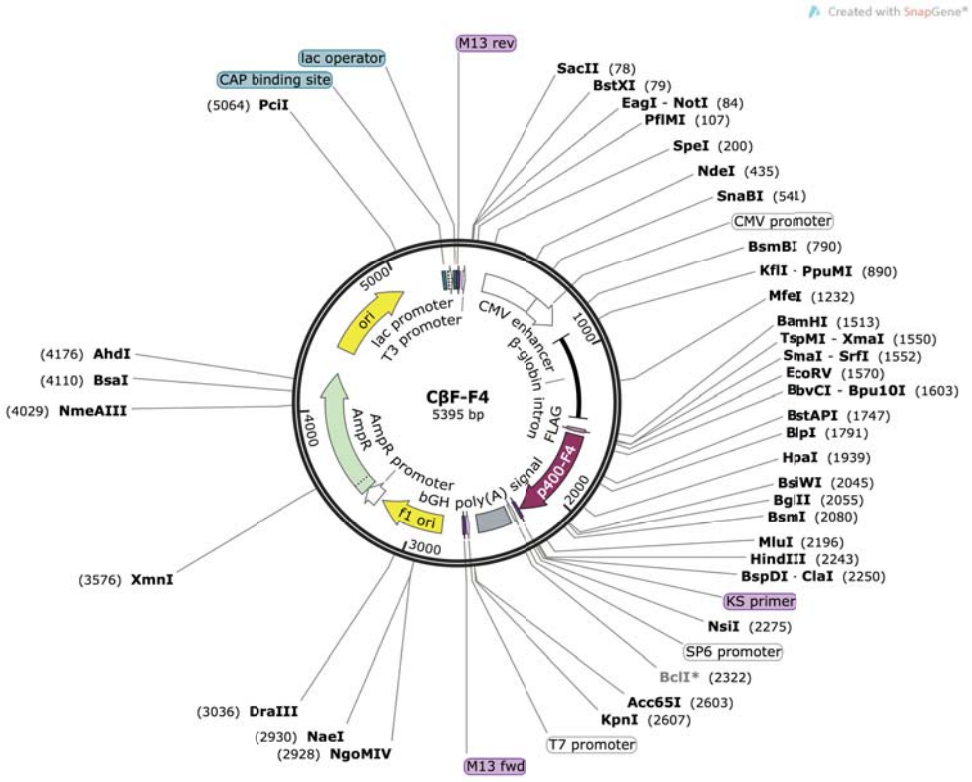

Figure A4.5 CβF-F4 Plasmid Map

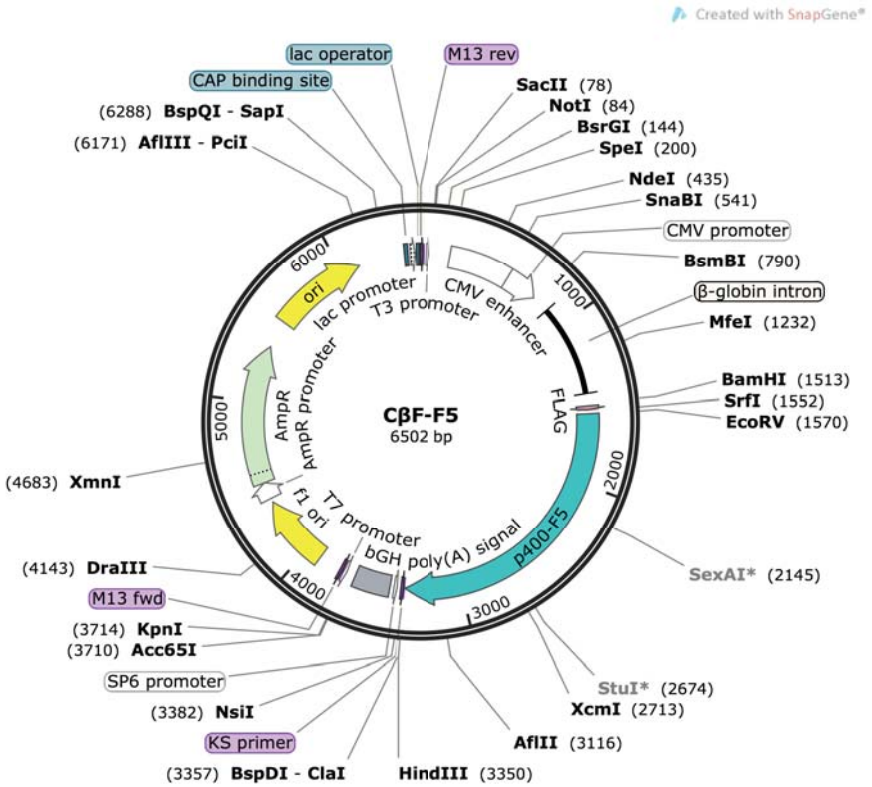

Figure A4.6 CβF-F5 Plasmid Map

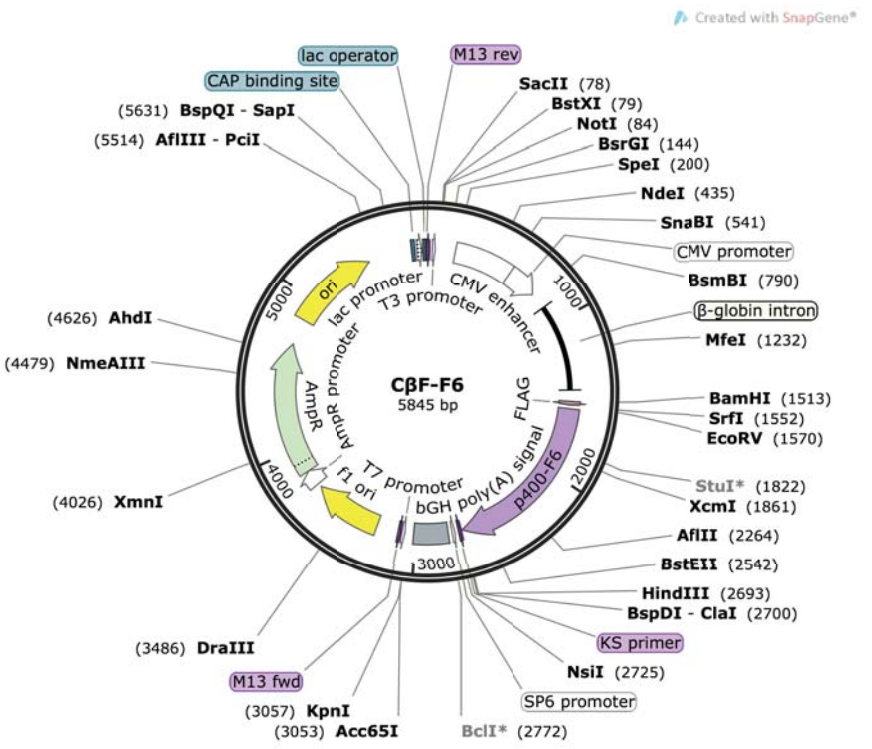

Figure A4.7 CβF-F6 Plasmid Map

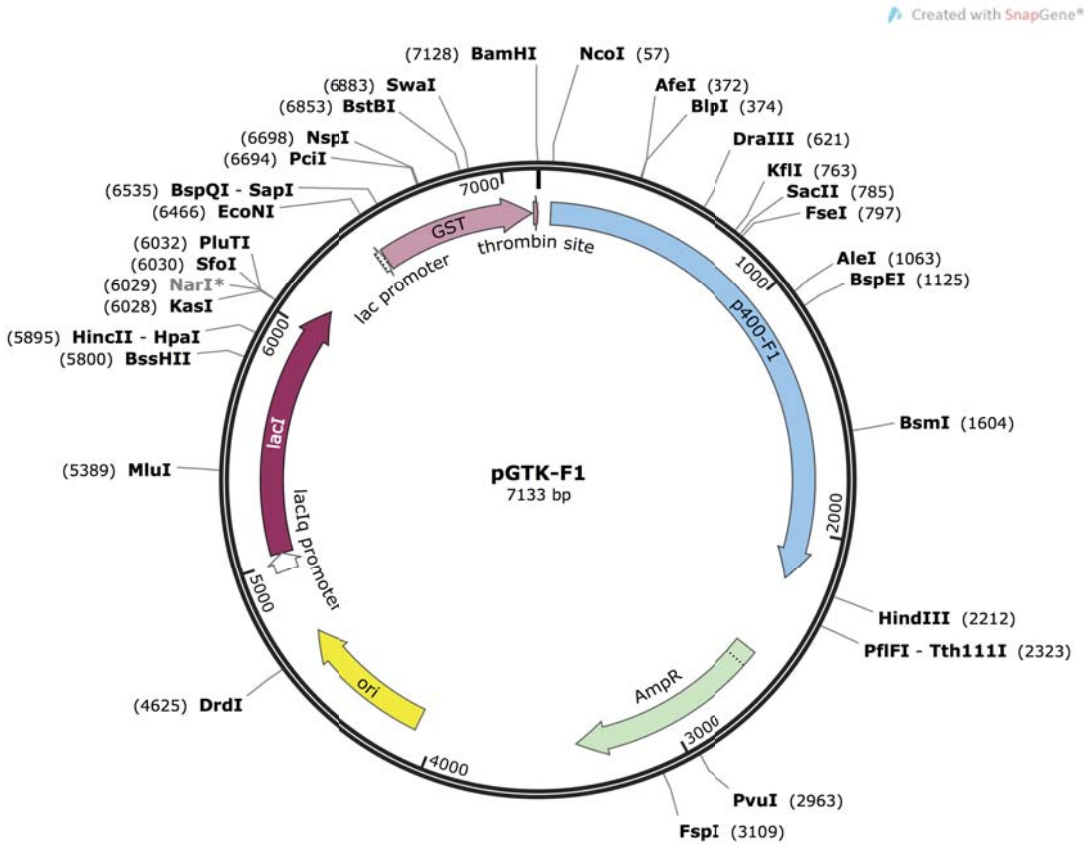

Figure A4.8 pGTK-F1 Plasmid Map The pGTK vector includes an ampicillin resistance gene for colony selection, the lacI gene which codes for lac repressor protein allowing for protein production only upon the addition of ITPG, the lac promoter, and a glutathione S-transferase (GST) sequence for N-terminal fusion proteins.

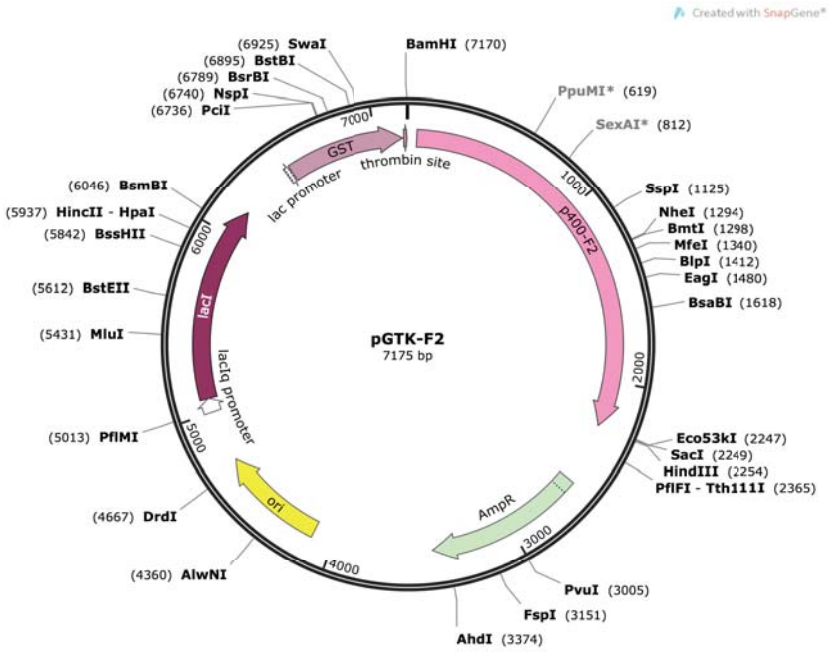

Figure A4.9 pGTK-F2 Plasmid Map

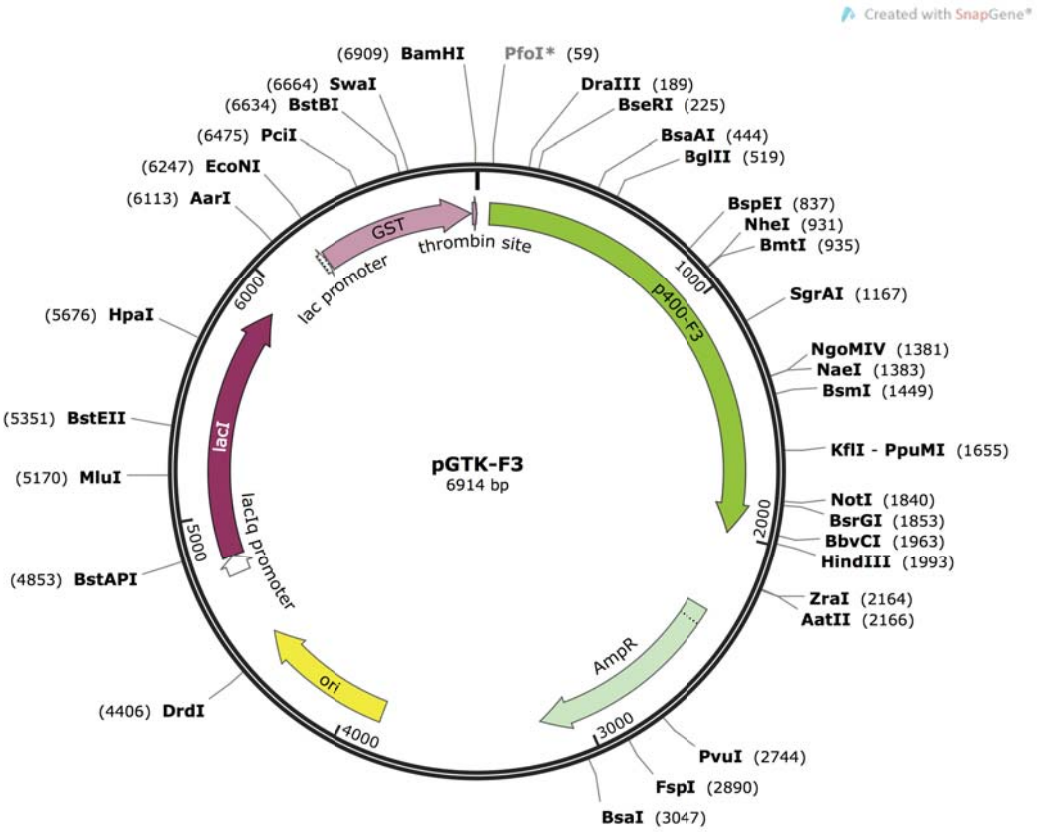

Figure A4.10 pGTK-F3 Plasmid Map

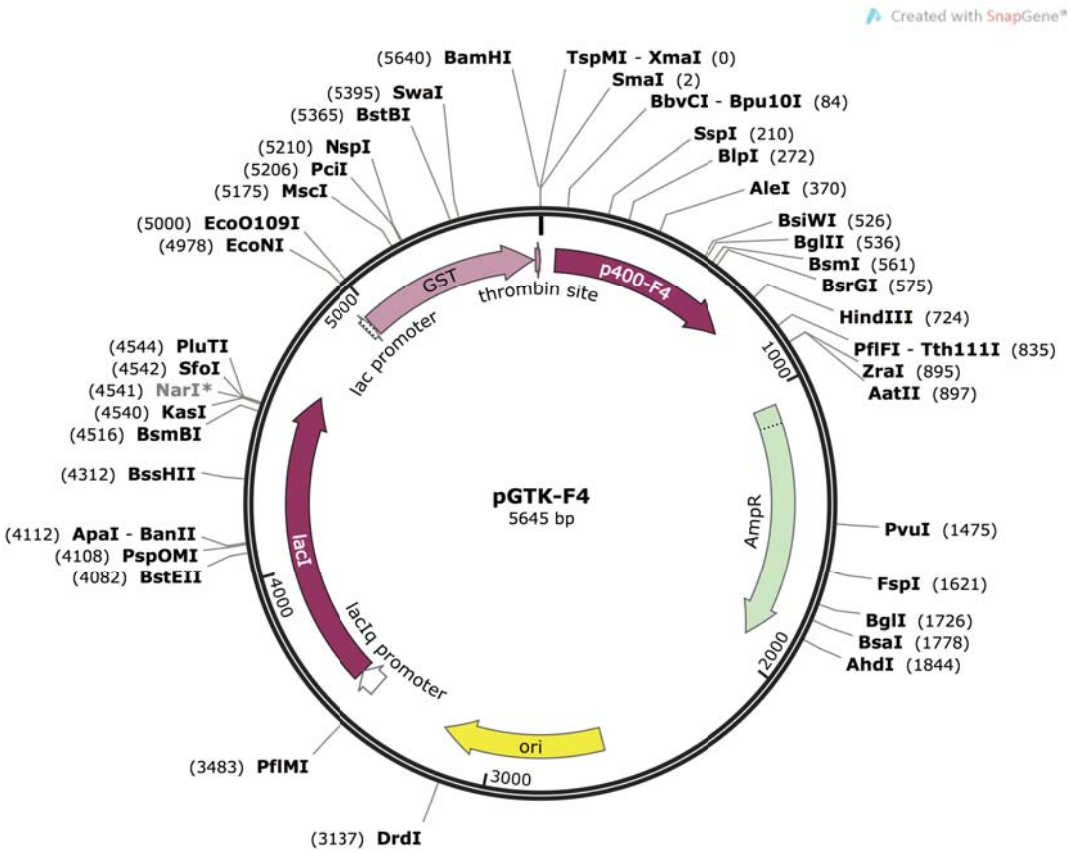

Figure A4.11 pGTK-F4 Plasmid Map

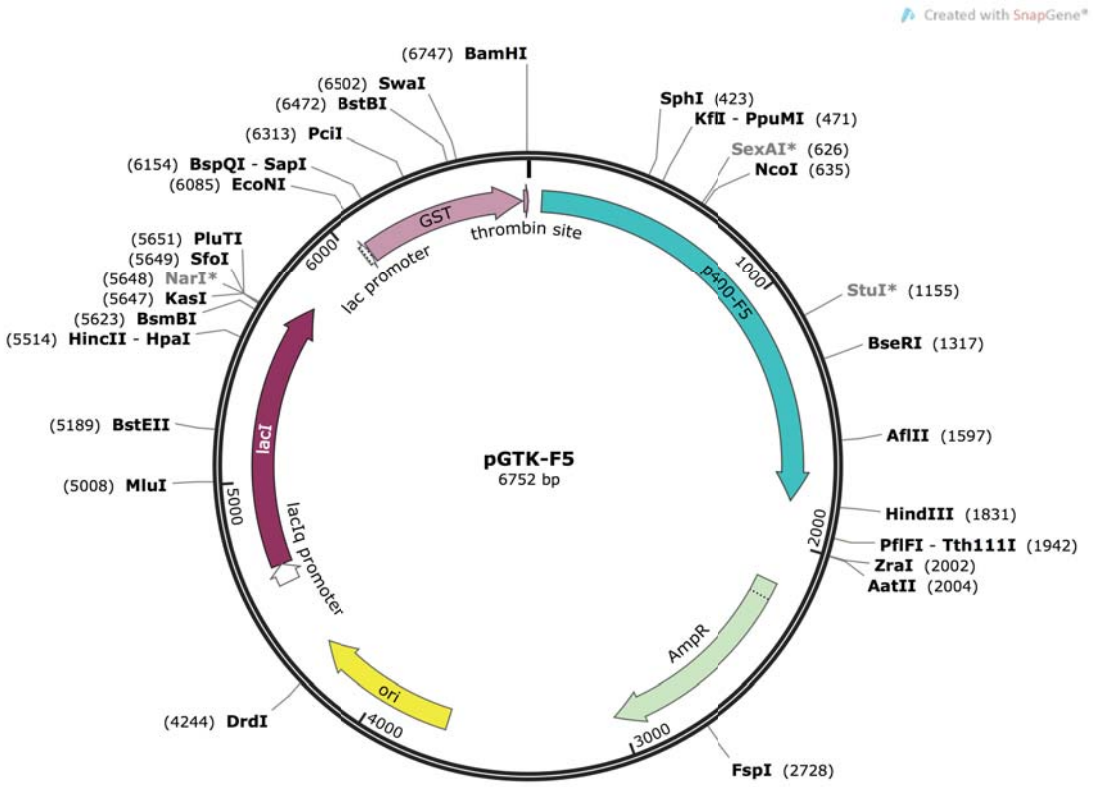

Figure A4.12 pGTK-F5 Plasmid Map

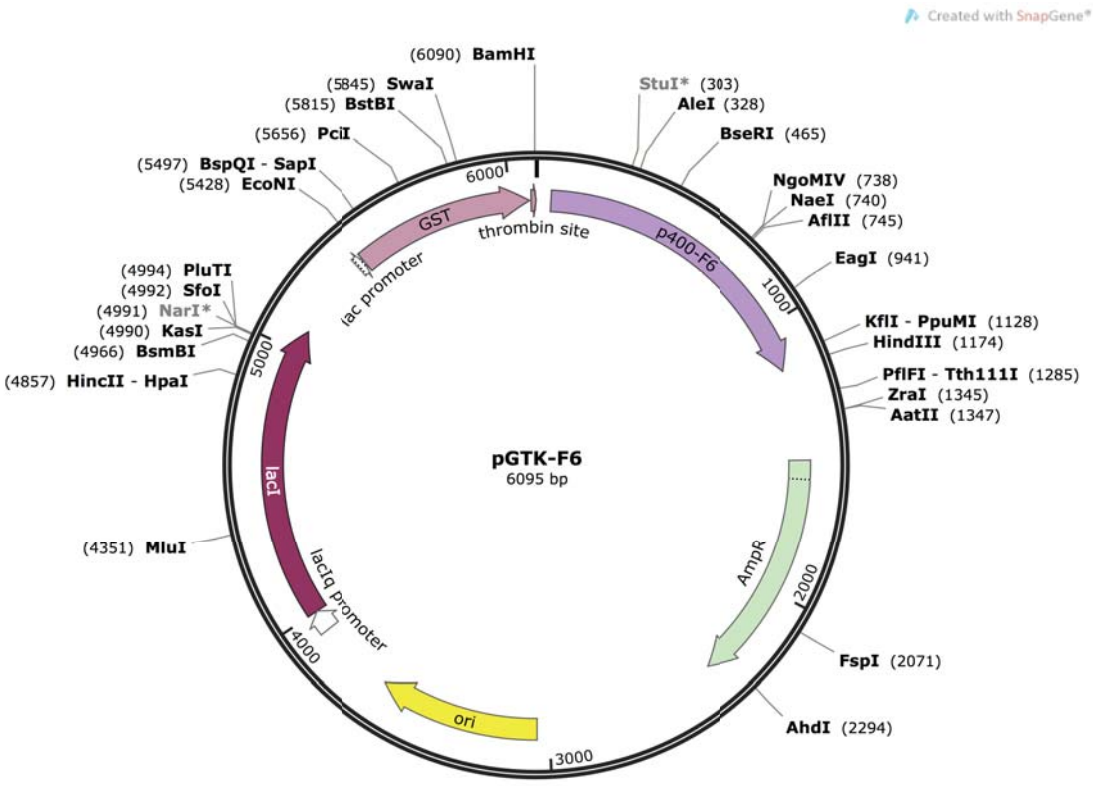

Figure A4.13 pGTK-F6 Plasmid Map

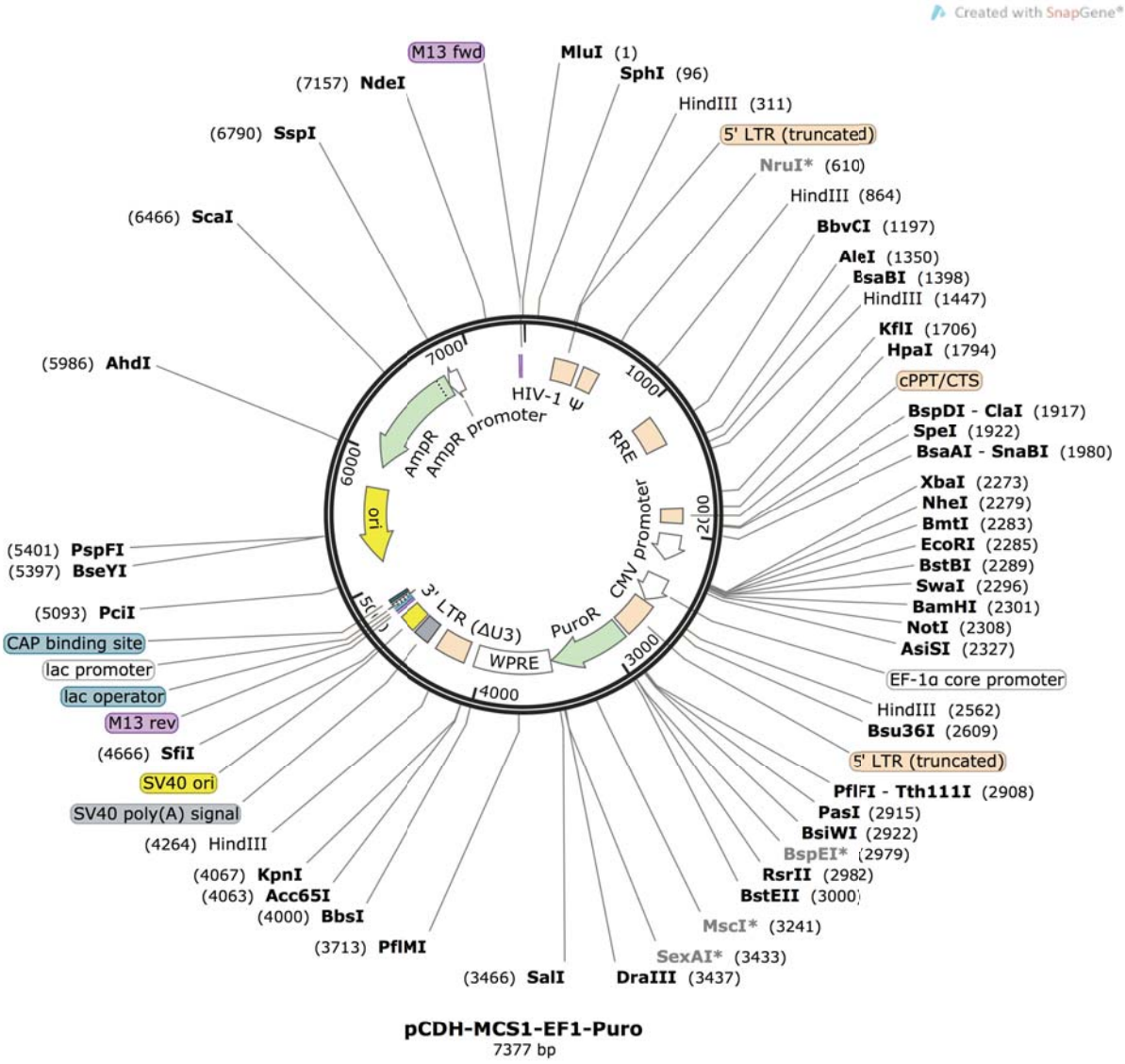

Figure A4.14 pCDH1 Plasmid Map

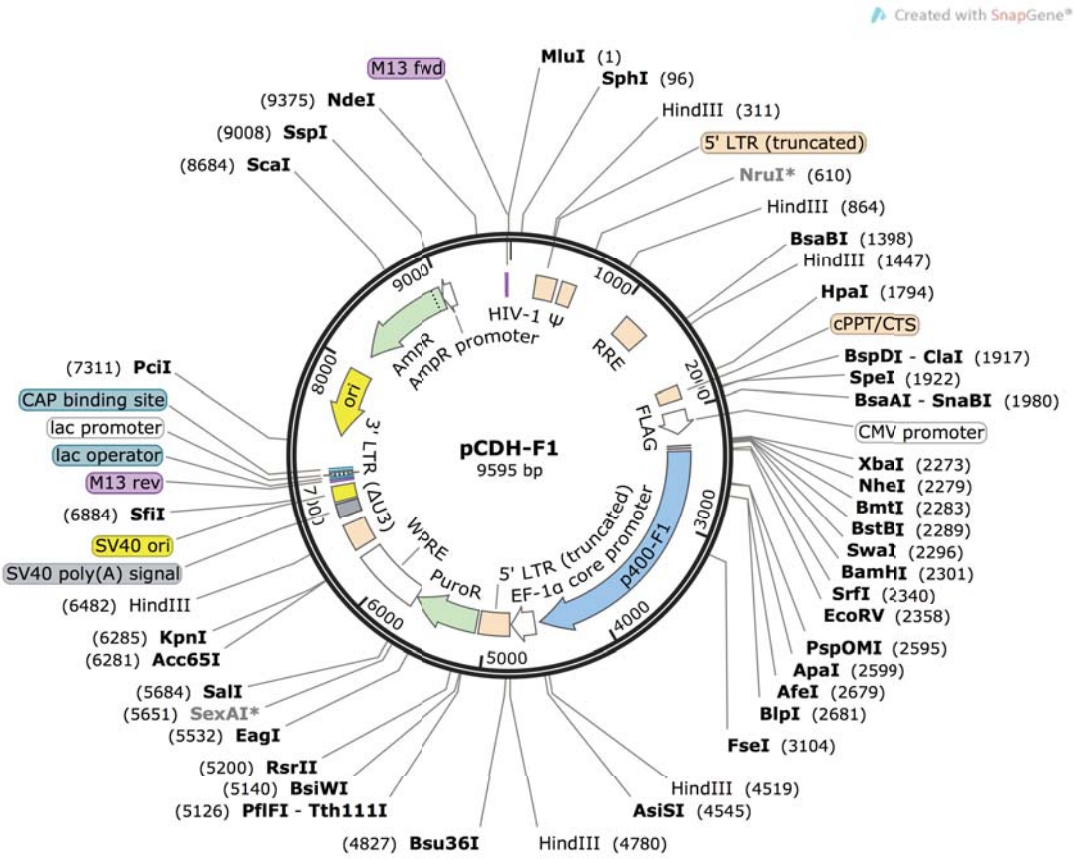

Figure A4.15 pCDH1-F1 Plasmid Map

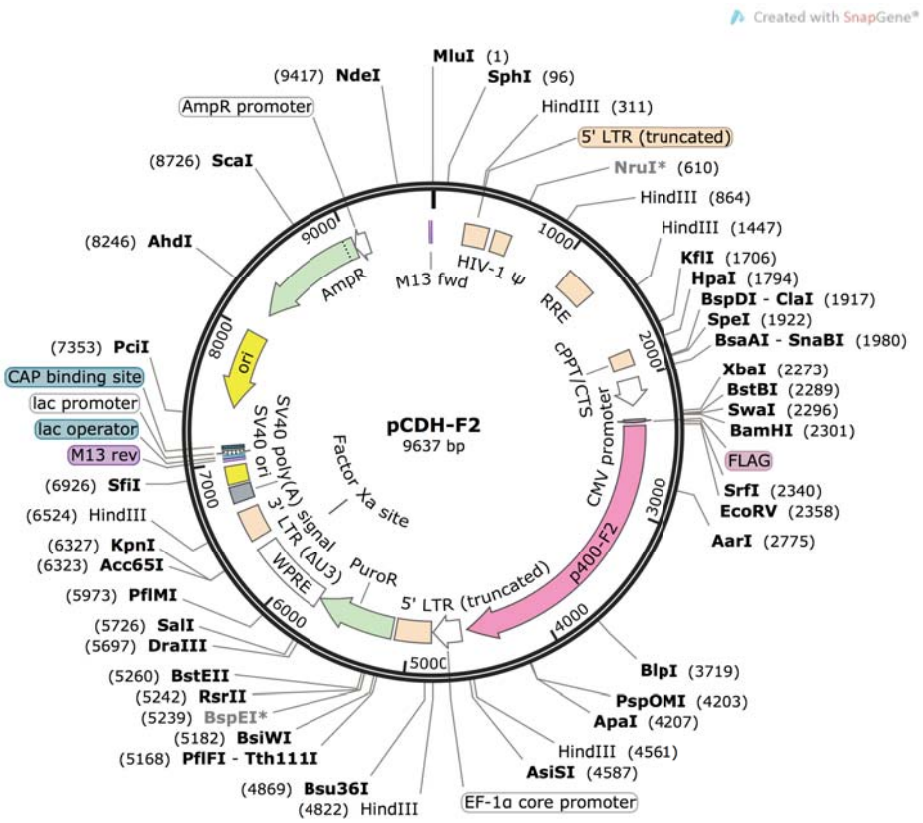

Figure A4.16 pCDH1-F2 Plasmid Map

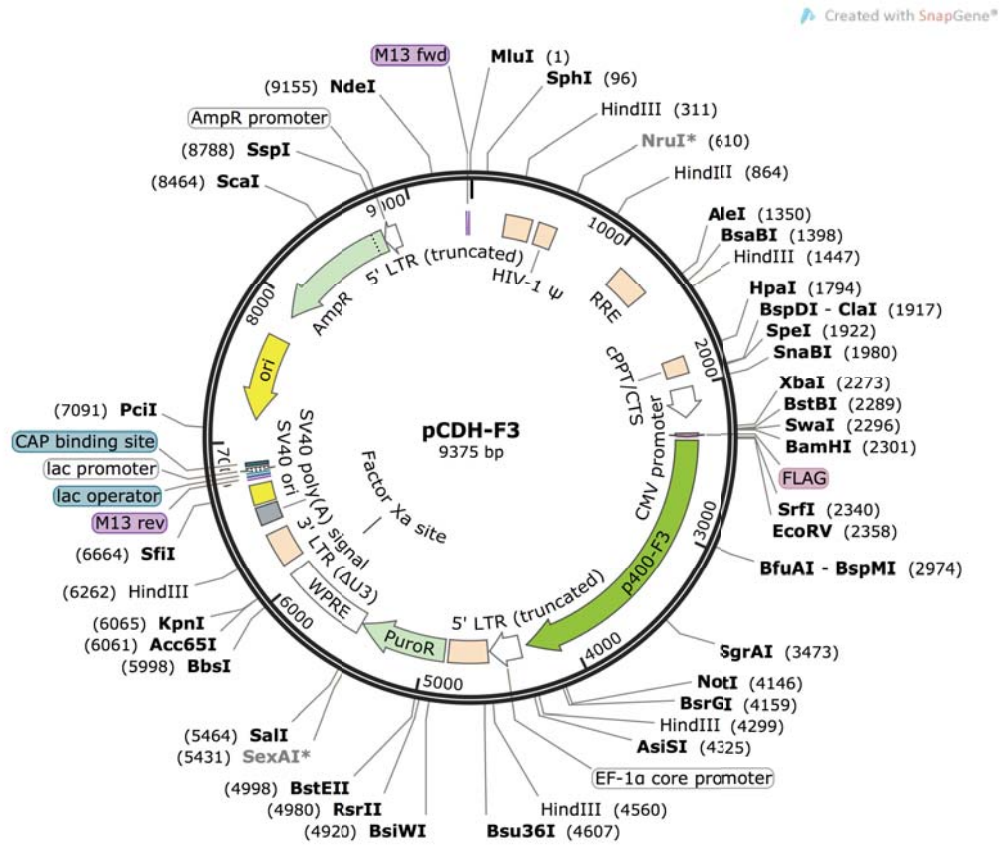

Figure A4.17 pCDH1-F3 Plasmid Map

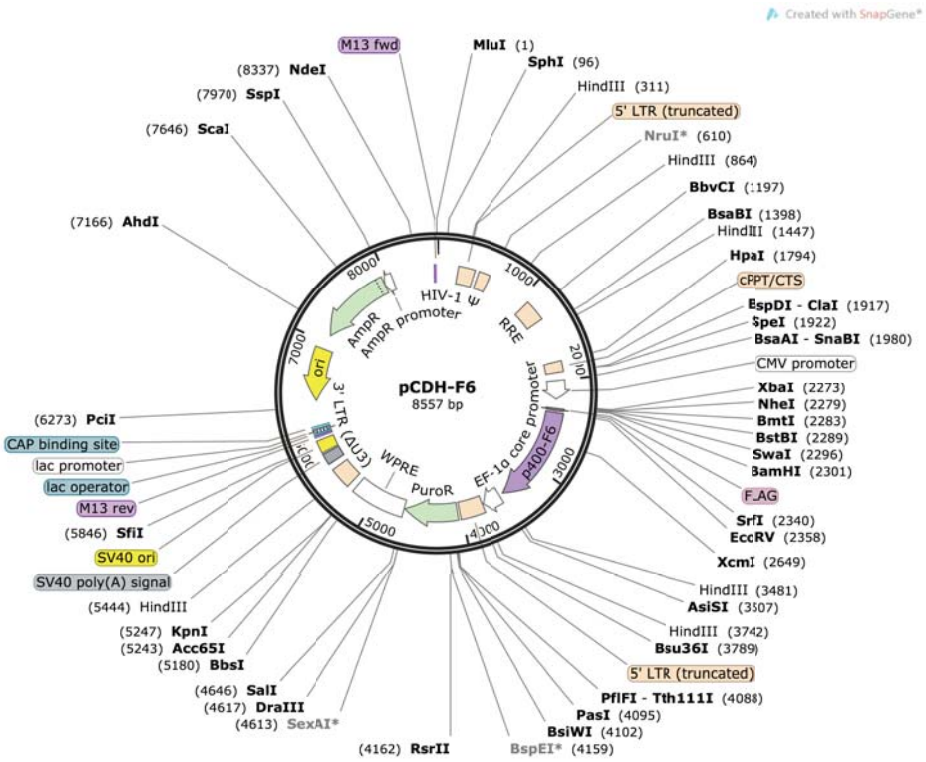

Figure A4.18 pCDH1-F6 Plasmid Map

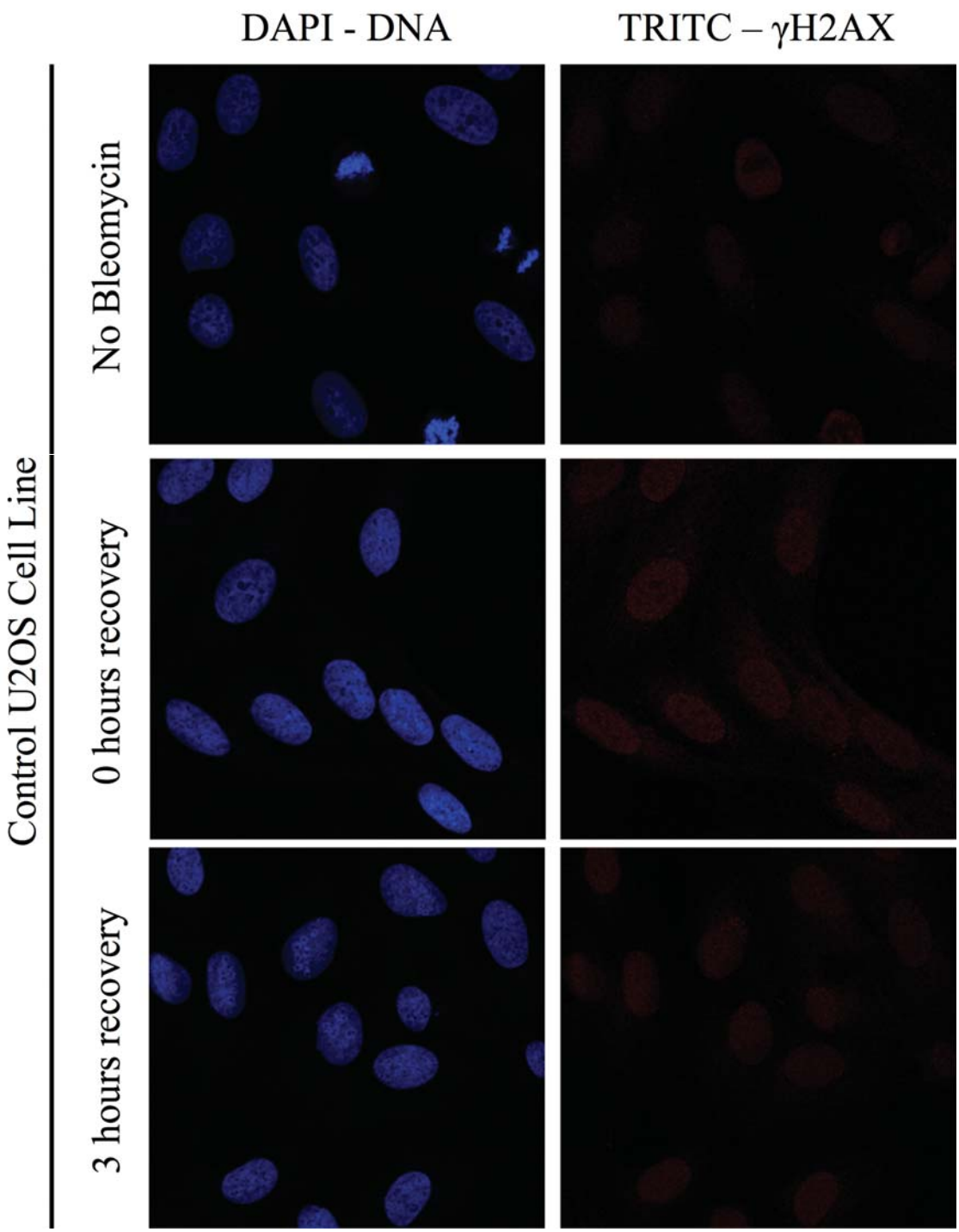
DAPI - DNA
TRITC – γH2AX
Control U2OS Cell Line
No Bleomycin
0 hours recovery
3 hours recovery